



AD A119827

12

# An Experimental Study of Dynamic Stall on Advanced Airfoil Sections Volume 1. Summary of the Experiment

W. J. McCroskey, K. W. McAlister, L. W. Carr, and  
S. L. Pucci

July 1982

DTIC FILE COPY

DTIC  
ELECTRONIC  
OCT 4 1982  
S H

DISTRIBUTION STATEMENT A  
Approved for public release  
Distribution Unlimited

**NASA**  
National Aeronautics and  
Space Administration

United States Army  
Aviation Research  
and Development  
Command



82 10 04 056

12

---

# An Experimental Study of Dynamic Stall on Advanced Airfoil Sections

## Volume 1. Summary of the Experiment

---

W. J. McCroskey

K. W. McAlister

L. W. Carr

S. L. Pucci, Aeromechanics Laboratory  
AVRADCOM Research and Technology Laboratories  
Ames Research Center, Moffett Field, California

**NASA**

National Aeronautics and  
Space Administration

**Ames Research Center**  
Moffett Field, California 94035

United States Army  
Aviation Research and  
Development Command  
St. Louis, Missouri 63166



TABLE OF CONTENTS

	<u>Page</u>
LIST OF TABLES . . . . .	v
LIST OF FIGURES . . . . .	vii
SYMBOLS . . . . .	ix
SUMMARY . . . . .	1
1. INTRODUCTION . . . . .	1
2. DESCRIPTION OF THE EXPERIMENT . . . . .	2
Test Apparatus . . . . .	2
Instrumentation . . . . .	3
Data Analysis and Measurement Accuracy . . . . .	4
Test Conditions . . . . .	7
3. GUIDE TO THE DATA . . . . .	8
4. RESULTS AND DISCUSSION . . . . .	10
Static Data . . . . .	10
Dynamic Data . . . . .	12
Comments on Wind-Tunnel Effects . . . . .	14
5. SUMMARY AND CONCLUSIONS . . . . .	14
REFERENCES . . . . .	16
TABLES . . . . .	19
FIGURES . . . . .	55

DTIC  
COPY  
INSPECTED  
2

Accession For	
NTIS GRA&I	✓
DTIC TAB	
Unannounced	
Justification	
By _____	
Distribution/	
Availability Codes	
Dist	Avail and/or Special
A	

LIST OF TABLES

		<u>Page</u>
1	Harmonic Coefficients of the Oscillation Mechanism . . . . .	19
2	Airfoil Coordinates: NACA 0012 and Ames A-01 Airfoils . . . . .	20
3	Airfoil Coordinates: Wortmann FX-098 and Sikorsky SC-1095 Airfoils . . . . .	21
4	Airfoil Coordinates: Hughes HH-02 (-5° Tab) and Vertol VR-7 (-3° Tab) Airfoils . . . . .	22
5	Airfoil Coordinates: NLR-1 and NLR-7301 Airfoils . . . . .	23
6	Transducer Locations on the Airfoils . . . . .	24
7	Static Drag Coefficients at $M_\infty = 0.30$ based on Wake Surveys . . . . .	25
8	Summary of the Measured Static Airfoil Characteristics at $M_\infty = 0.30$ , including Wind Tunnel Wall Corrections . . . . .	25
9	List of Test Points with Unusual Zero Drift of Pressure Transducers. . . . .	26
10	Coefficients of Linear Curve-Fit of Static Lift Data, without Wind-Tunnel Corrections . . . . .	27
11	List of Data Frames . . . . .	28
12	List of Static Data . . . . .	44
13	Mach Number Sweep at $\alpha = 15^\circ + 10^\circ \sin \omega t$ , $k = 0.10$ . . . . .	45
14	Frequency Sweep at $M_\infty = 0.29$ , $\alpha = 15^\circ + 10^\circ \sin \omega t$ . . . . .	45
15	Frequency Sweep at $M_\infty = 0.30$ , $\alpha = 10^\circ + 10^\circ \sin \omega t$ . . . . .	46
16	Frequency Sweep at $M_\infty = 0.30$ , $\alpha = 15^\circ + 5^\circ \sin \omega t$ . . . . .	46
17	Frequency Sweep at $M_\infty = 0.30$ , $\alpha = 10^\circ + 5^\circ \sin \omega t$ . . . . .	46
18	Stall Onset at $M_\infty = 0.30$ , $\alpha = \alpha_0 + 10^\circ \sin \omega t$ , $k = 0.10$ . . . . .	47
19	Stall Suppression at $M_\infty = 0.30$ , $\alpha = \alpha_0 + 10^\circ \sin \omega t$ . . . . .	47
20	Stall Suppression at $M_\infty = 0.18$ , $\alpha = \alpha_0 + 10^\circ \sin \omega t$ . . . . .	47
21	Pitch Damping Studies at $M_\infty = 0.30$ , $\alpha = \alpha_0 + 2^\circ \sin \omega t$ . . . . .	48
22	No Separation: $M_\infty = 0.30$ , $\alpha = 5^\circ + 5^\circ \sin \omega t$ . . . . .	50
23	Dynamic Boundary-Layer Trip Data . . . . .	50

	<u>Page</u>
24 Miscellaneous Dynamic Data . . . . .	51
25 Test Cases for Numerical Analysis (ref. 1) . . . . .	54

## LIST OF FIGURES

		<u>Page</u>
1	Airfoils tested in the experiment . . . . .	55
2	Model installation in the test section . . . . .	56
3	Photograph of the oscillation mechanism . . . . .	57
4	Sketch of the wooden model shells surrounding the steel spar . . . . .	58
5	Pressure transducer and hot-wire installation: view from inside the upper-surface shell . . . . .	59
6	Coordinate axes for the airfoils . . . . .	59
7	Sketch of the shadowgraph system for visualizing the leading- edge region . . . . .	60
8	Representative shadowgraphs before (upper) and during (lower) dynamic stall: Sikorsky SC-1095 airfoil, $M_\infty = 0.30$ , $\alpha = 10^\circ + 10^\circ \sin \omega t$ , $k = 0.10$ . . . . .	61
9	Static lift and moment data on the NACA 0012 airfoil at $M_\infty = 0.3$ ; shaded bands represent uncertainty limits of data corrected for wind-tunnel-wall effects . . . . .	62
10	Static lift and moment data on the Wortmann FX-098 airfoil at $M_\infty = 0.11$ . . . . .	63
11	Static lift and moment data on the Vertol VR-7 airfoil at $M_\infty = 0.30$ . . . . .	64
12	Comparison of measured lift-drag polars for the NACA 0012 airfoil at $M_\infty = 0.30$ , including wind-tunnel-wall corrections . . . . .	65
13	Comparison of lift-curve slopes on the NACA 0012 and SC-1095 airfoils, including wind-tunnel-wall corrections . . . . .	65
14	Typical data presentation from volume 2; no wall corrections . . . . .	66
15	Typical data presentation from volume 3 . . . . .	67
16	Static characteristics of the NACA 0012 airfoil at $M_\infty = 0.30$ , including wind-tunnel-wall corrections . . . . .	67
17	Static characteristics of the Ames A-01 airfoil at $M_\infty = 0.30$ , including wind-tunnel-wall corrections . . . . .	69
18	Static characteristics of the Wortmann FX-098 airfoil at $M_\infty = 0.30$ , including wind-tunnel-wall corrections . . . . .	71

	<u>Page</u>
19 Static characteristics of the Sikorsky SC-1095 airfoil at $M_\infty = 0.30$ , including wind-tunnel-wall corrections . . . . .	73
20 Static characteristics of the Hughes HH-02 airfoil at $M_\infty = 0.30$ , including wind-tunnel-wall corrections . . . . .	75
21 Static characteristics of the Vertol VR-7 airfoil at $M_\infty = 0.30$ , including wind-tunnel-wall corrections . . . . .	77
22 Static characteristics of the NLR-1 airfoil at $M_\infty = 0.30$ , including wind-tunnel-wall corrections . . . . .	79
23 Static characteristics of the NLR-7301 airfoil at $M_\infty = 0.30$ , including wind-tunnel-wall corrections . . . . .	81
24 Comparison of maximum static lift on the NACA 0012 airfoil . . . . .	83
25 Comparison of maximum static lift on the Ames A-01 airfoil . . . . .	83
26 Comparison of maximum static lift on the Wortmann FX-098 airfoil . . . . .	84
27 Comparison of maximum static lift on the Sikorsky SC-1095 airfoil . . . . .	84
28 Comparison of maximum static lift on the Hughes HH-02 airfoil . . . . .	85
29 Comparison of maximum static lift on the Vertol VR-7 airfoil . . . . .	85
30 Comparison of maximum static lift on the NLR-1 airfoil . . . . .	86
31 Comparison of maximum static lift on the NLR-7301 airfoil . . . . .	86
32 Maximum unsteady lift on the eight airfoils: solid symbols = stall onset; open symbols = deep stall . . . . .	87
33 Comparison of maximum lift on the eight airfoils at $M_\infty = 0.30$ . . . . .	88
34 Comparison of maximum lift on the NACA 0012 airfoil under deep-dynamic-stall conditions: $\alpha = 15^\circ + 10^\circ \sin \omega t$ , $k = 0.10$ . . . . .	89
35 Comparison of the lift hysteresis on the NACA 0012 airfoil: $M_\infty \approx 0.1$ , $\alpha = 15^\circ + 10^\circ \sin \omega t$ , $k = 0.10$ . . . . .	89
36 Comparison of maximum airloads on the NACA 0012 airfoil at $M_\infty = 0.30$ and $\alpha_1 k^2 \approx \text{constant}$ . . . . .	90
37 Comparison of maximum airloads on the Sikorsky SC-1095 airfoil at $M_\infty = 0.30$ and $\alpha_1 k^2 \approx \text{constant}$ . . . . .	91
38 Comparison of maximum airloads on the NLR-1 airfoil at $M_\infty = 0.3$ and $\alpha_{\text{max}} = 20^\circ$ . . . . .	92



## SYMBOLS

A	static lift coefficient at $\alpha = 0$ (see table 10)
B	static $C_{L\alpha} \sqrt{1 - M_\infty^2}$ (see table 10)
$C_C$	chord force coefficient
$C_D$	form drag coefficient derived from surface pressure measurements
$C_{DW}$	total drag coefficient derived from wake survey (see table 7)
$C_L$	lift coefficient
$C_{L\alpha}$	lift-curve slope at low $\alpha$ , per deg
$C_M$	quarter-chord pitching moment coefficient
$C_{M_0}$	static pitching-moment coefficient at zero angle of attack
$C_N$	normal force coefficient
$C_p$	pressure coefficient
c	airfoil chord, m
k	reduced frequency, $\omega c/2U_\infty$
L/D	ratio of lift to drag
$M_\infty$	free-stream Mach number (also M in table 11 and fig. 14)
$M_{\max}$	maximum local Mach number on the airfoil
$q_\infty$	free-stream dynamic pressure, $N/m^2$ (also Q, psi, in table 11)
Re	Reynolds number based on chord and free-stream conditions
$r_0$	leading-edge radius, m
t	time, sec
$U_\infty$	free-stream velocity, m/sec
$X_{a.c.}$	chordwise location of the aerodynamic center of pressure at zero lift
x	chordwise coordinate, m (see fig. 6)
y	normal coordinate, m (see fig. 6)
$\alpha$	angle of attack, deg
$\alpha_{C_{\min}}$	angle of attack for maximum negative chordwise force, deg

- $\alpha_{L_{max}}$  angle of attack for maximum lift, deg  
 $\alpha_{M_{max}}$  angle of attack for maximum local Mach number, deg  
 $\alpha_0$  mean angle, deg (also A0 in computer printouts); also angle for zero lift in table 8 and figs. 9-11  
 $\alpha_{ss}$  static-stall angle, corresponding to  $C_{L_{max}}$ , deg  
 $\alpha_1$  amplitude, deg (also A1 in table 11 and fig 14)  
 $\alpha_2$  magnitude of second harmonic of  $\alpha$ , deg  
 $\beta$   $\sqrt{1 - M_\infty^2}$   
 $\zeta$  aerodynamic pitch damping coefficient,  $-\frac{1}{4\alpha_1^2} \oint C_M d\alpha$   
 $\phi_2$  phase of second harmonic component of  $\alpha$ , deg  
 $\omega$  circular frequency, rad/sec

# AN EXPERIMENTAL STUDY OF DYNAMIC STALL ON ADVANCED AIRFOIL SECTIONS

## VOLUME 1. SUMMARY OF THE EXPERIMENT

W. J. McCroskey, K. W. McAlister, L. W. Carr, and S. L. Pucci

U.S. Army Aeromechanics Laboratory (AVRADCOM), Ames Research Center

### SUMMARY

The static and dynamic characteristics of seven helicopter sections and a fixed-wing supercritical airfoil were investigated over a wide range of nominally two-dimensional flow conditions, at Mach numbers up to 0.30 and Reynolds numbers up to  $4 \times 10^6$ . Details of the experiment, estimates of measurement accuracy, and test conditions are described in this volume (the first of three volumes). Representative results are also presented and comparisons are made with data from other sources. The complete results for pressure distributions, forces, pitching moments, and boundary-layer separation and reattachment characteristics are available in graphical form in volumes 2 and 3.

The results of the experiment show important differences between airfoils, which would otherwise tend to be masked by differences in wind tunnels, particularly in steady cases. All of the airfoils tested provide significant advantages over the conventional NACA 0012 profile. In general, however, the parameters of the unsteady motion appear to be more important than airfoil shape in determining the dynamic-stall airloads.

### 1. INTRODUCTION

Retreating-blade stall limits the high-speed performance of most modern helicopters. In the past decade, numerous new airfoils have been designed in attempts to improve the stall characteristics of rotors without compromising the advancing-blade performance. Only a few of these have been tested under unsteady conditions, and some have not been tested at all. Furthermore, there is almost no overlap between the existing data sets with regard to the important parameters of oscillatory motion.

The motivation of the present experimental investigation was the obvious need for a standard data base for a series of modern rotor-blade sections. The primary objective was to measure the unsteady airloads, over an extensive matrix of test conditions, on the eight profiles shown in figure 1. Other investigations were also overlapped as much as possible. The NACA 0012 served primarily as a standard reference section; the six modern helicopter sections were chosen as representative of contemporary designs from several different companies and research organizations. A modern fixed-wing supercritical profile was also included to extend the range of leading-edge geometries and to provide a basis for comparison with oscillating-airfoil results obtained in other wind tunnels.

Secondary objectives were to investigate the type of stall and boundary-layer separation characteristics for each profile, to provide guidelines for estimating the dynamic-stall characteristics of new airfoils in the future, to supplement the conventional lift and pitching-moment measurements with unsteady drag data and

stall-flutter boundaries, and to determine the effects of leading-edge roughness that is comparable to the erosion of blades in service or in incipient icing conditions.

Dynamic stall depends on a large number of parameters. Consequently, a very large number of unsteady test points (more than 600) plus 44 sets of static data were required to fulfill the objectives of this investigation. As a result, the complete report consists of three volumes. The present volume summarizes the experiment and some of the principal results, including comparisons with data from other sources. It also contains a comprehensive index of the individual unsteady data points. Volume 2 (Pressure and Force Data) contains the pressure, force, and moment data in graphical form. These data are also available upon request on digital computer tapes, one tape for each airfoil, as explained in volume 2. In addition, there is a single tape containing only the 10 test cases that were discussed in reference 1 for the NACA 0012, Vertol VR-7, and NLR-7301 airfoils. Boundary-layer transition, flow reversal, and reattachment results appear in volume 3 (Hot-Wire and Hot-Film Measurements).

This report is primarily intended to assist the users of the data; therefore, the results are not discussed at length. The principal results have been published in references 1 and 2.

## 2. DESCRIPTION OF THE EXPERIMENT

### Test Apparatus

The experiment was performed in the 2- by 3-m atmospheric-pressure, solid-wall Wind Tunnel at the U.S. Army Aeromechanics Laboratory. The tests were conducted in essentially the same manner as those in a previous experiment (refs. 3,4), except that the free-stream Mach number was extended to 0.3, the model chord  $c$  was reduced to 0.61 m (except for the Hughes HH-02 airfoil,  $c = 0.69$  m), the frequency of oscillation was extended to 11 Hz, and the data processing was refined considerably. The models spanned the 2.13-m vertical dimension of the wind tunnel, as indicated in figure 2, and were oscillated sinusoidally in pitch about the quarter chord. A gap of approximately 2 mm existed between the ends of the model and the wind-tunnel walls.

The drive mechanism used (fig. 3) was the same one described in references 3 and 4, with some notable improvements. In some cases, the connecting push rod was fitted with a remotely controlled jackscrew mechanism that allowed the mean angle,  $\alpha_0$ , to be varied continuously while the tunnel was operating. Discrete amplitudes of oscillation of 2°, 5°, 6°, 8°, 10°, or 14° could be set between runs. The motion of the airfoils was given by  $\alpha \approx \alpha_0 + \alpha_1 \sin \omega t$ , with maximum higher harmonic distortion approximately 2% of  $\alpha_1$ . Table 1 gives the harmonic content of the mechanism for various values of  $\alpha_0$  and  $\alpha_1$ . The frequency of oscillation could be varied between approximately 0.02 and 12 Hz.

The models of the eight airfoils (fig. 1) consisted of interchangeable shells constructed of wood and fiberglass. These shells surrounded a stainless steel spar that contained the instrumentation and wiring, as indicated schematically in figures 2 and 4. The shells contained special fittings for the pressure transducers and hot-wire or hot-film sensors (fig. 5) that facilitated model changes without disconnecting the instrumentation.

Each set of shells was precision-machined, while mounted on the spar, to a design accuracy of  $\pm 0.1$  mm. However, measurements after the test revealed that the rms standard deviation of the coordinates from the design values was about 0.4 mm, or 0.06% of chord, and that the maximum error was about 0.8 mm. The nominal design coordinates of the airfoils are given in tables 2-5, referred to the standard coordinate system sketched in figure 6. The coordinates were taken originally from references 5-9 and from Amer (K. Amer, private communication, 1977).

A limited amount of static and dynamic data were obtained on each airfoil at  $M_\infty = 0.185$  and 0.29 with a boundary-layer trip, consisting of a 3-mm-wide band of 0.10-mm-diam glass spheres glued to the leading edge. The purpose of the trip was to eliminate the laminar separation bubble that would normally form near the leading edge as the stall angle was approached. It also approximately simulated surface abrasion on helicopter blades operating under severe field conditions, as well as roughness caused by incipient icing conditions.

### Instrumentation

The primary data were obtained from 26 Kulite differential pressure transducers, types YCQH-250-1 and YCQL-093-15. Those of the latter type were used in the leading- and trailing-edge regions, because of their smaller size. The locations of the transducers for each airfoil are given in table 6. The back side of each transducer was referenced to the total pressure of the wind tunnel; total pressure was measured about 1.5 m upstream of the model. The measuring side of the transducers mated with the fittings shown in figure 5, which had 0.79-mm-diam orifices. The transducers thus installed had flat amplitude versus frequency responses of 250 Hz or better and typical cavity resonance frequencies of about 850 Hz.

Special on-line analog computers that calculated and displayed the instantaneous normal force, pitching moment, pitch damping, and pressure distributions proved to be extremely valuable in assessing the dynamic-stall behavior, as well as the performance of the instrumentation, while the tests were in progress. These devices also enabled the unsteady parameters to be adjusted until some desired result was obtained, such as the maximum lift condition in the absence of moment stall or neutral aerodynamic damping in pitch.

Boundary-layer transition, flow reversal, separation, and reattachment were studied with a variety of surface hot films and hot-wire sensors (single-, double-, and triple-element probes), using the techniques described in references 4, 10, and 11. Six sensors were used on the upper surface of each airfoil, at the locations given in table 6. In addition, a hot-wire probe protruding just outside the boundary layer was mounted near the leading edge of the NLR-1 profile to aid in diagnosing the local supersonic zone that was frequently inferred at high incidence.

The leading-edge region was also examined with a shadowgraph flow visualization system (fig. 7). The high-intensity strobe light was fired at selected phase angles during the oscillation, and the pattern that developed on the Scotchlite high-gain reflective sheeting on the floor of the tunnel was photographed by the pulse camera above the test section. A representative photograph is shown in figure 8.

Finally, a traversing pitot-static probe was used to survey the wake behind each airfoil under steady-flow conditions. The steady drag of the airfoils at  $M_\infty = 0.30$  was derived from these measurements; these drag coefficients are listed in table 7.

## Data Analysis and Measurement Accuracy

For quantitative purposes, the pressure transducer and hot-wire signals were amplified and recorded on a 32-channel analog tape recorder with 2500-Hz flat frequency response. In addition, the average free-stream dynamic pressure, the instantaneous angle of attack of the model, and 1/cycle and 200/cycle timing indicators were recorded simultaneously. Calibrations of the pressure transducers were recorded at the beginning and end of each analog tape. The unsteady data tapes were digitized and ensemble-averaged off line. At least 50 cycles of data were normally sampled 200 times per cycle; however, for the NACA 0012 airfoil at very low frequencies, that is,  $k < 0.002$ , only about 10 cycles were recorded. Reference and calibration signals and the steady pressure data were acquired with the same system and were digitally sampled 100 times over a 5-sec interval. The averaged pressure data were then processed and integrated numerically by trapezoidal rule to determine the unsteady lift, moment, and pressure drag.

End-to-end checks of the data acquisition and processing system indicated that the pressure signals were reproduced to within an rms error of approximately  $70 \text{ N/m}^2$  (0.01 psi), and that the transducer calibrations were reliable to better than  $\pm 150 \text{ N/m}^2$  (0.02 psi) or  $\pm 3\%$  of the reading, whichever was greater, over the range of tunnel speeds and temperatures. The model temperature, measured inside the shells, was closely monitored and not allowed to vary more than  $3^\circ\text{C}$  between records of no-flow pressure readings. Transducer zero drift was normally controlled to within the greater value of either  $\pm 150 \text{ N/m}^2$  (0.02 psi) or  $\pm 5\%$  of free-stream dynamic pressure. However, some exceptions are noted later in this section.

The hot-wire and hot-film signals were recorded as consecutive, separate data frames, and individual cycles of the analog records were examined to determine the boundary-layer characteristics, as discussed in references 4, 10, and 11. For these data, the results from three to eight cycles were averaged to obtain the relative times within the cycle,  $\omega t$ , at which the various boundary-layer events occurred.

The instantaneous angle of attack was measured with a potentiometer attached to the tubular portion of the model spar (fig. 3). The angle-of-attack signal was calibrated for each data point based on the value of  $\alpha_1$ , which was set by the oscillation linkage, and physical measurements of  $\alpha_{\max}$  and  $\alpha_{\min}$  that were obtained from the trailing-edge position relative to the centerline of the tunnel with the wind off. The maximum absolute error in  $\alpha$  was estimated to be  $\pm 0.2^\circ$ , with a relative uncertainty of  $\pm 0.05^\circ$  over the cycle. The maximum torsional deflection of the model at the centerline was calculated to be  $\pm 0.3^\circ$ . Table 1 gives the amplitude and phase of the second harmonic component of  $\alpha$  for various nominal values of  $\alpha_1$ . The frequency of the oscillation was maintained and measured to an estimated accuracy of  $\pm 0.03 \text{ Hz}$ .

The tunnel dynamic pressure was measured with a conventional pitot-static probe mounted approximately 1.5 m upstream of the model and connected to a pressure transducer and amplifier system with a net accuracy of approximately  $\pm 14 \text{ N/m}^2$  (0.002 psi) under steady conditions. The measured values ranged from  $90 \text{ N/m}^2$  (0.013 psi) at  $M_\infty = 0.04$  to  $6200 \text{ N/m}^2$  (0.90 psi) at  $M_\infty = 0.3$ . The output of this transducer was recorded by hand and on the 32-channel analog tape recorder. An average of these two values, which rarely differed by more than 2%, was used to compute  $q_\infty$ , except in a few cases in the early stages of the test program in which the tape-recorded value was obviously in error and was therefore ignored. The 25-mm-thick ground plane shown in figure 2 caused a 1% reduction in tunnel cross-sectional area between the pitot-static tube and the model; this was ignored except as noted in connection with the steady lift results presented in section 4 under the heading Static Data.

A detailed examination of the digitized data revealed that the 200/cycle sampling of the analog signals was not always synchronized perfectly with the 200/cycle timing indicators. That is, the effective time base of the digitized data was in error, the cumulative effect of which was either to leave a small gap in the data at the end of the cycle or to overlap the 200th sample of a given cycle with the first sample of the next cycle. Consequently, a corrected time base for the digital data arrays was obtained by least-squares curve-fitting a first- and second-harmonic sine wave to the angle-of-attack signal,  $\alpha$ . All of the pressure data were then linearly interpolated onto the new time base at 200 even intervals per cycle and stored in new arrays, with the first data point in each array corresponding to  $\omega t = 0$ . The end result is that the final data appear at the desired times, but suffer an effective "smearing" that would be, at worst, equivalent to sampling at a rate of 100 points per cycle instead of 200 per cycle.

Experimental uncertainty of the airloads- For the purposes of comparing the static and dynamic-stall characteristics of the eight airfoil sections, the absolute accuracy of the measurements and the consequences of wind-tunnel blockage, circulation interference, and sidewall boundary-layer interference are less important than the random experimental errors outlined above. However, an attempt was made to assess all of these, as described below.

The total measurement uncertainty in the pressure, force, and moment coefficients depends on the operating conditions. For example, the probable error in  $C_p$  based on the instrumentation characteristics quoted above varies from less than  $\pm 0.07$  at  $M_\infty = 0.3$  and  $\alpha = 0$  to about  $\pm 0.4$  near the leading edge at  $M_\infty = 0.11$  and  $\alpha$  approaching the stall angle. For most of the static data at  $M_\infty = 0.3$ , the measurement uncertainty is estimated at  $\pm 0.03$  for  $C_{Lmax}$ ,  $\pm 0.005$  for  $C_M$ , and  $\pm 0.0005$  for  $C_D$  derived from the wake measurements. However, the uncertainty in the SC-1095 lift and moment data is thought to be at least twice as large, because of some unresolved difficulties with the pressure measurements. These values increase with decreasing Mach number, rising by a factor of about 5 in the extreme case  $M_\infty = 0.035$ , where the pressure signals were very small.

Some representative examples of static  $C_L$  and  $C_M$  versus  $\alpha$  are given in figures 9-11, and the primary characteristics of each airfoil at  $M_\infty = 0.30$  are presented in table 8. The symbols in the figures indicate the individual uncorrected data points, as presented in volume 2 of this report; the shaded bands denote the estimated bounds of the airfoil characteristics. The bounds of the airfoil characteristic include static wind-tunnel-wall corrections according to Allen and Vincenti (ref. 12) and a 1% correction due to the reduction in test-section area at the model caused by the steel plate on the floor of the tunnel (fig. 2). (This wall correction method is only valid below stall, where the corrections are about 1% for  $\alpha$  and 1.5% for  $C_L$ .) These boundaries were derived based on the measurement uncertainties described above, on data that were obtained with the on-line analog computers, and on the dynamic data obtained at  $k \leq 0.01$ . It should be noted that the scatter in the data and the uncertainty bounds increase considerably for conditions above the stall angle. The last line in table 8 indicates the experimental uncertainties for the various quantities listed. The static data are discussed further in section 4.

A novel feature of the present experiment was the determination of unsteady pressure drag,  $C_D = C_C \cos \alpha + C_N \sin \alpha$ , where  $C_C$  and  $C_N$  are the chordwise and normal force coefficients derived from the upper and lower surface-pressure distributions. The two terms in this expression for  $C_D$  are approximately equal and opposite at high angles of attack below stall, so that the probable percentage errors of

$C_D$  are much greater than for  $C_C$ ,  $C_N$ ,  $C_L$ , or  $C_M$ . Figure 12 shows a typical static lift-drag polar based on pressure measurements and on the more accurate wake survey of the total drag (table 7). The measured pressure drag, which neglects the contribution due to skin friction, is less than the total drag at low lift coefficients, but it incorrectly exceeds the wake measurements by as much as 0.02 near the stall angle, that is, by as much as 100%. (It may be noted that Woodward (ref. 13) reported similar, unexplained discrepancies between measured pressure drag and  $C_D$  based on wake surveys.) However, the percentage errors are much less in the stall regime, where the magnitude of  $C_C$  decreases considerably and the maximum drag coefficient becomes of the order of  $C_L \tan \alpha$  (i.e., of the order of unity) for the deep-dynamic-stall cases studied.

The measurement uncertainty of the unsteady data is probably comparable to that of the static data, but fewer independent checks were available to assess the random experimental errors and the wind-tunnel interference, especially in the post-stall regime. Fromme and Golberg (ref. 14) have indicated that unsteady wall corrections can be greater than the corresponding static corrections, but it is not clear to what extent their potential flow analysis can be applied to the present measurements. Likewise, it is not possible to estimate reliably the post-stall tunnel sidewall effects nor how these vary from one airfoil to another, but tuft flow visualization and experience suggested that these problems became less important as the frequency of oscillation is increased. It is the authors' judgment that for  $M_\infty \geq 0.2$ , the unsteady data in the deep-dynamic-stall regime should be in error by no more than  $\pm 0.2$  for  $C_L$ ,  $\pm 0.05$  for  $C_M$ , and  $\pm 0.10$  for  $C_D$ , except as noted in the next section. The results are thought to be about twice this accurate below stall and in light stall, whereas the accuracy was seriously degraded for  $M_\infty < 0.1$  because of the small values of the pressure signals.

Special cases of questionable accuracy- Despite efforts to monitor the performance of the pressure instrumentation during the test and to control and minimize the measurement uncertainties, various problems sometimes arose that only became evident during the post-test reduction and analysis of the data. In most cases, it was possible to correct these problems on an individual basis, using redundant information or by interpolating in time or space between neighboring values, without significantly compromising the accuracy of the results. In other instances, the measurements appeared to be qualitatively correct, but the experimental uncertainty was likely to have been outside the normal bounds discussed in the previous section. These cases are identified below by data-point or "frame" number.

Frame 10202 for the NACA 0012 airfoil had an unusually large number of random irregularities, a total of 44 in the 5,200 pressure data samples. These were eliminated by linearly interpolating between data at preceding and succeeding time increments. Because some of these irregularities occurred during rapid fluctuations of the flow, the time-histories of part of the pressure data for this particular frame may have been degraded. However, the effect on the integrated force and moment coefficients was probably small.

Table 9 lists the frames for which the "zero" drift of one or more of the transducers appeared to have exceeded by a significant amount the nominal values quoted in the previous section. Also included are the low Mach-number cases for which the no-flow pressure readings taken before and after recording data varied by more than 50% of free-stream dynamic pressure, even though this drift amounted to less than the nominal measurement uncertainty of  $150 \text{ N/m}^2$  (0.02 psi). It should be mentioned that in all cases the differences between these pretest and post-test zeros were linearly interpolated with respect to elapsed time to obtain effective zeros for the individual



data frames. In principle, this should have reduced the effects of the transducer drift; however, the actual improvement in the measurement accuracy because of this technique remains unknown.

For the Hughes HH-02 airfoil, the responses of pressure transducers No. 1 (leading edge) and No. 25 ( $x/c = 0.0081$ , lower surface) were rather sluggish, possibly because the orifices were partially clogged. Therefore, the unsteady data from these two transducers are suspect. In calculating the force and moment data for this airfoil, transducer No. 25 was ignored and the pressure integrals

$$C_N = -\oint C_p dx/c \quad \text{etc.}$$

were replaced by

$$C_N = -2 \oint C_p \xi d\xi \quad \text{etc.}$$

where  $\xi = \sqrt{x/c}$ , thereby eliminating the influence of transducer No. 1, since  $C_{p1} \sqrt{x_1} = 0$ . Another problem with the HH-02 force and moment data is that the trailing-edge transducers were at  $x/c = 0.925$  instead of 0.98, so that the error in extrapolating to  $x/c = 1.0$  is greater for this airfoil. The net effect of these modifications is difficult to assess, but it probably increased the experimental uncertainties for the lift, pressure drag, and pitching moment data by no more than 50%.

The NLR-7301 airfoil had a large amount of concave curvature on the lower surface downstream of  $x/c = 0.5$ , which produced larger pressure gradients there than existed on the other airfoils. Therefore, the relatively sparse distribution of pressure transducers in that region may have led to larger errors in determining the forces and moments than the nominal values quoted in the preceding section.

The reduced data for the Sikorsky SC-1095 airfoil under static conditions and at low frequencies consistently exhibited values of maximum lift coefficient and lift-curve slope that appeared to be about 5% too large, based on comparisons with the other airfoils and with the results obtained from the special on-line analog computer described above under Instrumentation. In particular, the comparison with the present NACA 0012 data (fig. 13) contrasts significantly with the steady results of Noonam and Bingham (ref. 15) and Jepson (ref. 16), who found  $C_{L\alpha}$  to be approximately the same for both airfoils. A detailed examination of the present data and the transducer calibrations revealed somewhat erratic performance in a few cases, but no systematic behavior emerged that could explain the apparent problem. Therefore, the conclusion is that the SC-1095 results should be viewed with caution, even though they appear to be qualitatively correct.

#### Test Conditions

The primary reference conditions for the initial comparisons of the various airfoils were static and deep-dynamic stall at  $M_\infty = 0.3$ , with the nominal unsteady motion given by  $\alpha = 10^\circ + 10^\circ \sin \omega t$  and  $k = \omega c / 2U_\infty = 0.10$ . Limited but systematic variations in Mach number and the unsteady parameters were explored for all airfoils as indicated below and in section 3, where the specific test points are indexed and cross-referenced.

Static data- Pressure measurements were recorded at discrete values of  $\alpha$  between  $-5^\circ$  and  $20^\circ$  for  $M_\infty = 0.11, 0.185, 0.25,$  and  $0.30$  for all airfoils except the NACA 0012. In the latter case, static data were recorded only at  $M_\infty = 0.30$ ; quasi-steady data were obtained for a continuous range of  $\alpha = \alpha_0 + 10^\circ \sin \omega t$  for  $k \approx 0.001$  for nine values of  $M_\infty$  between  $0.035$  and  $0.30$ . A number of the static conditions were repeated with a boundary-layer trip at the leading edge. Wake surveys for static drag were obtained at  $M_\infty = 0.3$  for  $\alpha$  between  $-5^\circ$  and the static stall angle.

Unsteady data- The parameters that were varied under dynamic-stall conditions were Mach number, reduced frequency, mean angle, and amplitude of the oscillation. The effect of Mach number was studied between  $M_\infty = 0.035$  and  $0.30$ , primarily in the deep-stall regime for  $\alpha = 15^\circ + 10^\circ \sin \omega t$  and  $k = 0.10$ . In these cases, the Reynolds number also varied, proportional to Mach number, according to the relation  $Re \approx 14 \times 10^6 M_\infty$ .

The principal ranges of reduced frequency, mean angle, and amplitude were  $0.01 \leq k \leq 0.20$ ,  $\alpha_0 = 10^\circ$  and  $15^\circ$ , and  $\alpha_1 = 2^\circ, 5^\circ,$  and  $10^\circ$ , respectively; the effects of these parameters were studied primarily at  $M_\infty = 0.30$ . Additional variations in  $k$  and  $\alpha_0$  were effected to achieve specific dynamic effects, such as no stall, stall onset, stall suppression because of unsteady effects, and neutral aerodynamic damping in pitch.

Finally, additional test points were selected that duplicated some of the conditions of references 3 and 17-19 as closely as possible. A complete list of the unsteady test conditions and descriptions of the parametric variations are given in the following section.

### 3. GUIDE TO THE DATA

A very large data base was generated in this investigation. As mentioned in the Introduction, summary graphs of the pressure, force, and moment coefficients and selected results from the boundary-layer studies are contained in separate volumes. The airloads data are also stored on digital computer tapes, one for each airfoil, as explained in volume 2. This section describes briefly the data presentations to be found in the subsequent volumes and indicates by test point, or "frame number," the various types of data that are available.

Figure 14 illustrates the format of volume 2 for the unsteady pressure, force, and moment coefficient data, that is,  $C_L, C_M,$  and  $C_D$  versus  $\alpha$  and  $\omega t$ , and the upper-surface pressure distributions throughout the cycle. Additional information is listed at the top of the graphs. Following the airfoil name is the identification number for each test point. As explained in volume 2, these frame numbers comprise data at a single angle of attack for the steady data, and data at 200 evenly spaced time intervals throughout the cycle for the unsteady cases. The quantities  $A_0$  and  $A_1$  are the mean value and the first-harmonic amplitude, respectively, of the instantaneous angle of attack,  $\alpha$ ;  $M_{\max}$  is the estimated maximum value of the local Mach number at any time in the cycle, calculated from the classical gas-dynamic equations for steady isentropic flow and the measured pressure coefficient,  $-C_{p_{\min}}$  (cf. ref. 2);  $\alpha_{L_{\max}}, \alpha_{C_{\min}},$  and  $\alpha_{M_{\max}}$  are the angles of attack corresponding to maximum lift, minimum chord force (cf. ref. 3), and  $M_{\max}$ , respectively; and  $\zeta$  is

the aerodynamic damping in pitch. The asterisk on the ordinate of the pressure-coefficient graph represents sonic conditions.

The dotted line in the  $C_L$  vs  $\alpha$  curve in figure 14 is an approximation to the quasi-static lift behavior for this flow condition, according to the relation

$$C_L = A + \frac{B\alpha}{\sqrt{1 - M_\infty^2}}$$

where  $\alpha$  is in degrees and A and B were obtained from the relevant steady and very low-frequency data, that is, for  $k \leq 0.01$ . The values of A and B are given in table 10. Finally, it should be mentioned that in contrast to the data in table 8 and the static results presented in section 4 under the heading Static Data, wind-tunnel wall corrections have not been applied to A and B, to the data in volume 2, nor to the numerical data tapes.

Figure 15 shows two representative examples of the boundary-layer "flow reversal" information contained in volume 3. The abscissa in the figures show the position on the airfoil where the surface instrumentation first indicated a breakdown of the attached boundary-layer flow at the beginning of dynamic stall, as explained and discussed in volume 3 and in references 4, 10, and 11. This event either signifies or is closely associated with the separation that accompanies the beginning stages of dynamic stall. The ordinate indicates the nondimensional time in the cycle,  $\omega t$ , at which this event occurred.

Tables 11-24 provide a comprehensive summary and index of the entire experimental program. Table 11 lists the frame numbers of all the pressure data, in the sequence in which they appear on the data tapes. The airfoil and pertinent test conditions are also listed, and the conditions for which boundary-layer data were recorded are indicated in the last column. The letter "Y" in the "TRIP" column indicates the use of the boundary-layer trip; "N" denotes the standard smooth condition. The notations "ST" and "US" denote steady and unsteady data, respectively, and the frequency of oscillation in Hertz is given in the column labeled "FREQ."

Table 12 is an index of the steady-data sets, arranged by airfoil and Mach number. The use of a boundary-layer trip is indicated by the letter "T." The notation "Quasi-steady" indicates the data that were acquired on the NACA 0012 airfoil as unsteady data, but at very low frequency,  $k \leq 0.002$ .

A cross-reference index that groups the unsteady data by types for each of the eight airfoils is given in tables 13-24. There are some duplicate entries in these tables, in order to facilitate the identification of data sets with variations in the individual parameters of the unsteady motion. There are also blank entries, since not all conditions were recorded for all airfoils. The principal types of unsteady conditions are outlined below.

Variations in Mach number- Table 13 lists the test points concerned with the effect of Mach number on deep dynamic stall, for  $\alpha = 15^\circ + 10^\circ \sin \omega t$  and  $k = 0.10$ . Although the NLR-7301 airfoil was only tested at three values of  $M_\infty$  with  $\alpha_0 = 15^\circ$ , it was also tested with  $\alpha_0 = 10^\circ$  at  $M_\infty = 0.11, 0.18, 0.22,$  and  $0.30$ ; these frames are given in table 24. Stall-suppression conditions, tables 19 and 20, and the effects of leading-edge trips, table 23, were studied at  $M_\infty = 0.18$  and  $0.30$  for various values of  $\alpha_0$  and  $k$ . As stated in section 2 under Test Conditions, the variation of Reynolds number with Mach number was  $Re = 14 \times 10^6 M_\infty$ .

Reduced frequency sweeps- The test points concerned with the effect of frequency on dynamic stall are given in tables 14-17. These data cover the range  $0.01 \leq k \leq 0.20$  at  $M_\infty = 0.3$ , with mean angles of  $10^\circ$  and  $15^\circ$  and amplitudes of  $5^\circ$  and  $10^\circ$ . In addition, the NACA 0012 airfoil was tested over an extensive range of other values of  $\alpha_0$  (table 24).

Stall onset- This condition, defined in references 1 and 2 as obtaining the maximum possible lift without moment stall occurring at any time throughout the cycle of oscillation, was studied at  $M_\infty = 0.30$ ,  $k = 0.10$ ,  $\alpha_1 = 10^\circ$ , and variable mean angle, as indicated in table 18.

Stall suppression caused by unsteady effects- With  $\alpha_1$  fixed at  $10^\circ$ ,  $\alpha_0$  was varied so that  $\alpha_{\max}$  was slightly greater than the static-stall angle. Data were then recorded (tables 19 and 20) at various reduced frequencies to study whether stall would diminish or increase with increasing  $k$ .

Pitch damping boundaries- Stall conditions relevant to small-amplitude flutter boundaries are listed in table 21, at  $\alpha_1 = 2^\circ$  and  $M_\infty = 0.30$ . Mean angle and reduced frequency were varied to obtain approximate boundaries of neutral aerodynamic damping in pitch and to obtain the maximum negative value of pitch damping,  $-\zeta_{\min}$ . However, no data of this type were recorded for the NACA 0012 airfoil.

No separation- A limited number of test points were recorded at  $M_\infty = 0.30$  and  $\alpha = 5^\circ + 5^\circ \sin \omega t$ , as indicated in table 22. Some additional conditions for the NLR-1 and NLR-7301 profiles without separation are given in table 24.

Boundary-layer trip- Data with the leading-edge trip were obtained statically for  $\alpha$  between  $0^\circ$  and  $20^\circ$  and dynamically for  $\alpha = 15^\circ + 10^\circ \sin \omega t$  at two values of Mach number, 0.18 and 0.30. The values of  $k$  for the dynamic data are given in table 23; the static data with trip are so indicated in table 12. An exception was the NLR-7301 section at  $M_\infty = 0.30$ , for which  $\alpha = 10^\circ + 5^\circ \sin \omega t$  (table 24). In addition, the NLR-1 section with trip was studied with  $\alpha_0 = 2.5^\circ$  (table 24).

Miscellaneous- These test points are included in table 24. In addition to the cases mentioned above, the unsteady test conditions of references 3 and 17 for the NACA 0012, of reference 18 for the Sikorsky SC-1095, and of reference 19 for the NLR-1 airfoil were reproduced insofar as possible. Also, for the Vertol VR-7 airfoil,  $k$  was varied from 0.01 to 0.25 at  $M_\infty = 0.18$  with  $\alpha_0 = 10^\circ$  and  $15^\circ$  and  $\alpha_1 = 10^\circ$ . Finally, dynamic stall on the NLR-1 profile at negative incidence was studied at  $M_\infty = 0.30$  for  $\alpha = -2^\circ + 10^\circ \sin \omega t$  and  $0.01 \leq k \leq 0.10$ .

Selected test cases- Finally, table 25 lists the unsteady data that were proposed in reference 1 as specific test cases for evaluating unsteady viscous flow theories and computational methods. These data were obtained on the NACA 0012, Vertol VR-7, and NLR-7301 airfoils. They include conditions of no-stall, stall-onset, light-stall, and deep-dynamic-stall, all at  $M_\infty = 0.3$ .

#### 4. RESULTS AND DISCUSSION

##### Static Data

The measurements performed under steady or quasi-static flow conditions provide a frame of reference for the dynamic-stall results and a basis for comparison with

data from other wind tunnels. Some of the highlights of the static data are presented below, with particular reference to the force and moment coefficients at  $M_\infty = 0.3$ . With the exception of the drag data listed in table 7, wind-tunnel-wall corrections have been applied to all of the static results presented in this section, using the formulae of reference 12.

As noted earlier, table 8 gives a summary of the primary static characteristics of each airfoil at  $M_\infty = 0.30$ , and figures 16-23 show the basic variations of lift, pitching moment, and drag coefficients for the eight sections. The dashed lines in the "a" parts of figures 17-23 represent curve-fits of the lift data in the linear  $C_L - \alpha$  regime. The drag data derived from the wake surveys are listed in table 7. In the following discussions, some comparisons are made for each airfoil between the present measurements and data obtained elsewhere.

NACA 0012 airfoil- This profile has been tested by many investigators, with a wide range of results. Figure 24 shows the variation in  $C_{L_{max}}$  with Mach number, including results reported or summarized in references 3, 5, 15-17, and 20-24 over a wide range of Reynolds numbers. The present values of  $C_{L_{max}}$  increase with increasing Mach number for  $M_\infty < 0.22$ , probably because of the effects of increasing Reynolds number, whereas compressibility effects are thought to be responsible for the decrease in  $C_{L_{max}}$  for  $M_\infty > 0.22$ . The boundary-layer trip was found to be relatively unimportant for this airfoil at the Mach and Reynolds numbers of the test.

The present  $C_{L_{max}}$  data tend to lie near the upper range of the values from other sources. The same is true for the lift-curve slopes in the linear regime,  $C_{L_\alpha}$ , which is not shown.

Ames A-01 airfoil- Figure 25 compares the data from the present test with measurements made in a transonic wind tunnel at somewhat lower Reynolds numbers (ref. 6) for the A-01 airfoil. Although the lift-curve slopes for  $C_L < 1.0$  were not significantly different in the two tests, the airfoil stalled at lower angles of attack in the transonic tunnel. Consequently, lower values of maximum lift coefficient were measured and reported in reference 6 at  $M_\infty = 0.2$  and  $0.3$ , which was near the lower operating limit of that facility.

Wortmann FX-098 airfoil- Maximum-lift data from several investigations (refs. 8, 24-26) are compared with the present data in figure 26 for the FX-098 airfoil. All of the data agree reasonably well over the Mach-number range of the present test. However, there are marked differences at higher Mach numbers.

Sikorsky SC-1095 airfoil- Steady results for this section are shown in figure 27, where the comparison is generally unfavorable. The suspicious nature of the present lift data was mentioned earlier in section 2 under Data Analysis and Measurement Accuracy; here the open circles indicate the present data analyzed in the normal way and the solid symbols represent what are thought to be the true values. The latter, somewhat lower, values are based primarily on the on-line measurements. It should be mentioned that the data of Noonan and Bingham (ref. 15) were obtained on a modified profile with a reflex training edge that reduced  $C_{M_0}$  to approximately zero, compared with the present value of  $-0.027$  at  $M_\infty = 0.3$  (cf. table 8). Also, the data of Jepson (ref. 16) in figure 27 came from a slotted-wall tunnel with 12.5% porosity, which was thought to yield somewhat lower values of  $C_L$  than comparable tests in solid-wall tunnels. Furthermore, the Reynolds numbers in references 15 and 16 were

lower than those of the present tests. Nevertheless, the discrepancies in figure 27 seem to be too large to be attributed to these factors or to measurement uncertainties. It will be shown later that dynamic data on the SC-1095 section are generally in better agreement.

Hughes HH-02 airfoil- Figure 28 shows the measured maximum lift coefficients for the present HH-02 airfoil, in comparison with data from a section that is almost identical except for a slightly smaller leading-edge radius (ref. 27). Although the Mach number range does not overlap, the two sets of results seem consistent.

Vertol VR-7 airfoil- Results from four sources are plotted in figure 29 for the VR-7 profile. The present data are somewhat higher than those of Coulomb (ref. 28), primarily because the stall occurred at slightly higher angles of attack, but the lift-curve slopes (not shown) and the effect of a boundary-layer trip were approximately the same. The value of  $C_{L_{max}}$  at  $M_\infty = 0.3$  is slightly lower than that of Dadone (ref. 5), whose measurements at higher Mach numbers exceed considerably those of Bingham et al. (ref. 29).

NLR-1 airfoil- Figure 30 shows the good agreement of the present measurements with those of Dadone (ref. 19) for the NLR-1 airfoil. It should be mentioned, however, that the details of the pitching-moment behavior in the vicinity of  $C_{L_{max}}$  (not shown) were somewhat different. As in the previous example, the data of Noonan and Bingham (ref. 24) for  $C_{L_{max}}$  at  $M_\infty \geq 0.35$  tend to be lower than the data of Dadone (ref. 19). This airfoil appears to be more sensitive to Mach number than any of the other modern helicopter sections.

NLR-7301 airfoil- As shown in figure 31, the maximum static lift for the NLR-7301 airfoil exceeded that of the other sections by a considerable margin; however,  $C_{M_0}$  was  $-0.083$  (cf. table 8). The values of  $C_{L_{max}}$  shown are also greater than those obtained at NLR under virtually identical conditions (ref. 30). This was obtained at a significantly larger stall angle, more than  $1^\circ$  larger at  $M_\infty = 0.18$ , than in the NLR experiments, apparently because of different boundary-layer separation characteristics and sidewall interferences.

#### Dynamic Data

Although the static data described above comprised an essential part of the investigation, the primary objective was to obtain a common data base of unsteady characteristics for helicopter applications. In this section some representative examples are presented and comparisons made with other investigations. More complete discussions of the basic phenomena and of the results obtained are given in references 1 and 2.

The unsteady stall-onset and dynamic-stall counterparts of the static  $C_{L_{max}}$  results discussed above are shown in figures 32 and 33, reproduced from reference 2 with some minor corrections. The dashed lines in figure 33 indicate the estimated deep-stall  $C_{L_{max}}$  for the NLR-7301 airfoil; data were not obtained for this condition for  $M_\infty > 0.25$ . These results have not been corrected for wind-tunnel-wall interference.

Figures 32 and 33 illustrate an important general result of the investigation: the parameters of the unsteady motion tend to be more important than the airfoil geometry. For example, the differences in the values of  $C_{L_{max}}$  for the Wortmann, Sikorsky, and Hughes airfoils can hardly be discerned within the experimental uncertainty, but the unsteady stall-onset and deep-stall results are much higher than the static values shown in figures 26-28 and 33. It is also interesting to note that at least for  $M \leq 0.25$ , the deep-stall  $C_{L_{max}}$  values for the NLR-1 and NLR-7301 airfoils are almost identical. In contrast, the static and unsteady stall-onset results for these two very different profiles are considerably different and represent the lower and upper bounds, respectively, of all the airfoils tested.

In view of the aforementioned scatter in the static results from different wind tunnels, it is logical to inquire how different sets of dynamic data might compare. Because of the large number of parameters that affect dynamic stall and the tendency for past investigators to select different combinations of these parameters, the possibilities for direct comparison of unsteady results are much more limited. However, some examples are given below.

NACA 0012 airfoil- The first comparison for this profile is shown in figures 34 and 35, where data from reference 3 were obtained in the same wind tunnel as the present results, but with a model whose chord was twice as large. Figure 34 shows that the large values of  $C_{L_{max}}$  reported in reference 3 were not realized in the present experiment. Figure 35 shows  $C_L$  versus  $\alpha$ , where the two results are seen to differ by approximately 10% during the portion of the cycle when  $\alpha$  is increasing but before dynamic stall begins. This is approximately the same as the difference in the lift-curve slopes for the corresponding static data, and it is consistent with the differences that would be predicted for static wind-tunnel-wall corrections (ref. 12) for the two chord-to-height ratios. However, it can be inferred from the differences in the peaks of the lift curves in figure 35 that the organized vortex-shedding phenomenon was more pronounced on the larger model after stall began. Also, reattachment of the boundary layer on the downstroke occurred earlier. These do not seem to be solely Reynolds-number effects; rather, it is suspected that in the earlier tests there was excessive interference between the boundary layers on the upper and lower walls of the tunnel and the unsteady viscous flow on the ends of the vertically mounted airfoil.

St. Hilaire and Carta (ref. 17) have reported on dynamic-stall tests of the NACA 0012 airfoil at UTRC under conditions similar to those in the present experiment. Figure 36 compares some of the data from the two investigations. The format and choice of unsteady parameters is based on an extension of the observation in reference 2, that for sinusoidal pitching oscillations the values of  $\alpha_{max}$  and the product  $\alpha_1 k^2$  seem to be particularly important in determining the detailed time-history of the unsteady airloads during dynamic stall. In order to compare as many test points as possible, data were selected that satisfied the criterion  $0.0014 < \alpha_1 k^2 < 0.0022$ , where  $\alpha_1$  is in radians. The variations in  $C_{L_{max}}$  and  $C_{M_{min}}$  in figure 36 are seen to correlate reasonably well on this basis, and the results from the two sources are in fairly good agreement. Some of the  $C_{L_{max}}$  data from the UTRC wind tunnel are slightly higher than the present measurements.

SC-1095 airfoil- Gangwani (ref. 18) has reported data that were obtained on the SC-1095 section in the same facility that was used by St. Hilaire and Carta (ref. 17) to obtain the NACA 0012 data described in the preceding paragraph. The results are

compared with the present data in figure 37, following the same format as above. Fewer data points are available, but the degree of correlation is approximately comparable to that of the NACA 0012 results in figure 36. In contrast with that figure, however, the present values of  $C_{L_{max}}$  tend to be slightly higher than the UTRC data (ref. 18). In any case, the discrepancies generally appear to be within the measurement uncertainty, and the agreement is better than for the static results (fig. 27).

NLR-1 airfoil- This profile was tested by Dadone (ref. 19) over a wide range of Mach numbers, mean angles, and amplitudes. Based on the considerations outlined above regarding  $\alpha_{max}$  and  $\alpha_1 k^2$ , his results are compared with the present data in figure 38 as functions of  $\alpha_1 k^2$  at a constant value  $\alpha_{max} = 20^\circ$ , where  $\alpha_1$  is also in degrees. The lift data are in better agreement than in the previous examples, but more scatter appears in the pitching-moment results than before.

No unsteady results from other sources are presently available from other sources for comparison with the data obtained on the Wortmann FX-098, Ames A-01, Hughes HH-02, Vertol VR-7, and NLR 7301 airfoils.

#### Comments on Wind-Tunnel Effects

It is well known that testing the same airfoil in different wind tunnels often gives different results, especially for the static-stall characteristics. This is borne out in figures 24-31. In fact, if the results from these eight figures were overlaid, the real differences between the individual airfoils would be almost completely obscured by the differences attributable to the test facilities.

Although more limited in scope, the comparisons of dynamic-stall data shown in figures 36-38 are more encouraging than the static results. Since all of these data came from tests with either high aspect-ratio models or sidewall boundary-layer control, this suggests that the present dynamic data may be relatively free of wind-tunnel-wall contamination and other three-dimensional effects. A detailed examination of the complete time-histories of the unsteady airloads and further studies on models of various aspect ratios would be required to confirm this speculation.

A special feature of the present experiment is that a large number of airfoils were studied over a wide range of unsteady flow conditions in the same facility. This provides the basis for meaningful comparisons, even though wind-tunnel interference effects were not completely negligible. However, as stated in reference 1, it is recommended that the wind-tunnel walls be included or considered in any quantitative uses of the data.

#### 5. SUMMARY AND CONCLUSIONS

A large amount of steady and unsteady data has been obtained on eight airfoil sections over a wide range of test conditions, at Mach numbers up to 0.30. The details of the experimental arrangements, estimates of the measurement accuracy, and the test conditions are described in this volume. Some comparisons are also made with data from other sources. Volume 2 (Pressure and Force Data) presents the results in graphical form and describes the digital computer tapes that contain the extensive numerical data. Volume 3 (Hot-Wire and Hot-Film Measurements) describes the boundary-layer studies performed with surface-mounted hot wires and hot films.



The results of the experiment show important differences between airfoils, differences that would otherwise tend to be masked by differences in wind tunnels, particularly in steady cases. All of the airfoils tested offer significant advantages over the standard NACA 0012 profile. In general, however, the parameters of the unsteady motion appear to be more important than airfoil shape in determining the dynamic-stall airloads.

#### REFERENCES

1. McCroskey, W. J.; and Pucci, S. L.: Viscous-Inviscid Interaction on Oscillating Airfoils in Subsonic Flow. AIAA J., vol. 20, no. 2, Feb. 1982, pp. 167-174.
2. McCroskey, W. J.; McAlister, K. W.; et al.: Dynamic Stall on Advanced Airfoil Sections. J. American Helicopter Soc., vol. 26, no. 3, July 1981, pp. 40-50.
3. McAlister, K. W.; Carr, L. W.; and McCroskey, W. J.: Dynamic Stall Experiments on the NACA 0012 Airfoil. NASA TP-1100, 1978.
4. Carr, L. W.; McAlister, K. W.; and McCroskey, W. J.: Analysis of the Development of Dynamic Stall Based on Oscillating Airfoil Experiments. NASA TN D-8382, 1977.
5. Dadone, L. U.: U.S. Army Helicopter Design Datcom. Vol. I - Airfoils. NASA CR-153247, 1976.
6. Hicks, R. M.; and McCroskey, W. J.: An Experimental Evaluation of a Helicopter Rotor Section Design by Numerical Optimization. NASA TM-78622, 1980.
7. Balch, D. T.: Helicopter Blade. U.S. Patent 3,728,045, 1973.
8. Kemp, L. D.: An Analytical Study for the Design of Advanced Rotor Airfoils. NASA CR-112297, 1973.
9. Barche, J., ed.: Experimental Data Base for Computer Program Assessment. AGARD Advisory Report 138, Advisory Group for Aerospace Research and Development, Neuilly-sur-Seine, France, 1979.
10. Carr, L. W.; and McCroskey, W. J.: A Directionally Sensitive Hot-Wire Probe for Detection of Flow Reversal in Highly Unsteady Flows. International Congress on Instrumentation in Aerospace Facilities, 1979 Record, Sept. 1979, pp. 154-162.
11. McCroskey, W. J.; McAlister, K. W.; and Carr, L. W.: Dynamic Stall Experiments on Oscillating Airfoils. AIAA J., vol. 14, no. 1, Jan. 1976, pp. 57-63.
12. Allen, H. J.; and Vincenti, W. G.: Wall Interference in a Two-Dimensional Flow Wind Tunnel with Consideration of the Effect of Compressibility. NACA Report 782, 1944.
13. Woodward, D. S.: The Twodimensional Characteristics of a 12.2% Thick R.A.E. Aerofoil Section. RAE Technical Report 68303, Royal Aircraft Establishment, Farnborough Hants, England, Jan. 1969.
14. Fromme, J. A.; and Golberg, M. A.: Unsteady Two-Dimensional Airloads Acting on Oscillating Airfoils in Subsonic Ventilated Wind Tunnels. NASA CR-2914, 1977.
15. Noonan, K. W.; and Bingham, G. J.: Aerodynamic Characteristics of Three Helicopter Rotor Airfoil Sections at Reynolds Numbers from Model Scale to Full Scale at Mach Numbers from 0.35 to 0.90. NASA TP-1701, 1980.

16. Jepson, W. D.: Two Dimensional Test of Four Airfoil Configurations with an Aspect Ratio of 7.5 and a 16 Inch Chord up to a Mach Number of 1.1. Report SER-50977, Sikorsky Aircraft, Stratford, Conn., Apr. 1977.
17. St. Hilaire, A. L.; and Carta, F. O.: The Influence of Sweep on the Aerodynamic Loading of an Oscillating NACA 0012 Airfoil. Vol. II - Data Report. NASA CR-145350, 1979.
18. Gangwani, S. T.: Prediction of Dynamic Stall and Unsteady Airloads for Rotor Blades. American Helicopter Society Paper 81-01, May 1981.
19. Dadone, L. U.: Two-Dimensional Wind Tunnel Test of an Oscillating Rotor Airfoil. NASA CR-2915, 1977.
20. Lizak, A. A.: Two-Dimensional Wind Tunnel Tests of an H-34 Main Rotor Airfoil Section. TREC Technical Report 60-53, U.S. Army Transportation Research Command, Ft. Eustis, VA, 1960.
21. Prouty, R. W.: A State-of-the-Art Survey of Two-Dimensional Airfoil Data. J. American Helicopter Soc., vol. 20, no. 4, Oct. 1975, pp. 14-25.
22. Bevert, A.: Essais Comparatifs en Courant Plan des Profils "G.1" et NACA 0012. ONERA Doc. No. 76/1157.AN, Office National d'Etudes et de Recherches Aérospatiales, Châtillon, France, Mar. 1970.
23. Harris, C. D.: Two-Dimensional Aerodynamic Characteristics of the NACA 0012 Airfoil in the Langley 8-Foot Transonic Pressure Tunnel. NASA TM-81927, 1981.
24. Noonan, K. W.; and Bingham, G. J.: Two-Dimensional Aerodynamic Characteristics of Several Rotorcraft Airfoils at Mach Numbers from 0.35 to 0.90. NASA TM X-73990, Jan. 1977.
25. Bingham, G. J.; and Noonan, K. W.: Low-Speed Aerodynamic Characteristics of Five Helicopter Blade Sections at Reynolds Numbers from  $2.4 \times 10^5$  to  $8.4 \times 10^6$ . NASA TM X-2467, 1972.
26. Wortmann, F. X.: Design of Airfoils with High Lift at Low and Medium Subsonic Mach Numbers. Paper No. 7, AGARD Conference Proceedings CP-102, Advisory Group for Aerospace Research and Development, Neuilly-sur-Seine, France, 1972.
27. Prouty, R. W.: Airfoil Section Data Report. Report No. 150-A-1012, Hughes Helicopters, Culver City, Calif., Mar. 1978.
28. Coulomb, J.: Caractéristiques Stationnaires du Profil VR 7. Procès-verbal No. 102 B/SC, Centre d'Essais Aéronautique de Toulouse, Toulouse, France, June 1979.
29. Bingham, G. J.; Noonan, K. W.; and Jones, H. E.: Results of an Investigation of Several New Rotorcraft Airfoils as Related to Airfoil Requirements. Paper No. 8, NASA Conference Publication 2046, Mar. 1978.

30. Joosen, C. J. J.; and Kho, C. G.: Two Dimensional Low-Speed Wind Tunnel Investigation on a NLR 73-108-10 Airfoil with Fowler Type Flap, Part 1: Text, Tables, and Figures. NLR TR 74058 C, National Lucht- en Ruimtevaartlaboratorium, Amsterdam, The Netherlands, Sept. 1975.

TABLE 1.- HARMONIC COEFFICIENTS  
OF THE OSCILLATION MECHANISM

$$\alpha = \alpha_0 + \alpha_1 \sin \omega t + \alpha_2 \sin(\omega t + \phi_2)$$

$\alpha_0$	Nominal $\alpha_1$	$\alpha_1$	$\alpha_2$	$\phi_2$
5	5	5.00	0.05	(a)
10	5	4.90	.05	(a)
0	10	10.20	.20	(a)
5	10	10.05	.20	(a)
10	10	9.90	.20	260°
15	10	9.90	.20	(a)
15	14	14.10	.38	200°

<sup>a</sup>Not measured.

TABLE 2. - AIRFOIL COORDINATES: NACA 0012 AND AMES A-01 AIRFOILS

x/c	NACA 0012, y/c		AMES A-01, y/c	
	upper	lower	upper	lower
0.0000	0.00000	0.00000	0.00000	0.00000
0.0005	0.00395	-0.00395	0.00377	-0.00338
0.0010	0.00556	-0.00556	0.00541	-0.00472
0.0020	0.00781	-0.00781	0.00766	-0.00651
0.0035	0.01027	-0.01027	0.01013	-0.00844
0.0050	0.01221	-0.01221	0.01214	-0.00994
0.0065	0.01386	-0.01386	0.01388	-0.01120
0.0080	0.01531	-0.01531	0.01543	-0.01227
0.0100	0.01704	-0.01704	0.01732	-0.01350
0.0125	0.01894	-0.01894	0.01945	-0.01481
0.0160	0.02127	-0.02127	0.02214	-0.01634
0.0200	0.02360	-0.02360	0.02490	-0.01777
0.0250	0.02615	-0.02615	0.02801	-0.01922
0.0350	0.03043	-0.03043	0.03335	-0.02137
0.0500	0.03555	-0.03555	0.03991	-0.02365
0.0650	0.03966	-0.03966	0.04523	-0.02549
0.0800	0.04307	-0.04307	0.04961	-0.02710
0.1000	0.04683	-0.04683	0.05421	-0.02902
0.1250	0.05055	-0.05055	0.05829	-0.03104
0.1500	0.05345	-0.05345	0.06098	-0.03277
0.2000	0.05737	-0.05737	0.06344	-0.03551
0.2500	0.05941	-0.05941	0.06431	-0.03727
0.3000	0.06002	-0.06002	0.06446	-0.03828
0.3500	0.05949	-0.05949	0.06409	-0.03866
0.4000	0.05803	-0.05803	0.06316	-0.03848
0.4500	0.05581	-0.05581	0.06154	-0.03782
0.5000	0.05294	-0.05294	0.05924	-0.03665
0.5500	0.04952	-0.04952	0.05623	-0.03501
0.6000	0.04563	-0.04563	0.05249	-0.03297
0.6500	0.04132	-0.04132	0.04792	-0.03056
0.7000	0.03664	-0.03664	0.04246	-0.02785
0.7500	0.03160	-0.03160	0.03600	-0.02486
0.8000	0.02623	-0.02623	0.02860	-0.02153
0.8500	0.02053	-0.02053	0.02064	-0.01786
0.9000	0.01448	-0.01448	0.01260	-0.01374
0.9250	0.01132	-0.01132	0.00899	-0.01144
0.9500	0.00807	-0.00807	0.00598	-0.00888
0.9750	0.00472	-0.00472	0.00392	-0.00603
0.9900	0.00265	-0.00265	0.00322	-0.00421
1.0000	0.00126	-0.00126	0.00299	-0.00300
	$r_o/c = 0.0158$		$r_o/c = 0.012$	

TABLE 3. - AIRFOIL COORDINATES: WORTMANN FX-098 AND SIKORSKY SC-1095 AIRFOILS

x/c	WORTMANN FX-098, y/c		SIKORSKY SC-1095, y/c	
	upper	lower	upper	lower
0.0000	0.00000	0.00000	0.00000	0.00000
0.0005	0.00293	-0.00249	0.00307	-0.00257
0.0010	0.00426	-0.00343	0.00443	-0.00368
0.0020	0.00619	-0.00471	0.00640	-0.00535
0.0035	0.00837	-0.00609	0.00865	-0.00724
0.0050	0.01017	-0.00717	0.01054	-0.00880
0.0065	0.01175	-0.00807	0.01221	-0.01016
0.0080	0.01319	-0.00886	0.01374	-0.01138
0.0100	0.01494	-0.00978	0.01560	-0.01285
0.0125	0.01692	-0.01079	0.01771	-0.01450
0.0160	0.01944	-0.01202	0.02041	-0.01657
0.0200	0.02204	-0.01321	0.02320	-0.01865
0.0250	0.02501	-0.01451	0.02635	-0.02092
0.0350	0.03021	-0.01664	0.03140	-0.02454
0.0500	0.03681	-0.01913	0.03677	-0.02842
0.0650	0.04234	-0.02111	0.04070	-0.03108
0.0800	0.04705	-0.02277	0.04374	-0.03295
0.1000	0.05222	-0.02464	0.04680	-0.03464
0.1250	0.05714	-0.02658	0.04963	-0.03619
0.1500	0.06073	-0.02819	0.05174	-0.03739
0.2000	0.06491	-0.03059	0.05447	-0.03884
0.2500	0.06650	-0.03198	0.05548	-0.03933
0.3000	0.06630	-0.03251	0.05524	-0.03918
0.3500	0.06515	-0.03242	0.05437	-0.03858
0.4000	0.06336	-0.03184	0.05299	-0.03760
0.4500	0.06097	-0.03096	0.05105	-0.03622
0.5000	0.05798	-0.02982	0.04854	-0.03446
0.5500	0.05445	-0.02843	0.04555	-0.03234
0.6000	0.05040	-0.02678	0.04212	-0.02985
0.6500	0.04586	-0.02487	0.03819	-0.02702
0.7000	0.04085	-0.02273	0.03375	-0.02384
0.7500	0.03543	-0.02034	0.02887	-0.02034
0.8000	0.02962	-0.01768	0.02362	-0.01658
0.8500	0.02337	-0.01473	0.01808	-0.01265
0.9000	0.01642	-0.01134	0.01235	-0.00865
0.9250	0.01253	-0.00932	0.00943	-0.00664
0.9500	0.00856	-0.00702	0.00642	-0.00454
0.9750	0.00476	-0.00423	0.00328	-0.00233
0.9900	0.00255	-0.00237	0.00132	-0.00093
1.0000	0.00110	-0.00110	0.00000	0.00000
	$r_o/c = 0.007$		$r_o/c = 0.008$	

TABLE 4. - AIRFOIL COORDINATES: HUGHES HH-02 (-5° TAB) AND VERTOL VR-7 (-3° TAB) AIRFOILS

x/c	HUGHES HH-02, y/c		VERTOL VR-7, y/c	
	upper	lower	upper	lower
0.0000	0.00000	0.00000	0.00000	0.00000
0.0005	0.00283	-0.00284	0.00337	-0.00330
0.0010	0.00405	-0.00388	0.00483	-0.00460
0.0020	0.00594	-0.00532	0.00696	-0.00633
0.0035	0.00819	-0.00683	0.00943	-0.00800
0.0050	0.01009	-0.00800	0.01149	-0.00919
0.0065	0.01176	-0.00895	0.01330	-0.01010
0.0080	0.01327	-0.00978	0.01494	-0.01086
0.0100	0.01510	-0.01072	0.01695	-0.01172
0.0125	0.01717	-0.01172	0.01923	-0.01263
0.0160	0.01975	-0.01290	0.02213	-0.01367
0.0200	0.02237	-0.01404	0.02512	-0.01467
0.0250	0.02531	-0.01524	0.02846	-0.01575
0.0350	0.03029	-0.01714	0.03423	-0.01751
0.0500	0.03640	-0.01943	0.04144	-0.01966
0.0650	0.04137	-0.02127	0.04759	-0.02154
0.0800	0.04553	-0.02276	0.05299	-0.02320
0.1000	0.05012	-0.02432	0.05922	-0.02516
0.1250	0.05468	-0.02575	0.06565	-0.02709
0.1500	0.05828	-0.02675	0.07091	-0.02855
0.2000	0.06328	-0.02793	0.07887	-0.03055
0.2500	0.06608	-0.02843	0.08378	-0.03186
0.3000	0.06738	-0.02834	0.08592	-0.03273
0.3500	0.06750	-0.02755	0.08574	-0.03308
0.4000	0.06640	-0.02600	0.08365	-0.03271
0.4500	0.06391	-0.02377	0.07984	-0.03148
0.5000	0.06008	-0.02104	0.07451	-0.02952
0.5500	0.05504	-0.01797	0.06781	-0.02712
0.6000	0.04891	-0.01482	0.05996	-0.02464
0.6500	0.04174	-0.01176	0.05171	-0.02207
0.7000	0.03344	-0.00952	0.04322	-0.01929
0.7500	0.02403	-0.00851	0.03442	-0.01639
0.8000	0.01436	-0.00889	0.02527	-0.01346
0.8500	0.00481	-0.00984	0.01575	-0.01050
0.9000	-0.00431	-0.01041	0.00558	-0.00744
0.9250	-0.00394	-0.00777	0.00117	-0.00609
0.9500	-0.00203	-0.00583	-0.00016	-0.00512
0.9750	-0.00006	-0.00387	0.00115	-0.00380
0.9900	0.00112	-0.00269	0.00194	-0.00300
1.0000	0.00190	-0.00190	0.00247	-0.00247
	$r_o/c = 0.008$		$r_o/c = 0.011$	



TABLE 5. - AIRFOIL COORDINATES: NLR-1 AND NLR-7301 AIRFOILS

x/c	NLR-1, y/c		NLR-7301, y/c	
	upper	lower	upper	lower
0.0000	0.00000	0.00000	0.00000	0.00000
0.0005	0.00359	-0.00288	0.00730	-0.00748
0.0010	0.00499	-0.00388	0.01051	-0.01020
0.0020	0.00687	-0.00518	0.01518	-0.01373
0.0035	0.00890	-0.00643	0.02030	-0.01735
0.0050	0.01053	-0.00730	0.02424	-0.02016
0.0065	0.01194	-0.00799	0.02756	-0.02252
0.0080	0.01321	-0.00858	0.03043	-0.02455
0.0100	0.01475	-0.00929	0.03375	-0.02688
0.0125	0.01648	-0.01006	0.03729	-0.02935
0.0160	0.01868	-0.01101	0.04140	-0.03225
0.0200	0.02097	-0.01196	0.04514	-0.03502
0.0250	0.02358	-0.01301	0.04873	-0.03794
0.0350	0.02799	-0.01477	0.05372	-0.04264
0.0500	0.03328	-0.01688	0.05920	-0.04806
0.0650	0.03750	-0.01859	0.06321	-0.05229
0.0800	0.04093	-0.02007	0.06636	-0.05576
0.1000	0.04435	-0.02179	0.06985	-0.05962
0.1250	0.04701	-0.02363	0.07347	-0.06358
0.1500	0.04905	-0.02522	0.07648	-0.06689
0.2000	0.05200	-0.02775	0.08115	-0.07194
0.2500	0.05386	-0.02958	0.08441	-0.07527
0.3000	0.05489	-0.03082	0.08649	-0.07713
0.3500	0.05528	-0.03154	0.08755	-0.07763
0.4000	0.05511	-0.03185	0.08764	-0.07672
0.4500	0.05443	-0.03176	0.08678	-0.07412
0.5000	0.05327	-0.03126	0.08495	-0.06934
0.5500	0.05164	-0.03025	0.08206	-0.06237
0.6000	0.04948	-0.02882	0.07789	-0.05386
0.6500	0.04677	-0.02707	0.07212	-0.04397
0.7000	0.04348	-0.02503	0.06458	-0.03316
0.7500	0.03892	-0.02276	0.05551	-0.02227
0.8000	0.03172	-0.02028	0.04523	-0.01221
0.8500	0.02368	-0.01756	0.03415	-0.00409
0.9000	0.01562	-0.01427	0.02269	0.00108
0.9250	0.01179	-0.01199	0.01696	0.00228
0.9500	0.00811	-0.00903	0.01129	0.00246
0.9750	0.00454	-0.00511	0.00577	0.00153
0.9900	0.00244	-0.00253	0.00258	0.00042
1.0000	0.00103	-0.00103	0.00055	-0.00055
	$r_o/c = 0.007$		$r_o/c = 0.055$	

TABLE 6.- TRANSDUCER LOCATIONS ON THE AIRFOILS

Transducer Number <sup>a</sup>	Nominal <sup>b</sup> x/c		Actual pressure transducer location									
	Pressure	Hot wire	0012	A-01	FX-098	SC-1095	VR-7	NLR-1	NLR-7301	HH-02		
1 LE	0.		0.	0.	0.0002U	0.	0.	0.	0.0015U	0.		
2 U	.005 (.004)		.0060	.0054	.0038	.0040	.0044	.0054	.0101	.0050		
3	.010 (.010)		.0103	.010	.0067	.0110	.0083	.0108	.0165	.0087		
4	.025 (.030)	0.025 (.025)	.0242	.024	.0196	.0275	.0225	.028	.0335	.0326		
5	.050 (.06)		.052	.050	.051	.053	.050	.051	.0512	.0581		
6	.100 (.12)	.10 (.12)	.102	.100	.101	.1025	.100	.101	.102	.1167		
7	.175 (.18)		.176	.175	.177	.178	.175	.177	.177	.183		
8	.25 (.25)		.252	.250	.252	.252	.250	.250	.252	.250		
9	.325 (.32)		.326	.325	.326	.325	.325	.325	.326	.317		
10	.40 (.38)	.40 (.38)	.40	.40	.40	.40	.40	.40	.40	.383		
11	.50 (.48)		.50	.50	.50	.50	.50	.50	.50	.472		
12	.60 (.56)	.60 (.56)	.60	.60	.60	.60	.60	.60	.60	.561		
13	.70 (.65)		.70	.70	.70	.70	.70	.70	.70	.650		
14	.80 (.74)	.80 (.74)	.80	.80	.80	.80	.80	.80	.80	.739		
15	.90 (.84)		.899	.90	.90	.90	.90	.90	.90	.840		
16 U	.98 (.93)		.98	.98	.98	.98	.98	.98	.98	.925		
17 L	.98 (.93)		.979	.98	.98	.98	.98	.98	.98	.925		
18	.90 (.84)		.90	.90	.90	.90	.90	.90	.90	.840		
19	.70 (.65)		.70	.70	.70	.70	.70	.70	.70	.650		
20	.50 (.48)		.50	.50	.50	.50	.50	.50	.50	.472		
21	.30 (.29)		.30	.30	.30	.30	.30	.30	.30	.294		
22	.15 (.16)		.153	.150	.153	.150	.150	.150	.155	.161		
23	.05 (.072)		.0504	.050	.051	.052	.050	.051	.0517	.0730		
24	.025 (.030)		.023	.026	.027	.028	.0246	.0220	.0194	.0293		
25	.010 (.010)		.0093	.0130	.0125	.009	.0094	.0108	.0051	.0081		
26 L	.005 (.004)		.0049	.0073	.0061	.005	.0040	.0062	.0021	.0044		

<sup>a</sup>LE = leading edge; U = upper surface; L = lower surface.

<sup>b</sup>Locations for HH-02, for which c = 68.6 cm, are shown in parentheses; for all other airfoils shown, c = 61.0 cm.

TABLE 7. - STATIC DRAG COEFFICIENTS AT M = 0.30 BASED ON WAKE SURVEYS

$\alpha$ , deg	N-0012	AMES-01	W-098	SC-1095	HH-02	VR-7	NLR-1	NLR-7301
-5.0	0.00843	0.00851	0.00886	0.00739	0.00846	0.00899	0.02602	0.00952
-2.0	0.00729	0.00832	0.00771	0.00713	0.00719	0.00759	0.00743	0.00780
0.0	0.00711	0.00794	0.00683	0.00708	0.00679	0.00723	0.00710	0.00968
2.0	0.00718	0.00662	0.00664	0.00670	0.00655	0.00707	0.00745	0.00891
5.0	0.00865	0.00767	0.00755	0.00807	0.00816	0.00800	0.00831	0.01011
8.0	0.01031	0.00965	0.01142	0.01013	0.01112	0.01059	0.01086	0.01305
10.0	0.01190	0.01248	0.01405	0.01127	0.01382	0.01353	0.01322	0.01569
12.0	0.01711	0.01600	0.01773	0.01586	0.01849	0.02156	0.02006	0.02022
13.0	--	--	--	0.02015	0.02236	--	--	--
14.0	0.02901	--	0.08922	--	--	--	--	--
-4.0	--	--	--	--	--	--	0.00773	0.00843
-1.75	--	--	--	--	--	--	--	0.00874
-1.0	--	--	--	--	--	--	--	0.00962
1.0	--	0.00738	--	--	--	--	--	0.00973
1.5	--	--	--	--	--	--	--	0.00910
2.5	--	--	--	--	--	--	--	0.00896
3.0	--	0.00702	--	--	--	--	--	--
4.0	--	0.00712	--	--	--	--	--	--
6.0	--	0.00791	--	--	--	--	--	--
9.9	--	0.01218	--	--	--	--	--	--

TABLE 8.- SUMMARY OF THE MEASURED STATIC AIRFOIL CHARACTERISTICS AT  $M_\infty = 0.30$ , INCLUDING WIND TUNNEL WALL CORRECTIONS

Airfoil	$C_{L\alpha}$	$\alpha_o$	$C_{M_o}$	$C_{D_{min}}$	$X_{a.c.}$	$C_{L_{max}}$	$\alpha_{ss}$	$(L/D)_{max}$
NACA 0012	0.109	-0.1°	-0.007	0.0072	0.24	1.33	13.7°	90
Ames-01	.111	-.6	-.005	.0070	.25	1.45	13.6	100
FX-098	.109	-1.3	-.026	.0066	.24	1.43	13.1	94
SC-1095	(.110) <sup>a</sup>	-.9	-.027	.0073	.245	(1.46) <sup>a</sup>	13.5	(98) <sup>a</sup>
HH-02	.114	-.6	-.002	.0066	.255	1.42	13.2	92
VR-7	.117	-1.6	-.016	.0071	.26	1.51	12.6	107
NLR-1	.102	-1.0	-.025	.0071	.22	1.29	12.4	87
NLR-7301	.117	-1.9	-.083	.0078	.25	(1.83) <sup>a</sup>	(17.2) <sup>a</sup>	89
Nominal uncertainty	±.003	.2	.005	.0005	.005	.03	.3	5

<sup>a</sup>Uncertainty larger than nominal value in table.

TABLE 9.- LIST OF TEST POINTS WITH UNUSUAL ZERO DRIFT OF PRESSURE TRANSDUCERS

Airfoil	Frame	M <sub>∞</sub>	Type <sup>a</sup>	Problem transducers	Airfoil	Frame	M <sub>∞</sub>	Type <sup>a</sup>	Problem transducers	
NACA 0012	8019	0.035	U	All	Wortmann FX-098	18414	.11	S	20,22	
	8021					19401	.25		2,3,4	
	8023					19402	.25			
	8102					19405	.25			
	8104					19406	.25			
	8106					20103	.25		2,3	
	8114	.07		23		20104	.25			
	8116	.07		23		20122	.30			
	8118	.07		23		20123	.30			
	8210	.11		4		20203	.30			
	12118	.26	Q.S.	3		20204	.30			
	13107	.11		1,4,20		Sikorsky SC-1095	33022	.07	U	1,17,18,25
	13115	.07		Many			33106	.11	U	Many
	13120	.07		1,3,4,18, 24,26			33110	.11	U	Many
	13205	.035		Many			34409	.29	U	2,3
	13217	.035		Many			35021	.30	S	11
	14104	.18	U	3,8			35023	.30		11
	14106	.18	U	3,8			35100	.30		11
	14108	.18	U	3,8			35102	.30		11
	Ames A-01	26306	.30	S			2,3	35103	.30	
26307		.30		2,3	36209		.11		1,20,22	
28019		.11		1,20	36210		.11		1,20,22	
28021				1,20	35211		.11		1,20,22	
28023				1,20	35212		.11		1,20,22	
28101				1,20	35213		.11		1,20,22	
28106				All	Hughes HH-02		42309	.22	U	6
28107						42313	.25		6	
28109						43308	.30		13	
28110						43309	.30		13	
28115						Vertol VR-7	47213	.18		1,4,24
28116							47217	.22		1,4,24
28117					47301		.25		3,24	
28119					47305		.28		3,24	
28120					NLR-1		62020	.07		1,16,18
29317	.035	U	5,12,14,23	63018		.30		2		
Wortmann FX-098	16019	.035	U	Many		63019	.30		2	
	16200	.18	U	4,11		63020	.30		2	
	17220	.30	U	2		63021	.30		2	
	18102	.18	S	2,3,4		65207	.20		2,3,4	
	18106	.18		2,3,4		65209	.30		2,3,4	
	18108	.18		2,3,4	NLR-7301	66616	.11	S	Many	
	18410	.11		20,22		66617	.11	S	Many	
	18411	.11		20,22						
	18413	.11		20,22						

<sup>a</sup>S = steady; U = unsteady; Q = quasi-steady, k ≤ 0.002.

TABLE 10.- COEFFICIENTS OF LINEAR CURVE-FIT OF STATIC LIFT DATA  
WITHOUT WIND-TUNNEL CORRECTIONS

$$C_L = A + \frac{B\alpha}{\sqrt{1 - M_\infty^2}}$$

Airfoil	A = C <sub>L</sub> (0)	B = βC <sub>Lα</sub>
NACA 0012	0	0.110
Ames 01	.15	.108
Wortmann FX-098	.07	.111
Sikorsky SC-1095	.11	.110
Hughes HH-02	.07	.116
Vertol VR-7	.19	.117
NLR-1	.11	.102
NLR-7301	.24	.116

TABLE 11.- LIST OF DATA FRAMES

(a) NACA 0012 airfoil.

A										B										
FRAME	TRIP	TYPE	A0	A1	Q	M	RE	K	FREQ	FRAME	TRIP	TYPE	A0	A1	Q	M	RE	K	FREQ	FRAME
4019	N	ST	-5.0	0.0	875	301	3957803	0.0000	0.00	4020	N	US	9.0	5.0	878	301	3909814	0.1496	8.10	7102
4100	N	ST	-2.0	0.0	877	301	3932537	0.0000	0.00	4101	N	US	9.0	5.0	878	301	3901884	0.0249	1.35	7105
4102	N	ST	2.0	0.0	877	301	3923848	0.0000	0.00	4103	N	US	8.0	5.0	878	301	3920784	0.0350	1.35	
4109	N	ST	4.0	0.0	885	299	39110221	0.0000	0.00	4110	N	US	8.0	5.0	878	301	3923187	0.0997	5.40	
4111	N	ST	4.0	0.0	877	302	3931136	0.0000	0.00	4112	N	US	8.0	5.0	877	301	3924727	0.0997	10.80	
4113	N	ST	8.0	0.0	877	302	3989235	0.0000	0.00	4114	N	US	10.0	5.0	877	301	3937891	0.0252	1.37	
4119	N	ST	10.0	0.0	877	301	3900522	0.0000	0.00	4120	N	US	10.0	5.0	877	301	3872995	0.0994	5.40	
4123	N	ST	13.0	0.0	877	302	3876047	0.0000	0.00	4200	N	US	11.0	5.0	878	301	3891815	0.0249	1.35	
4201	N	ST	13.5	0.0	874	302	3970568	0.0000	0.00	4202	N	US	11.0	5.0	878	301	3875085	0.0437	2.70	
4203	N	ST	14.0	0.0	877	302	3867132	0.0000	0.00	4204	N	US	11.0	5.0	877	301	3865664	0.0933	5.40	
4209	N	ST	14.5	0.0	868	305	3861326	0.0000	0.00	4210	N	US	11.0	5.0	877	301	3860258	0.1488	8.10	
4211	N	ST	15.0	0.0	877	302	3822671	0.0000	0.00	4212	N	US	11.0	5.0	878	301	3852461	0.1983	10.80	
4213	N	ST	15.0	0.0	877	302	3643407	0.0000	0.00	4214	N	US	12.0	5.0	878	301	3876632	0.0249	1.35	
4215	N	ST	15.0	0.0	878	284	3628769	0.0000	0.00	4216	N	US	12.0	5.0	877	302	3853339	0.0991	5.40	
4217	N	ST	16.0	0.0	888	266	3398340	0.0000	0.00	4218	N	US	12.0	5.0	877	302	3845471	0.1981	10.80	
4219	N	ST	17.8	0.0	717	271	3462550	0.0000	0.00	4220	N	US	8.8	5.0	877	302	3844684	0.1488	8.10	
4301	N	ST	20.0	0.0	700	266	3485278	0.0000	0.00	4302	N	US	8.8	5.0	877	302	3859691	0.0992	5.40	
4401	N	ST	11.0	0.0	877	302	3795037	0.0000	0.00	4402	N	US	8.8	5.0	877	302	3856685	0.0496	2.70	
4403	N	ST	11.0	0.0	877	302	3783629	0.0000	0.00	7300	N	US	10.0	5.0	877	300	3986300	0.1513	8.10	
4404	N	ST	8.0	0.0	877	302	37801176	0.0000	0.00	7302	N	US	10.0	5.0	877	300	3957627	0.0745	8.10	
4405	N	ST	8.0	0.0	877	302	3781319	0.0000	0.00	7305	N	US	12.0	5.0	877	300	3966326	0.1510	8.10	
4410	N	ST	2.0	0.0	877	302	3787016	0.0000	0.00	8019	N	US	10.0	10.0	0.13	0.35	468697	0.1038	6.6	
4411	N	ST	2.0	0.0	877	302	3781623	0.0000	0.00	8021	N	US	10.0	10.0	0.13	0.35	486001	0.1515	9.7	
4412	N	ST	-2.0	0.0	877	302	3778643	0.0000	0.00	8023	N	US	10.0	10.0	0.13	0.35	485755	0.2529	1.62	
11018	N	ST	-5.0	0.0	875	302	3989932	0.0000	0.00	8102	N	US	15.0	10.0	0.13	0.36	485630	0.1032	6.6	
11019	N	ST	-2.0	0.0	875	301	3989948	0.0000	0.00	8104	N	US	15.0	10.0	0.13	0.36	484039	0.1529	9.8	
11020	N	ST	2.0	0.0	875	302	3978039	0.0000	0.00	8106	N	US	15.0	14.0	0.13	0.36	483453	0.1039	6.7	
11101	N	ST	2.0	0.0	875	302	3974780	0.0000	0.00	8114	N	US	15.0	10.0	0.054	0.72	980395	0.0992	1.30	
11102	N	ST	4.0	0.0	875	301	3958641	0.0000	0.00	8116	N	US	15.0	10.0	0.054	0.72	979893	0.1487	1.95	
11105	N	ST	8.1	0.0	876	301	3939640	0.0000	0.00	8118	N	US	15.0	10.0	0.054	0.72	978493	0.2477	3.25	
11110	N	ST	10.0	0.0	875	301	3936424	0.0000	0.00	8123	N	US	15.0	14.0	0.054	0.72	980066	0.0991	1.30	
11111	N	ST	12.3	0.0	875	301	3921945	0.0000	0.00	8203	N	US	10.0	10.0	0.054	0.72	978307	0.2476	3.25	
11112	N	ST	13.4	0.0	875	301	3912483	0.0000	0.00	8210	N	US	10.0	10.0	0.122	1.09	1491495	0.2497	4.90	
11113	N	ST	13.8	0.0	875	301	3904607	0.0000	0.00	8214	N	US	15.0	10.0	0.122	1.09	1450389	0.0996	1.96	
11121	N	ST	14.6	0.0	875	302	3913072	0.0000	0.00	8218	N	US	15.0	10.0	0.339	1.84	2432854	0.0993	3.30	
11122	N	ST	15.0	0.0	867	304	3929975	0.0000	0.00	8222	N	US	15.0	10.0	0.339	1.84	2423357	0.1487	4.95	
11123	N	ST	15.0	0.0	811	289	3925323	0.0000	0.00	8306	N	US	15.0	14.0	0.339	1.84	2404523	0.0988	3.30	
11200	N	ST	15.0	0.0	811	289	3745403	0.0000	0.00	9022	N	US	15.0	6.0	0.339	1.84	2358259	0.2352	7.92	
11201	N	ST	16.0	0.0	811	290	3733698	0.0000	0.00	9101	N	US	15.0	5.0	0.339	1.84	2358520	0.2642	9.57	
11204	N	ST	17.0	0.0	841	295	3793167	0.0000	0.00	9106	N	US	10.0	10.0	0.339	1.84	2365336	0.2453	8.25	
11205	N	ST	17.9	0.0	803	288	3725491	0.0000	0.00	9110	N	US	8.0	10.0	0.339	1.84	2476299	0.1000	1.33	
11208	N	ST	20.0	0.0	764	280	3616412	0.0000	0.00	9112	N	US	8.0	10.0	0.341	1.84	2475104	0.0500	1.65	
11209	N	ST	24.9	0.0	610	249	3252565	0.0000	0.00	9118	N	US	8.0	10.0	0.339	1.84	2449160	0.1990	6.60	
11211	N	ST	30.0	0.0	561	239	3105558	0.0000	0.00	9202	N	US	15.0	10.0	0.479	2.20	2847551	0.0985	3.93	
11212	N	ST	25.0	0.0	619	251	3254780	0.0000	0.00	9203	N	US	15.0	10.0	0.479	2.20	3187113	0.0484	4.46	
11213	N	ST	20.0	0.0	725	273	3515071	0.0000	0.00	9208	N	US	15.0	10.0	0.610	2.49	3187113	0.0975	4.98	
11214	N	ST	18.0	0.0	764	280	3628495	0.0000	0.00	9210	N	US	15.0	10.0	0.762	2.80	3520275	0.0098	1.53	
11215	N	ST	16.0	0.0	875	302	3566108	0.0000	0.00	9213	N	US	15.0	10.0	0.842	2.95	3672459	0.0098	1.53	
11216	N	ST	15.0	0.0	875	302	3861556	0.0000	0.00	9213	N	US	15.0	10.0	0.831	2.94	3596380	0.0243	1.31	
11221	N	ST	14.0	0.0	869	301	3846733	0.0000	0.00	9214	N	US	15.0	10.0	0.821	2.92	3566725	0.0489	2.62	
11222	N	ST	13.1	0.0	875	302	3594818	0.0000	0.00	9217	N	US	15.0	10.0	0.812	2.90	3549571	0.0983	5.24	
11223	N	ST	11.0	0.0	875	302	3876254	0.0000	0.00	9218	N	US	15.0	10.0	0.773	2.83	3450727	0.1509	7.86	
11304	N	ST	8.0	0.0	875	302	3870718	0.0000	0.00	9221	N	US	10.0	10.0	0.876	3.02	3672528	0.0098	1.54	
11305	N	ST	5.0	0.0	875	302	3864492	0.0000	0.00	9222	N	US	10.0	10.0	0.876	3.02	3660134	0.0241	1.34	
11308	N	ST	2.0	0.0	875	302	386782	0.0000	0.00	9223	N	US	10.0	10.0	0.876	3.02	3652176	0.0481	2.68	
11309	N	ST	0.0	0.0	875	301	3873667	0.0000	0.00	9302	N	US	10.0	10.0	0.876	3.02	3659205	0.0963	5.36	
7019	N	US	9.0	5.0	878	297	3894008	0.0538	2.70	7020	N	US	12.0	10.0	0.877	3.02	3670847	0.1447	8.04	
7021	N	US	9.0	5.0	886	299	3962010	0.1004	5.40	7022	N	US	20.0	10.0	0.688	2.65	3769502	0.0976	5.36	
7023	N	US	9.0	5.0	886	299	3944777	0.2005	10.80	7100	N	US	12.0	8.0	0.877	3.02	3711352	0.0485	2.68	

TABLE 11.- Continued.

(a) Concluded.

A	FRAME	TRIP	TYPE	A0	A1	Q	M	RE	K	FREQ	B
10105	N	US	12.0	8.0	878	302	3694271	.0568			12023
10108	N	US	12.0	8.0	847	294	3635589	.1253			12105
10113	N	US	15.0	5.0	876	285	3866845	.0998			12112
10114	N	US	15.0	5.0	841	285	3801337	.0252			12121
10118	N	US	15.0	5.0	823	294	3748526	.1020			12121
10120	N	US	15.0	5.0	842	294	3785165	.1511			12306
10123	N	US	15.0	5.0	832	293	3758528	.2024			
10202	N	US	10.0	5.0	877	301	3658103	.0098			
10204	N	US	10.0	5.0	877	301	3647481	.0246			
10204	N	US	10.0	5.0	870	300	3826614	.0493			
10207	N	US	10.0	5.0	877	302	3834529	.0740			
10208	N	US	10.0	5.0	870	300	3859785	.0990			
10211	N	US	10.0	5.0	870	300	3863353	.1486			
10212	N	US	10.0	5.0	870	300	3850737	.1979			
10218	N	US	10.0	5.0	880	300	3933484	.0098			
10221	N	US	5.0	5.0	878	301	3925387	.0993			
10222	N	US	5.0	5.0	878	301	3912114	.1983			
10303	N	US	5.0	10.0	877	301	3910580	.0991			
10305	N	US	3.8	10.0	877	301	3911328	.0991			
10309	N	US	2.8	10.0	877	301	3896261	.0989			
12020	N	US	20.0	10.0	718	270	3490909	.0010			
12102	N	US	5.0	10.0	882	302	3820000	.0009			
12109	N	US	6.0	10.0	756	279	3455765	.0010			
12118	N	US	20.0	10.0	676	262	3246704	.0010			
12203	N	US	20.0	10.0	531	231	2887477	.0011			
12208	N	US	7.0	10.0	587	244	3269975	.0010			
12300	N	US	20.0	10.0	421	204	2706734	.0011			
12305	N	US	20.0	10.0	292	169	2252844	.0010			
12310	N	US	7.0	10.0	350	186	2469266	.0010			
13021	N	US	7.0	10.0	120	108	1502757	.0017			
13107	N	US	20.0	10.0	113	105	1421201	.0017			
13115	N	US	20.0	10.0	048	068	916563	.0027			
13120	N	US	5.0	10.0	053	072	962303	.0025			
13205	N	US	5.0	10.0	014	036	488772	.0026			
13217	N	US	20.0	10.0	013	036	485631	.0026			
13222	N	US	20.0	10.0	749	276	3456957	.0010			
13303	N	US	7.0	10.0	603	247	3298109	.0010			
13308	N	US	7.0	10.0	461	215	2884310	.0010			
13310	Y	US	7.0	10.0	466	216	2884723	.0010			
13313	Y	US	7.0	10.0	332	181	2404990	.0010			
13321	Y	US	7.0	10.0	839	294	3740954	.0009			
14019	Y	US	15.0	10.0	339	183	2453890	.0499			
14021	Y	US	15.0	10.0	336	182	2434182	.1001			
14023	Y	US	15.0	10.0	335	182	2426579	.1504			
14104	Y	US	15.0	10.0	338	183	2448651	.0499			
14106	Y	US	15.0	10.0	340	184	2449389	.0994			
14108	Y	US	15.0	10.0	339	183	2443079	.1493			
14117	Y	US	15.0	10.0	837	293	3843264	.0257			
14119	Y	US	15.0	10.0	836	293	3818332	.0509			
14200	Y	US	15.0	10.0	843	294	3822179	.0253			
14202	Y	US	15.0	10.0	839	293	3792702	.0506			
14208	Y	US	15.0	10.0	828	291	3764396	.1019			
14210	Y	US	15.0	10.0	832	292	3760353	.1014			
14218	N	US	15.0	10.0	820	292	3762798	.0254			
14219	N	US	15.0	10.0	824	291	3735990	.0509			
14220	N	US	15.0	10.0	805	287	3683317	.1031			
15218	N	US	15.0	10.0	818	290	3678973	.0994			
10117	N	US	15.0	5.0	843	295	3802563	.0504			
7202	N	US	12.0	5.0	877	302	3861194	.0496			
7222	N	US	10.0	5.0	876	298	3975490	.0509			





TABLE 11.- Continued.  
(b) Concluded.

FRAME	TRIP	TYPE	AO	A1	Q	H	RE	K	FREQ	B
25102	N	US	10	0	881	302	3831527	0489	2.68	29100
25104	N	US	10	0	880	302	3816708	.0978	5.36	25103
25109	N	US	10	0	879	302	3810775	1.468	8.04	25108
25117	N	US	10	0	884	303	3824075	.0242	1.34	25110
25118	N	US	10	0	879	302	3803407	.0489	2.68	
25119	N	US	10	0	883	303	3805390	.0975	5.36	
25121	N	US	10	0	881	302	3813088	1.465	8.04	
25122	N	US	10	0	884	303	3819823	1.462	8.04	
25123	N	US	10	0	885	303	3816827	1.947	10.72	
29023	Y	US	15	0	820	291	3637799	.0248	1.34	29100
29101	Y	US	15	0	805	288	3634654	.0500	2.62	29102
29106	Y	US	15	0	806	298	3646183	1.001	5.24	29107
29115	Y	US	15	0	340	194	2418131	.0494	1.65	29116
29117	Y	US	15	0	341	184	2418248	.0987	3.30	29118
29119	Y	US	15	0	341	184	2417060	1.481	4.95	29121
29205	N	US	5	0	876	301	3947215	.0098	5.3	29206
29207	N	US	5	0	877	301	3918856	.0496	2.68	29210
29211	N	US	5	0	877	301	3902857	.0991	5.36	29212
29213	N	US	5	0	879	301	3896095	1.483	8.04	29214
29215	N	US	5	0	879	301	3891313	1.481	8.04	
29223	N	US	13	5	876	301	3611877	1.965	10.72	29300
29304	N	US	14	5	870	300	3777473	1.967	10.72	29306
29309	N	US	16	5	852	296	3722411	1.986	10.72	29310
29317	N	US	15	0	013	035	473349	1.021	65	29318
30019	N	US	15	0	865	298	3856941	.0097	52	30021
30020	N	US	15	0	864	298	3828146	.0096	52	30021
30105	N	US	10	0	880	301	3844592	.0097	53	30106
30119	N	US	15	0	877	301	3817844	.0097	53	30111
30201	N	US	11	0	874	300	3819552	.0097	53	30120
30206	N	US	11	0	877	301	3814196	.0099	54	30202
30215	N	US	7	5	838	183	2415733	.0099	53	30208
31102	N	US	10	0	877	302	3680208	.0099	33	30216
31104	N	US	10	0	878	302	3659857	.0247	1.34	31103
31110	N	US	10	0	880	302	3841535	.0492	2.68	31105
31112	N	US	10	0	880	302	3841535	1.471	8.04	31111
31119	N	US	10	0	880	302	3832051	1.469	8.04	31111
31121	N	US	5	0	884	303	3856266	.0245	1.34	31120
31123	N	US	5	0	880	302	3826984	.0489	2.68	31122
31201	N	US	5	0	884	303	3823741	.0975	5.36	31200
31209	N	US	5	0	883	303	3816623	1.463	8.04	31202
31215	N	US	5	0	341	184	2421435	.0987	3.30	31210
31217	N	US	7	5	341	184	2425489	.0494	1.65	31216
31302	N	US	14	5	852	297	3765532	1.972	6.60	31218
31310	N	US	14	5	854	298	3731989	1.485	8.04	31304
25204	N	US	15	0	877	301	3973275	.0249	1.34	31312
25205	N	US	15	0	878	301	3952662	.0497	2.68	
25208	N	US	15	0	878	301	3950602	.0994	5.36	
25209	N	US	15	0	852	298	3687213	1.506	8.04	
25210	N	US	15	0	852	297	3865306	.2013	10.72	
25214	N	US	11	0	880	302	3726436	.0495	2.68	25215
25216	N	US	11	0	883	302	3909711	.0986	5.36	25217
25301	N	US	5	0	884	302	3903998	.0984	5.36	25302
25303	N	US	5	0	865	303	3878688	1.962	10.72	25304
25311	N	US	5	0	881	302	3852707	.0982	5.36	25312
25319	N	US	5	5	881	302	3833693	.0980	5.36	25320

TABLE 11.- Continued.  
(c) Wortmann FX-098 airfoil.

A										B																			
FRAME	TRIP	TYPE	AO	AI	Q	M	RE	K	FREQ	FRAME	TRIP	TYPE	AO	AI	Q	M	RE	K	FREQ	FRAME									
17208	Y	ST	5.0	0.0	0.877	301	3975279.	0.0000	0.00	17209	N	ST	13.0	0.0	0.340	185	2353097.	0.0000	0.00	19021	N	ST	20.0	0.0	0.342	185	2454849.	0.0000	0.00
17212	Y	ST	5.0	0.0	0.880	301	3928557.	0.0000	0.00	17213	N	ST	11.0	0.0	0.341	185	2354196.	0.0000	0.00	19022	N	ST	2.0	0.0	0.340	185	2361633.	0.0000	0.00
17220	Y	ST	10.0	0.0	0.879	302	3911481.	0.0000	0.00	17221	N	ST	5.0	0.0	0.340	185	2357348.	0.0000	0.00	19101	N	ST	2.0	0.0	0.341	185	2399877.	0.0000	0.00
17303	Y	ST	12.0	0.0	0.847	296	3802285.	0.0000	0.00	17304	N	ST	0.0	0.0	0.340	185	2354786.	0.0000	0.00	19116	N	ST	8.0	0.0	0.340	185	2378719.	0.0000	0.00
17305	Y	ST	13.0	0.0	0.870	300	3835722.	0.0000	0.00	17306	N	ST	-5.0	0.0	0.614	250	3151118.	0.0000	0.00	19119	N	ST	10.0	0.0	0.343	185	2379520.	0.0000	0.00
17310	Y	ST	14.0	0.0	0.866	299	3820076.	0.0000	0.00	17311	N	ST	2.0	0.0	0.611	250	3138172.	0.0000	0.00	19121	N	ST	12.0	0.0	0.338	183	2355087.	0.0000	0.00
17312	Y	ST	15.0	0.0	0.866	299	3805980.	0.0000	0.00	17313	N	ST	0.0	0.0	0.612	250	3137611.	0.0000	0.00	19122	N	ST	13.5	0.0	0.340	185	2370521.	0.0000	0.00
17314	Y	ST	16.0	0.0	0.828	292	3710084.	0.0000	0.00	17315	N	ST	2.0	0.0	0.616	251	3300956.	0.0000	0.00	19205	N	ST	14.0	0.0	0.342	185	2361633.	0.0000	0.00
18019	Y	ST	0.0	0.0	0.341	184	2348709.	0.0000	0.00	18020	N	ST	4.0	0.0	0.616	251	3297074.	0.0000	0.00	19208	N	ST	15.0	0.0	0.342	185	2361273.	0.0000	0.00
18102	Y	ST	5.0	0.0	0.343	185	2400750.	0.0000	0.00	18103	N	ST	8.0	0.0	0.617	251	3297867.	0.0000	0.00	19214	N	ST	16.0	0.0	0.341	185	2365586.	0.0000	0.00
18106	Y	ST	10.0	0.0	0.339	184	2378846.	0.0000	0.00	18107	N	ST	10.0	0.0	0.614	250	3275608.	0.0000	0.00	19216	N	ST	15.0	0.0	0.340	185	2364851.	0.0000	0.00
18108	Y	ST	12.0	0.0	0.343	185	2388927.	0.0000	0.00	18109	N	ST	12.0	0.0	0.618	251	3278455.	0.0000	0.00	19218	N	ST	18.0	0.0	0.341	185	2368218.	0.0000	0.00
18115	Y	ST	13.0	0.0	0.346	185	2394744.	0.0000	0.00	18116	N	ST	13.0	0.0	0.618	251	3268218.	0.0000	0.00	19219	N	ST	18.0	0.0	0.341	184	2452121.	0.0000	0.00
18117	Y	ST	14.0	0.0	0.345	185	2388872.	0.0000	0.00	18118	N	ST	13.5	0.0	0.620	251	3264994.	0.0000	0.00	19219	Y	UN	15.0	10.0	0.341	184	2452121.	0.0000	0.00
18119	Y	ST	15.0	0.0	0.341	184	2374587.	0.0000	0.00	18120	N	ST	14.0	0.0	0.613	250	3264994.	0.0000	0.00	19219	Y	UN	15.0	10.0	0.341	184	2452121.	0.0000	0.00
18121	Y	ST	16.0	0.0	0.340	184	2369089.	0.0000	0.00	18122	N	ST	15.0	0.0	0.613	250	3263310.	0.0000	0.00	19219	Y	UN	15.0	10.0	0.341	184	2452121.	0.0000	0.00
18123	Y	ST	19.9	0.0	0.342	184	2370588.	0.0000	0.00	18200	N	ST	16.0	0.0	0.602	248	3194789.	0.0000	0.00	19219	Y	UN	15.0	10.0	0.341	184	2452121.	0.0000	0.00
18206	Y	ST	0.0	0.0	0.341	184	2379635.	0.0000	0.00	18207	N	ST	18.0	0.0	0.602	248	3194789.	0.0000	0.00	19219	Y	UN	15.0	10.0	0.341	184	2452121.	0.0000	0.00
18215	N	ST	-5.0	0.0	0.122	110	1500031.	0.0000	0.00	18216	N	ST	25.0	0.0	0.610	249	3162267.	0.0000	0.00	19219	Y	UN	15.0	10.0	0.341	184	2452121.	0.0000	0.00
18217	N	ST	-2.0	0.0	0.123	110	1502458.	0.0000	0.00	18217	N	ST	20.0	0.0	0.612	250	3158666.	0.0000	0.00	19219	Y	UN	15.0	10.0	0.341	184	2452121.	0.0000	0.00
18218	N	ST	0.0	0.0	0.121	109	1487692.	0.0000	0.00	18219	N	ST	14.0	0.0	0.614	250	3163174.	0.0000	0.00	19219	Y	UN	15.0	10.0	0.341	184	2452121.	0.0000	0.00
18220	N	ST	2.0	0.0	0.122	110	1494149.	0.0000	0.00	18220	N	ST	13.0	0.0	0.610	249	3155282.	0.0000	0.00	19219	Y	UN	15.0	10.0	0.341	184	2452121.	0.0000	0.00
18221	N	ST	4.0	0.0	0.121	109	1486754.	0.0000	0.00	18221	N	ST	11.0	0.0	0.609	249	3150506.	0.0000	0.00	19219	Y	UN	15.0	10.0	0.341	184	2452121.	0.0000	0.00
18304	N	ST	8.0	0.0	0.121	109	1480425.	0.0000	0.00	18304	N	ST	5.0	0.0	0.613	250	3157103.	0.0000	0.00	19219	Y	UN	15.0	10.0	0.341	184	2452121.	0.0000	0.00
18305	N	ST	10.0	0.0	0.122	110	1483466.	0.0000	0.00	18305	N	ST	5.0	0.0	0.615	250	3152218.	0.0000	0.00	19219	Y	UN	15.0	10.0	0.341	184	2452121.	0.0000	0.00
18307	N	ST	12.0	0.0	0.122	109	1476483.	0.0000	0.00	18308	N	ST	-5.0	0.0	0.893	304	3774892.	0.0000	0.00	19219	Y	UN	15.0	10.0	0.341	184	2452121.	0.0000	0.00
18312	N	ST	13.0	0.0	0.121	109	1466753.	0.0000	0.00	18312	N	ST	-2.0	0.0	0.883	303	3776701.	0.0000	0.00	19219	Y	UN	15.0	10.0	0.341	184	2452121.	0.0000	0.00
18319	N	ST	13.5	0.0	0.123	109	1469738.	0.0000	0.00	18320	N	ST	0.0	0.0	0.879	303	3758789.	0.0000	0.00	19219	Y	UN	15.0	10.0	0.341	184	2452121.	0.0000	0.00
18321	N	ST	14.0	0.0	0.124	110	1474082.	0.0000	0.00	18322	N	ST	2.0	0.0	0.876	302	3748627.	0.0000	0.00	19219	Y	UN	15.0	10.0	0.341	184	2452121.	0.0000	0.00
18323	N	ST	15.0	0.0	0.122	110	1463922.	0.0000	0.00	18323	N	ST	4.0	0.0	0.878	303	3748627.	0.0000	0.00	19219	Y	UN	15.0	10.0	0.341	184	2452121.	0.0000	0.00
18401	N	ST	18.0	0.0	0.122	109	1461183.	0.0000	0.00	18402	N	ST	8.0	0.0	0.860	299	3709078.	0.0000	0.00	19219	Y	UN	15.0	10.0	0.341	184	2452121.	0.0000	0.00
18410	N	ST	16.0	0.0	0.124	111	1459953.	0.0000	0.00	18412	N	ST	12.0	0.0	0.860	299	3709078.	0.0000	0.00	19219	Y	UN	15.0	10.0	0.341	184	2452121.	0.0000	0.00
18413	N	ST	20.0	0.0	0.123	109	1447617.	0.0000	0.00	18412	N	ST	10.0	0.0	0.860	299	3709078.	0.0000	0.00	19219	Y	UN	15.0	10.0	0.341	184	2452121.	0.0000	0.00
18414	N	ST	20.0	0.0	0.122	110	1439675.	0.0000	0.00	18412	N	ST	10.0	0.0	0.860	299	3709078.	0.0000	0.00	19219	Y	UN	15.0	10.0	0.341	184	2452121.	0.0000	0.00
18421	N	ST	20.0	0.0	0.123	109	1439675.	0.0000	0.00	18412	N	ST	10.0	0.0	0.860	299	3709078.	0.0000	0.00	19219	Y	UN	15.0	10.0	0.341	184	2452121.	0.0000	0.00
18422	N	ST	14.0	0.0	0.122	110	1459948.	0.0000	0.00	18412	N	ST	10.0	0.0	0.860	299	3709078.	0.0000	0.00	19219	Y	UN	15.0	10.0	0.341	184	2452121.	0.0000	0.00
18423	N	ST	13.0	0.0	0.122	109	1439933.	0.0000	0.00	18412	N	ST	10.0	0.0	0.860	299	3709078.	0.0000	0.00	19219	Y	UN	15.0	10.0	0.341	184	2452121.	0.0000	0.00
18500	N	ST	11.0	0.0	0.122	110	1437504.	0.0000	0.00	18501	N	ST	20.0	0.0	0.737	294	3811625.	0.0000	0.00	19219	Y	UN	15.0	10.0	0.341	184	2452121.	0.0000	0.00
18501	N	ST	5.0	0.0	0.122	109	1436482.	0.0000	0.00	18502	N	ST	20.0	0.0	0.668	261	3411407.	0.0000	0.00	19219	Y	UN	15.0	10.0	0.341	184	2452121.	0.0000	0.00
18502	N	ST	5.0	0.0	0.342	185	2454849.	0.0000	0.00	19021	N	ST	20.0	0.0	0.740	275	3578432.	0.0000	0.00	19219	Y	UN	15.0	10.0	0.341	184	2452121.	0.0000	0.00
19020	N																												

TABLE 11.- Continued.  
(c) Concluded.

A	FRAME	TRIP	Y	TYPE	AO	A1	Q	M	RE	K	FREQ	B	FRAME
17200	N	UN	15.0	10.0	10.0	814	290	3702477	0999	5.24	21201		
21107	N	UN	10.0	10.0	823	291	3718613	0099	5.24	21102			
21200	N	UN	10.0	10.0	857	299	3792469	0098	5.3	21201			
21208	N	UN	10.0	5.0	875	301	3922117	0098	5.3	21209			
21219	N	UN	3.3	10.0	882	302	3833549	0097	5.3	21220			
22023	N	UN	6.5	10.0	339	184	2455159	0098	3.3	21220			
22103	N	UN	15.0	10.0	627	293	3727583	0247	1.31	22104			
22201	N	UN	15.0	10.0	837	294	3749080	0492	2.62	22104			
22206	N	UN	15.0	10.0	785	285	3552419	1008	5.24	22202			
22208	N	UN	15.0	10.0	754	279	3477029	1542	7.86	22207			
22216	N	UN	15.0	10.0	763	281	3483672	0969	4.98	22209			
22217	N	UN	10.0	10.0	875	302	3732111	0243	1.34				
22218	N	UN	10.0	10.0	875	302	3720266	0485	2.68				
22219	N	UN	10.0	10.0	862	300	3694571	0977	5.36				
22307	N	UN	10.0	10.0	835	294	3618609	1490	8.04	22223			
22308	N	UN	10.0	5.0	875	301	3654387	0246	1.34	22300			
22309	N	UN	10.0	5.0	880	303	3857324	0491	2.68	22301			
22311	N	UN	10.0	5.0	881	303	3853491	0980	5.36	22302			
22312	N	UN	10.0	5.0	877	292	3649798	1475	8.04	22302			
23021	N	UN	15.0	5.0	882	303	3849072	1957	10.72	22303			
23022	N	UN	15.0	5.0	858	298	3792196	0248	1.34				
23023	N	UN	15.0	5.0	851	297	3750472	0497	2.68				
23100	N	UN	15.0	5.0	840	295	3716891	1000	5.36				
23107	N	UN	15.0	5.0	822	292	3670934	1515	8.04				
23109	N	UN	5.0	5.0	867	300	3802836	0986	5.36	23108			
23117	N	UN	5.0	5.0	867	300	3769174	1970	10.72	23110			
23201	N	UN	5.0	10.0	869	300	3803440	0985	5.36	23118			
23206	N	UN	3.8	10.0	866	299	3948210	1003	5.36	23202			
23208	N	UN	3.3	10.0	871	300	3924045	0500	2.68	23207			
23211	N	UN	3.3	10.0	871	300	3914485	0596	5.36	23210			
23219	N	UN	12.0	2.0	870	300	3896319	1492	8.04	23212			
23305	N	UN	14.0	2.0	864	298	3865609	1994	10.72	23220			
23310	N	UN	16.0	2.0	858	298	3831711	1995	10.72	23306			
21112	N	UN	15.0	5.0	873	301	3940131	2014	10.72	23311			
23101	N	UN	15.0	5.0	800	287	3617353	0099	5.3				
								2049	10.72				

TABLE 11.- Continued.  
(d) Sikorsky SC-1095 airfoil.

A										B										
FRAME	TRIP	TYPE	AO	AI	Q	M	RE	K	FREQ	FRAME	TRIP	TYPE	AO	AI	Q	M	RE	K	FREQ	FRAME
34022	Y	ST	5.0	0.0	.878	.301	3985083.	0.0000	0.00	34023	N	ST	16.0	0.0	.340	184	2432059.	0.0000	0.00	36119
34100	Y	ST	5.0	0.0	.880	.301	3976998.	0.0000	0.00	34101	N	ST	20.0	0.0	.341	185	2424852.	0.0000	0.00	36120
34102	Y	ST	10.0	0.0	.884	.301	3969476.	0.0000	0.00	34103	N	ST	-5.0	0.0	.123	110	1457009.	0.0000	0.00	36121
34107	Y	ST	12.0	0.0	.879	.302	3961576.	0.0000	0.00	34108	N	ST	0.0	0.0	.124	111	1461763.	0.0000	0.00	36122
34109	Y	ST	13.0	0.0	.883	.302	3956692.	0.0000	0.00	34110	N	ST	5.0	0.0	.122	110	1455304.	0.0000	0.00	36123
34111	Y	ST	13.0	0.0	.886	.297	3956692.	0.0000	0.00	34111	N	ST	10.0	0.0	.122	110	1429342.	0.0000	0.00	36124
34113	Y	ST	14.0	0.0	.886	.287	3953399.	0.0000	0.00	34112	N	ST	12.0	0.0	.121	109	1430840.	0.0000	0.00	36125
34115	Y	ST	16.0	0.0	.890	.301	3902976.	0.0000	0.00	34114	N	ST	13.5	0.0	.122	110	1428033.	0.0000	0.00	36126
34200	Y	ST	0.0	0.0	.841	.184	2464109.	0.0000	0.00	34201	N	ST	14.0	0.0	.124	110	1430614.	0.0000	0.00	36127
34202	Y	ST	5.0	0.0	.842	.184	2463733.	0.0000	0.00	34203	N	ST	15.0	0.0	.122	110	1421260.	0.0000	0.00	36128
34204	Y	ST	10.0	0.0	.842	.184	2455124.	0.0000	0.00	34205	N	ST	15.5	0.0	.123	110	1425215.	0.0000	0.00	36129
34208	Y	ST	13.0	0.0	.842	.184	2449358.	0.0000	0.00	34209	N	ST	16.0	0.0	.121	109	1413387.	0.0000	0.00	36130
34210	Y	ST	14.0	0.0	.842	.184	2447959.	0.0000	0.00	34211	N	ST	20.0	0.0	.120	109	1408711.	0.0000	0.00	36131
34212	Y	ST	16.0	0.0	.841	.184	2441097.	0.0000	0.00	34212	N	UN	15.0	10.0	.054	073	975044.	0.0000	0.00	36132
34214	Y	ST	0.0	0.0	.841	.184	2444858.	0.0000	0.00	34213	N	UN	15.0	10.0	.087	073	975044.	0.0000	0.00	36133
35021	N	ST	-2.0	0.0	.880	.301	3835776.	0.0000	0.00	35022	N	UN	15.0	10.0	.124	110	1462074.	.0979	1.30	33023
35100	N	ST	0.0	0.0	.878	.301	3819752.	0.0000	0.00	35101	N	UN	15.0	10.0	.339	183	2400379.	.0990	3.30	33111
35102	N	ST	0.0	0.0	.877	.301	3816485.	0.0000	0.00	35102	N	UN	6.2	10.0	.334	182	2390916.	.0499	1.65	33120
35103	N	ST	0.0	0.0	.877	.301	3815931.	0.0000	0.00	35103	N	UN	6.2	10.0	.340	184	2409037.	.1975	6.60	33122
35111	N	ST	0.0	0.0	.877	.301	3811571.	0.0000	0.00	35104	N	UN	15.0	10.0	.479	219	2837984.	.0985	3.93	33206
35112	N	ST	8.0	0.0	.881	.302	4009328.	0.0000	0.00	35105	N	UN	15.0	10.0	.612	249	3185055.	.0984	4.46	33208
35114	N	ST	10.0	0.0	.879	.302	3971392.	0.0000	0.00	35106	N	UN	15.0	10.0	.855	297	3744923.	.1002	4.98	33216
35116	N	ST	13.0	0.0	.877	.301	3903577.	0.0000	0.00	35107	N	UN	15.0	10.0	.852	296	3886915.	.0494	2.62	33223
35118	N	ST	13.5	0.0	.845	.293	3867672.	0.0000	0.00	35108	N	UN	15.0	10.0	.828	292	3817843.	.0997	5.24	33303
35123	N	ST	14.0	0.0	.879	.302	3927789.	0.0000	0.00	35109	N	UN	15.0	10.0	.840	288	3800453.	.0503	2.62	34307
35206	N	ST	16.0	0.0	.832	.293	3806814.	0.0000	0.00	35207	N	UN	15.0	10.0	.340	184	2482777.	.1017	5.24	34309
35207	N	ST	14.0	0.0	.874	.301	3893325.	0.0000	0.00	35208	N	UN	15.0	10.0	.341	184	2476494.	.0998	3.30	34322
35208	N	ST	13.0	0.0	.845	.291	3760893.	0.0000	0.00	35209	N	UN	15.0	10.0	.762	279	3920520.	.1495	4.95	34400
35213	N	ST	5.0	0.0	.878	.295	3602021.	0.0000	0.00	35210	N	UN	4.1	10.0	.881	302	3894279.	.1480	8.04	37113
35214	N	ST	0.0	0.0	.883	.302	3894699.	0.0000	0.00	35211	N	UN	4.1	10.0	.879	302	3866563.	.0492	2.68	37120
35220	N	ST	-2.0	0.0	.611	.249	3231739.	0.0000	0.00	35212	N	UN	4.1	10.0	.886	303	3859634.	.0978	5.36	37122
35221	N	ST	-2.0	0.0	.610	.249	3231739.	0.0000	0.00	35213	N	UN	4.1	10.0	.879	302	3836077.	.1471	8.04	37201
35222	N	ST	0.0	0.0	.613	.250	3233953.	0.0000	0.00	35214	N	UN	4.1	10.0	.880	302	3894279.	.1480	8.04	37113
35223	N	ST	2.0	0.0	.612	.249	3228312.	0.0000	0.00	35215	N	UN	4.1	10.0	.879	302	3894279.	.1480	8.04	37113
35300	N	ST	5.0	0.0	.613	.250	3228749.	0.0000	0.00	35216	N	UN	4.1	10.0	.886	303	3866563.	.0492	2.68	37120
35305	N	ST	8.0	0.0	.612	.249	3194450.	0.0000	0.00	35217	N	UN	4.1	10.0	.879	302	3894279.	.1480	8.04	37113
35307	N	ST	10.0	0.0	.614	.249	3194450.	0.0000	0.00	35218	N	UN	4.1	10.0	.886	303	3866563.	.0492	2.68	37120
35308	N	ST	12.0	0.0	.609	.248	3176162.	0.0000	0.00	35219	N	UN	4.1	10.0	.879	302	3894279.	.1480	8.04	37113
35309	N	ST	13.5	0.0	.605	.247	3151475.	0.0000	0.00	35220	N	UN	4.1	10.0	.880	302	3894279.	.1480	8.04	37113
35310	N	ST	14.1	0.0	.614	.250	3175031.	0.0000	0.00	35221	N	UN	4.1	10.0	.879	302	3894279.	.1480	8.04	37113
35313	N	ST	16.0	0.0	.614	.249	3171847.	0.0000	0.00	35222	N	UN	4.1	10.0	.886	303	3866563.	.0492	2.68	37120
35314	N	ST	18.0	0.0	.611	.249	3155127.	0.0000	0.00	35223	N	UN	4.1	10.0	.886	303	3866563.	.0492	2.68	37120
35315	N	ST	20.0	0.0	.609	.248	3132360.	0.0000	0.00	35224	N	UN	4.1	10.0	.879	302	3894279.	.1480	8.04	37113
35316	N	ST	25.0	0.0	.612	.250	3135933.	0.0000	0.00	35225	N	UN	4.1	10.0	.886	303	3866563.	.0492	2.68	37120
35317	N	ST	14.0	0.0	.611	.249	3142583.	0.0000	0.00	35226	N	UN	4.1	10.0	.879	302	3894279.	.1480	8.04	37113
35318	N	ST	13.0	0.0	.612	.250	3143100.	0.0000	0.00	35227	N	UN	4.1	10.0	.886	303	3866563.	.0492	2.68	37120
35319	N	ST	12.5	0.0	.611	.249	3139723.	0.0000	0.00	35228	N	UN	4.1	10.0	.879	302	3894279.	.1480	8.04	37113
35400	N	ST	5.0	0.0	.614	.249	3166450.	0.0000	0.00	35229	N	UN	4.1	10.0	.886	303	3866563.	.0492	2.68	37120
35401	N	ST	0.0	0.0	.611	.249	3155127.	0.0000	0.00	35230	N	UN	4.1	10.0	.879	302	3894279.	.1480	8.04	37113
35409	N	ST	-5.0	0.0	.342	.184	2509809.	0.0000	0.00	35231	N	UN	12.0	8.0	.878	301	3752961.	.0972	5.36	37222
35420	N	ST	0.0	0.0	.341	.185	2503010.	0.0000	0.00	35232	N	UN	12.0	8.0	.878	301	3752961.	.0972	5.36	37222
35422	N	ST	5.0	0.0	.341	.185	2493947.	0.0000	0.00	35233	N	UN	12.0	8.0	.878	301	3752961.	.0972	5.36	37222
35406	N	ST	10.0	0.0	.341	.185	2467697.	0.0000	0.00	35234	N	UN	12.0	8.0	.878	301	3752961.	.0972	5.36	37222
35408	N	ST	12.0	0.0	.341	.185	2461702.	0.0000	0.00	35235	N	UN	12.0	8.0	.878	301	3752961.	.0972	5.36	37222
35410	N	ST	13.5	0.0	.340	.184	2452406.	0.0000	0.00	35236	N	UN	12.0	8.0	.878	301	3752961.	.0972	5.36	37222
35411	N	ST	14.0	0.0	.341	.185	2447787.	0.0000	0.00	35237	N	UN	12.0	8.0	.878	301	3752961.	.0972	5.36	37222
35412	N	ST	15.0	0.0	.338	.183	2428196.	0.0000	0.00	35238	N	UN	12.0	8.0	.878	301	3752961.	.0972	5.36	37222

TABLE 11.- Continued.

(d) Concluded.

A												B	
FRAME	TRIP	TYPE	AO	A1	Q	M	RE	K	FREQ	FRAME			
39110	N	UN	11.0	5.0	.869	.299	3896687.	.0099	.53				
39115	N	UN	14.0	2.0	.865	.298	3838822.	.0100	.54				
38110	N	UN	16.0	2.0	.832	.293	3754517.	.2023	10.72	38111			
39107	N	UN	10.0	5.0	.876	.300	3939495.	.0098	.53				



TABLE 11.- Continued.

(e) Concluded.

A	FRAME	TRIP	TYPE	AO	A1	G	M	RE	K	FREQ	B
44112	N	US	10.0	5.0	.880	.303	4003278.	.1989	10.72	44113	
44118	N	US	10.0	5.0	.880	.302	4037690.	.0999	5.36		
44119	N	US	10.0	5.0	.876	.302	4019097.	.0250	1.34		
44120	N	US	10.0	5.0	.878	.302	4007236.	.1997	10.72		
44202	N	US	14.0	2.0	.875	.301	4004232.	.1001	5.36	44203	
44204	N	US	14.0	2.0	.872	.301	3987136.	.2002	10.72	44205	
44209	N	US	17.5	2.0	.773	.282	3756572.	.2132	10.72		
44212	N	US	15.5	2.0	.854	.297	3961107.	.0102	.54		
44214	N	US	15.5	2.0	.851	.297	3917470.	.0253	1.34		
44215	N	US	15.5	2.0	.849	.296	3904494.	.0506	2.68		
44216	N	US	15.5	2.0	.829	.293	3854681.	.1024	5.36		
44217	N	US	15.5	2.0	.820	.291	3826794.	.1545	8.04		
44218	N	US	15.5	2.0	.824	.292	3832243.	.2054	10.72		
44221	N	US	12.5	2.0	.871	.301	3956605.	.0101	.54		
44222	N	US	12.5	2.0	.877	.302	3945321.	.0248	1.34		
44223	N	US	12.5	2.0	.871	.301	3926050.	.0493	2.68		
44300	N	US	12.5	2.0	.874	.301	3929775.	.0994	5.36		
44303	N	US	12.5	2.0	.877	.302	3922217.	.1490	8.04		
44304	N	US	12.5	2.0	.878	.302	3945918.	.1984	10.72		
44308	N	US	15.0	5.0	.813	.290	3809287.	.1549	8.04		

TABLE II.- Continued.  
(f) Vertol VR-7 airfoil.

A										B										
FRAME	TRIP	TYPE	A0	A1	Q	M	RE	K	FREQ	FRAME	TRIP	TYPE	A0	A1	Q	M	RE	K	FREQ	FRAME
46018	N	ST	-5.0	0.0	121	108	1551001.	0.0000	0.00	46009	N	ST	13.0	0.0	876	299	4071175.	0.0000	0.00	46708
46019	N	ST	0.0	0.0	121	108	1546271.	0.0000	0.00	46810	N	ST	12.0	0.0	881	299	4055190.	0.0000	0.00	46713
46020	N	ST	5.0	0.0	123	109	1557517.	0.0000	0.00	46621	N	ST	0.0	0.0	861	300	4057411.	0.0000	0.00	46715
46101	N	ST	10.0	0.0	118	107	1512690.	0.0000	0.00	46623	Y	ST	5.0	0.0	340	163	2522757.	0.0000	0.00	46717
46102	N	ST	12.5	0.0	122	109	1540066.	0.0000	0.00	46701	Y	ST	10.0	0.0	340	183	2514978.	0.0000	0.00	46719
46103	N	ST	12.5	0.0	123	109	1547844.	0.0000	0.00	46703	Y	ST	10.0	0.0	341	183	2513421.	0.0000	0.00	46704
46104	N	ST	13.5	0.0	123	109	1543789.	0.0000	0.00	46705	Y	ST	13.0	0.0	340	183	2515138.	0.0000	0.00	46706
46105	N	ST	13.5	0.0	123	109	1542255.	0.0000	0.00	46707	Y	ST	14.0	0.0	338	182	2501582.	0.0000	0.00	46708
46106	N	ST	14.0	0.0	122	109	1533972.	0.0000	0.00	46712	Y	ST	15.0	0.0	340	183	2518275.	0.0000	0.00	46713
46107	N	ST	15.0	0.0	122	109	1537932.	0.0000	0.00	46714	Y	ST	16.0	0.0	341	184	2516975.	0.0000	0.00	46715
46108	N	ST	17.0	0.0	123	109	1541148.	0.0000	0.00	46716	Y	ST	20.0	0.0	342	184	2517610.	0.0000	0.00	46717
46109	N	ST	20.0	0.0	122	109	1534206.	0.0000	0.00	46718	Y	ST	20.0	0.0	342	183	2519323.	0.0000	0.00	46719
46110	N	ST	25.0	0.0	120	108	1523001.	0.0000	0.00	46802	Y	ST	0.0	0.0	881	300	4204772.	0.0000	0.00	46803
46116	N	ST	-5.0	0.0	341	184	2550698.	0.0000	0.00	46804	Y	ST	5.0	0.0	881	300	4185103.	0.0000	0.00	46805
46117	N	ST	0.0	0.0	342	183	2552564.	0.0000	0.00	46806	Y	ST	10.0	0.0	886	301	4170536.	0.0000	0.00	46807
46119	N	ST	5.0	0.0	341	183	2546284.	0.0000	0.00	46808	Y	ST	12.0	0.0	882	300	4168330.	0.0000	0.00	46809
46203	N	ST	10.0	0.0	343	184	2562110.	0.0000	0.00	46809	Y	ST	13.0	0.0	883	301	4199718.	0.0000	0.00	46811
46205	N	ST	12.0	0.0	341	183	2551368.	0.0000	0.00	46810	Y	ST	14.0	0.0	881	300	4137342.	0.0000	0.00	46816
46207	N	ST	12.5	0.0	342	183	2553262.	0.0000	0.00	46815	Y	ST	15.0	0.0	877	300	4108330.	0.0000	0.00	46818
46209	N	ST	13.0	0.0	342	184	2553793.	0.0000	0.00	46816	Y	ST	15.0	0.0	877	299	4091352.	0.0000	0.00	46820
46211	N	ST	13.5	0.0	341	183	2550511.	0.0000	0.00	46819	Y	ST	16.0	0.0	877	299	3893404.	0.0000	0.00	46822
46211	N	ST	14.0	0.0	342	183	2637541.	0.0000	0.00	46821	Y	ST	20.0	0.0	876	287	4085157.	0.0000	0.00	46822
46219	N	ST	15.0	0.0	341	183	2630320.	0.0000	0.00	46822	Y	ST	0.0	0.0	881	300	4085157.	0.0000	0.00	46822
46221	N	ST	17.0	0.0	340	183	2624424.	0.0000	0.00	46823	Y	ST	0.0	0.0	873	300	4082142.	0.0000	0.00	46822
46221	N	ST	20.0	0.0	340	183	2622591.	0.0000	0.00	46821	N	UN	15.0	10.0	830	292	3937973.	0.0000	0.00	46822
46301	N	ST	25.0	0.0	340	183	2614669.	0.0000	0.00	46823	N	UN	15.0	10.0	835	293	3931111.	0.0000	0.00	46822
46307	N	ST	-5.0	0.0	612	248	3482182.	0.0000	0.00	45101	N	UN	10.0	10.0	793	285	3624874.	0.0000	0.00	45100
46308	N	ST	-2.0	0.0	613	249	3476509.	0.0000	0.00	45109	N	UN	10.0	10.0	873	301	4033426.	0.0000	0.00	45102
46309	N	ST	0.0	0.0	612	248	3469801.	0.0000	0.00	45111	N	UN	10.0	10.0	873	301	4010514.	0.0000	0.00	45110
46310	N	ST	2.0	0.0	611	248	3461144.	0.0000	0.00	45113	N	UN	10.0	10.0	875	301	4010372.	0.0000	0.00	45112
46311	N	ST	5.0	0.0	614	249	3462655.	0.0000	0.00	45117	N	UN	10.0	10.0	879	301	4019136.	0.0000	0.00	45118
46317	N	ST	8.0	0.0	615	249	3457898.	0.0000	0.00	45119	N	UN	10.0	10.0	879	302	4015236.	0.0000	0.00	45120
46318	N	ST	10.0	0.0	611	248	3435015.	0.0000	0.00	45205	N	UN	15.0	5.0	869	300	4019028.	0.0000	0.00	45204
46319	N	ST	12.0	0.0	613	248	3433344.	0.0000	0.00	45207	N	UN	15.0	5.0	876	301	4006473.	0.0000	0.00	45206
46320	N	ST	12.5	0.0	615	249	3429825.	0.0000	0.00	45209	N	UN	15.0	5.0	877	301	4005939.	0.0000	0.00	45208
46321	N	ST	13.0	0.0	612	248	3419429.	0.0000	0.00	45211	N	UN	15.0	5.0	871	300	3986030.	0.0000	0.00	45210
46322	N	ST	13.5	0.0	610	248	3409796.	0.0000	0.00	45213	N	UN	15.0	5.0	860	298	3957187.	0.0000	0.00	45212
46323	N	ST	14.0	0.0	613	249	3417715.	0.0000	0.00	45219	N	UN	15.0	5.0	881	295	3908733.	0.0000	0.00	45214
46400	N	ST	15.0	0.0	613	249	3413348.	0.0000	0.00	45221	N	UN	10.0	5.0	878	302	4054475.	0.0000	0.00	45222
46403	N	ST	17.0	0.0	616	249	3427697.	0.0000	0.00	45223	N	UN	10.0	5.0	877	301	4032781.	0.0000	0.00	45301
46404	N	ST	20.0	0.0	615	249	3412222.	0.0000	0.00	45300	N	UN	10.0	5.0	878	301	4031948.	0.0000	0.00	45304
46405	N	ST	25.0	0.0	614	248	3396768.	0.0000	0.00	45302	N	UN	10.0	5.0	879	302	4030474.	0.0000	0.00	45304
46406	N	ST	12.0	0.0	610	248	3391942.	0.0000	0.00	45303	N	UN	10.0	5.0	878	301	4025973.	0.0000	0.00	45304
46407	N	ST	12.0	0.0	614	248	3391942.	0.0000	0.00	47020	Y	UN	15.0	10.0	859	299	4059175.	0.0000	0.00	47021
46412	N	ST	0.0	0.0	877	300	3964285.	0.0000	0.00	47100	Y	UN	15.0	10.0	859	299	3926981.	0.0000	0.00	47101
46418	N	ST	-5.0	0.0	877	300	3964105.	0.0000	0.00	47110	Y	UN	15.0	10.0	859	299	3926981.	0.0000	0.00	47101
46420	N	ST	-2.0	0.0	878	301	3926471.	0.0000	0.00	47112	Y	UN	15.0	10.0	859	299	3926981.	0.0000	0.00	47101
46423	N	ST	2.0	0.0	875	300	3966654.	0.0000	0.00	47114	Y	UN	15.0	10.0	859	299	3926981.	0.0000	0.00	47101
46500	N	ST	5.0	0.0	877	300	3965878.	0.0000	0.00	47114	Y	UN	15.0	10.0	859	299	3926981.	0.0000	0.00	47101
46508	N	ST	8.0	0.0	878	300	4161706.	0.0000	0.00	47206	N	UN	15.0	10.0	859	299	3926981.	0.0000	0.00	47207
46509	N	ST	10.0	0.0	876	299	4126333.	0.0000	0.00	47217	N	UN	15.0	10.0	859	299	3926981.	0.0000	0.00	47218
46511	N	ST	12.0	0.0	876	299	4119351.	0.0000	0.00	47301	N	UN	15.0	10.0	859	299	3926981.	0.0000	0.00	47302
46513	N	ST	12.5	0.0	874	299	4096603.	0.0000	0.00	47305	N	UN	15.0	10.0	859	299	3926981.	0.0000	0.00	47302
46515	N	ST	13.0	0.0	867	298	4070743.	0.0000	0.00	47305	N	UN	15.0	10.0	859	299	3926981.	0.0000	0.00	47302
46517	N	ST	13.5	0.0	879	300	4087558.	0.0000	0.00	54019	N	UN	10.0	10.0	340	183	2632968.	0.0000	0.00	54020
46519	N	ST	14.0	0.0	878	300	4077474.	0.0000	0.00	54022	N	UN	10.0	10.0	340	183	2616265.	0.0000	0.00	54023
46600	N	ST	15.0	0.0	873	299	4089463.	0.0000	0.00	54101	N	UN	10.0	10.0	339	183	2607326.	0.0000	0.00	54102
46602	N	ST	17.0	0.0	878	300	4078318.	0.0000	0.00	54101</										



TABLE 11.- Continued.

(f) Concluded.

A	FRAME	TRIP	TYPE	AO	A1	G	M	RE	K	FREQ	B
54216	N	UN	15.0	10.0	.340	184	2547606.		.1514	4.95	48218
48019	N	UN	4.1	10.0	.874	299	4215503.		.0103	.54	48020
48023	N	UN	4.1	10.0	.880	300	4189985.		.0255	1.34	48100
48101	N	UN	4.1	10.0	.877	299	4160141.		.0509	2.68	48102
48103	N	UN	4.1	10.0	.879	300	4154411.		.1016	5.36	48104
48116	N	UN	13.0	2.0	.878	299	4054662.		.0253	1.34	48117
48118	N	UN	13.0	2.0	.876	299	4057323.		.0504	2.68	48119
48122	N	UN	13.0	2.0	.878	299	4057706.		.1010	5.36	48123
48209	N	UN	16.0	2.0	.870	298	4059728.		.2028	10.72	48211
48215	N	UN	14.0	2.0	.877	300	4057579.		.0504	2.68	
48216	N	UN	14.0	2.0	.879	300	4047826.		.1005	5.36	
48217	N	UN	14.0	2.0	.879	300	4035080.		.2009	10.72	
48300	N	UN	12.5	2.0	.878	300	4033369.		.0101	.54	
48301	N	UN	12.5	2.0	.878	300	4011900.		.0251	1.34	
48302	N	UN	12.5	2.0	.881	301	4009053.		.0500	2.68	
48303	N	UN	12.5	2.0	.874	299	3686169.		.1004	5.36	
48304	N	UN	12.5	2.0	.873	299	3980450.		.1505	8.04	
48308	N	UN	12.5	2.0	.875	300	3998448.		.2007	10.72	48309
49110	N	UN	15.0	10.0	.339	184	2634248.		.0257	.83	49111
49117	N	UN	15.0	10.0	.342	185	2619396.		.0507	1.65	49118
49120	N	UN	15.0	10.0	.340	185	2599912.		.1014	3.30	49121
49203	N	UN	15.0	10.0	.341	185	2592737.		.1518	4.95	49204
49206	N	UN	15.0	10.0	.341	185	2564616.		.2020	6.60	49207
49216	N	UN	4.7	10.0	.340	184	2504339.		.0254	.83	49217
49300	N	UN	4.7	10.0	.338	184	2535655.		.1009	3.30	49301
49307	N	UN	4.7	10.0	.342	185	2546693.		.2005	6.60	49308
49310	N	UN	4.7	10.0	.343	185	2543519.		.2503	8.25	49311
49323	N	UN	15.0	10.0	.338	184	2543127.		.0101	.33	49100
50116	N	UN	4.7	10.0	.339	183	2531156.		.0101	.33	50117
57018	N	UN	15.0	10.0	.340	184	2555187.		.1516	4.95	57019
58018	N	UN	15.0	10.0	.338	183	2437793.		.1495	4.95	58019
58102	N	UN	15.0	10.0	.014	037	496703.		.0983	.65	58103
58111	N	UN	15.0	10.0	.121	109	1528745.		.1010	1.96	58112
58120	N	UN	15.0	10.0	.340	184	2536174.		.1511	4.95	
58121	N	UN	15.0	10.0	.340	184	2532230.		.1007	3.30	
47022	Y	UN	15.0	10.0	.841	296	3990015.		.0501	2.62	47023
48200	N	UN	13.0	2.0	.884	301	4062447.		.2006	10.72	48201

TABLE 11.- Continued.  
(g) NLR-1 airfoil.

A										B																	
FRAME	TRIP	TYPE	AO	A1	Q	M	RE	K	FREQ	FRAME	TRIP	TYPE	AO	A1	Q	M	RE	K	FREQ	FRAME							
61018	N	ST	5.0	0.0	.122	.109	1524150.	0.0000	0.00	61408	N	ST	5.0	0.0	.122	.110	1534313.	0.0000	0.00	61408	N	ST	5.0	0.0	.122	.109	1524150.
61019	N	ST	5.0	0.0	.123	.110	1534313.	0.0000	0.00	61409	N	ST	5.0	0.0	.123	.110	1509433.	0.0000	0.00	61409	N	ST	5.0	0.0	.123	.110	1509433.
61020	N	ST	5.0	0.0	.125	.111	1529480.	0.0000	0.00	61410	N	ST	5.0	0.0	.125	.111	1537127.	0.0000	0.00	61410	N	ST	5.0	0.0	.125	.111	1537127.
61101	N	ST	10.0	0.0	.125	.111	1537127.	0.0000	0.00	61102	N	ST	12.0	0.0	.122	.109	1517792.	0.0000	0.00	61102	N	ST	12.0	0.0	.122	.109	1517792.
61102	N	ST	12.0	0.0	.122	.109	1517792.	0.0000	0.00	61103	N	ST	14.0	0.0	.122	.110	1522421.	0.0000	0.00	61103	N	ST	14.0	0.0	.122	.110	1522421.
61103	N	ST	14.0	0.0	.122	.110	1522421.	0.0000	0.00	61104	N	ST	15.0	0.0	.122	.110	1517668.	0.0000	0.00	61104	N	ST	15.0	0.0	.122	.110	1517668.
61104	N	ST	15.0	0.0	.122	.110	1517668.	0.0000	0.00	61105	N	ST	16.5	0.0	.122	.110	1511515.	0.0000	0.00	61105	N	ST	16.5	0.0	.122	.110	1511515.
61105	N	ST	16.5	0.0	.122	.110	1511515.	0.0000	0.00	61106	N	ST	18.0	0.0	.121	.109	1502495.	0.0000	0.00	61106	N	ST	18.0	0.0	.121	.109	1502495.
61106	N	ST	18.0	0.0	.121	.109	1502495.	0.0000	0.00	61107	N	ST	20.0	0.0	.123	.110	1511233.	0.0000	0.00	61107	N	ST	20.0	0.0	.123	.110	1511233.
61107	N	ST	20.0	0.0	.123	.110	1511233.	0.0000	0.00	61108	N	ST	5.0	0.0	.341	.301	3790531.	0.0000	0.00	61108	N	ST	5.0	0.0	.341	.301	3790531.
61108	N	ST	5.0	0.0	.341	.301	3790531.	0.0000	0.00	61114	N	ST	5.0	0.0	.342	.301	3782112.	0.0000	0.00	61114	N	ST	5.0	0.0	.342	.301	3782112.
61114	N	ST	5.0	0.0	.342	.301	3782112.	0.0000	0.00	61115	N	ST	5.0	0.0	.342	.301	3786607.	0.0000	0.00	61115	N	ST	5.0	0.0	.342	.301	3786607.
61115	N	ST	5.0	0.0	.342	.301	3786607.	0.0000	0.00	61116	N	ST	5.0	0.0	.341	.301	3783080.	0.0000	0.00	61116	N	ST	5.0	0.0	.341	.301	3783080.
61116	N	ST	5.0	0.0	.341	.301	3783080.	0.0000	0.00	61201	N	ST	5.0	0.0	.341	.301	3784580.	0.0000	0.00	61201	N	ST	5.0	0.0	.341	.301	3784580.
61201	N	ST	5.0	0.0	.341	.301	3784580.	0.0000	0.00	61202	N	ST	10.0	0.0	.341	.301	3785621.	0.0000	0.00	61202	N	ST	10.0	0.0	.341	.301	3785621.
61202	N	ST	10.0	0.0	.341	.301	3785621.	0.0000	0.00	61204	N	ST	12.0	0.0	.345	.301	3814433.	0.0000	0.00	61204	N	ST	12.0	0.0	.345	.301	3814433.
61204	N	ST	12.0	0.0	.345	.301	3814433.	0.0000	0.00	61206	N	ST	12.0	0.0	.344	.301	3814433.	0.0000	0.00	61206	N	ST	12.0	0.0	.344	.301	3814433.
61206	N	ST	12.0	0.0	.344	.301	3814433.	0.0000	0.00	61214	N	ST	16.5	0.0	.342	.301	3790531.	0.0000	0.00	61214	N	ST	16.5	0.0	.342	.301	3790531.
61214	N	ST	16.5	0.0	.342	.301	3790531.	0.0000	0.00	61215	N	ST	18.0	0.0	.341	.301	3786607.	0.0000	0.00	61215	N	ST	18.0	0.0	.341	.301	3786607.
61215	N	ST	18.0	0.0	.341	.301	3786607.	0.0000	0.00	61218	N	ST	18.0	0.0	.341	.301	3784574.	0.0000	0.00	61218	N	ST	18.0	0.0	.341	.301	3784574.
61218	N	ST	18.0	0.0	.341	.301	3784574.	0.0000	0.00	61221	N	ST	5.0	0.0	.342	.301	3785621.	0.0000	0.00	61221	N	ST	5.0	0.0	.342	.301	3785621.
61221	N	ST	5.0	0.0	.342	.301	3785621.	0.0000	0.00	61222	N	ST	5.0	0.0	.342	.301	3786607.	0.0000	0.00	61222	N	ST	5.0	0.0	.342	.301	3786607.
61222	N	ST	5.0	0.0	.342	.301	3786607.	0.0000	0.00	61223	N	ST	5.0	0.0	.342	.301	37870314.	0.0000	0.00	61223	N	ST	5.0	0.0	.342	.301	37870314.
61223	N	ST	5.0	0.0	.342	.301	37870314.	0.0000	0.00	61300	N	ST	2.0	0.0	.613	.250	3194392.	0.0000	0.00	61300	N	ST	2.0	0.0	.613	.250	3194392.
61300	N	ST	2.0	0.0	.613	.250	3194392.	0.0000	0.00	61301	N	ST	2.0	0.0	.612	.250	3191078.	0.0000	0.00	61301	N	ST	2.0	0.0	.612	.250	3191078.
61301	N	ST	2.0	0.0	.612	.250	3191078.	0.0000	0.00	61302	N	ST	2.0	0.0	.612	.250	3192688.	0.0000	0.00	61302	N	ST	2.0	0.0	.612	.250	3192688.
61302	N	ST	2.0	0.0	.612	.250	3192688.	0.0000	0.00	61303	N	ST	5.0	0.0	.612	.251	3401495.	0.0000	0.00	61303	N	ST	5.0	0.0	.612	.251	3401495.
61303	N	ST	5.0	0.0	.612	.251	3401495.	0.0000	0.00	61306	N	ST	8.0	0.0	.616	.251	3401495.	0.0000	0.00	61306	N	ST	8.0	0.0	.616	.251	3401495.
61306	N	ST	8.0	0.0	.616	.251	3401495.	0.0000	0.00	61307	N	ST	10.0	0.0	.619	.251	3402068.	0.0000	0.00	61307	N	ST	10.0	0.0	.619	.251	3402068.
61307	N	ST	10.0	0.0	.619	.251	3402068.	0.0000	0.00	61308	N	ST	12.5	0.0	.613	.249	3381325.	0.0000	0.00	61308	N	ST	12.5	0.0	.613	.249	3381325.
61308	N	ST	12.5	0.0	.613	.249	3381325.	0.0000	0.00	61309	N	ST	13.0	0.0	.610	.250	3381216.	0.0000	0.00	61309	N	ST	13.0	0.0	.610	.250	3381216.
61309	N	ST	13.0	0.0	.610	.250	3381216.	0.0000	0.00	61310	N	ST	13.0	0.0	.610	.249	3384760.	0.0000	0.00	61310	N	ST	13.0	0.0	.610	.249	3384760.
61310	N	ST	13.0	0.0	.610	.249	3384760.	0.0000	0.00	61311	N	ST	14.0	0.0	.619	.251	3385628.	0.0000	0.00	61311	N	ST	14.0	0.0	.619	.251	3385628.
61311	N	ST	14.0	0.0	.619	.251	3385628.	0.0000	0.00	61312	N	ST	15.0	0.0	.611	.249	3361196.	0.0000	0.00	61312	N	ST	15.0	0.0	.611	.249	3361196.
61312	N	ST	15.0	0.0	.611	.249	3361196.	0.0000	0.00	61315	N	ST	16.0	0.0	.611	.249	3363488.	0.0000	0.00	61315	N	ST	16.0	0.0	.611	.249	3363488.
61315	N	ST	16.0	0.0	.611	.249	3363488.	0.0000	0.00	61316	N	ST	20.0	0.0	.612	.250	3357544.	0.0000	0.00	61316	N	ST	20.0	0.0	.612	.250	3357544.
61316	N	ST	20.0	0.0	.612	.250	3357544.	0.0000	0.00	61317	N	ST	25.0	0.0	.612	.250	3344638.	0.0000	0.00	61317	N	ST	25.0	0.0	.612	.250	3344638.
61317	N	ST	25.0	0.0	.612	.250	3344638.	0.0000	0.00	61318	N	ST	14.0	0.0	.612	.250	3349019.	0.0000	0.00	61318	N	ST	14.0	0.0	.612	.250	3349019.
61318	N	ST	14.0	0.0	.612	.250	3349019.	0.0000	0.00	61319	N	ST	12.5	0.0	.614	.250	3357487.	0.0000	0.00	61319	N	ST	12.5	0.0	.614	.250	3357487.
61319	N	ST	12.5	0.0	.614	.250	3357487.	0.0000	0.00	61400	N	ST	5.0	0.0	.613	.249	3372794.	0.0000	0.00	61400	N	ST	5.0	0.0	.613	.249	3372794.
61400	N	ST	5.0	0.0	.613	.249	3372794.	0.0000	0.00	61401	N	ST	5.0	0.0	.612	.250	3264756.	0.0000	0.00	61401	N	ST	5.0	0.0	.612	.250	3264756.
61401	N	ST	5.0	0.0	.612	.250	3264756.	0.0000	0.00	61407	N	ST	5.0	0.0	.612	.250	3961952.	0.0000	0.00	61407	N	ST	5.0	0.0	.612	.250	3961952.
61407	N	ST	5.0	0.0	.612	.250	3961952.	0.0000	0.00	61409	N	ST	2.0	0.0	.878	.302	3970720.	0.0000	0.00	61409	N	ST	2.0	0.0	.878	.302	3970720.
61409	N	ST	2.0	0.0	.878	.302	3970720.	0.0000	0.00	61410	N	ST	2.0	0.0	.877	.302	3963168.	0.0000	0.00	61410	N	ST	2.0	0.0	.877	.302	3963168.
61410	N	ST	2.0	0.0	.877	.302	3963168.	0.0000	0.00	61411	N	ST	2.0	0.0	.877												

TABLE 11.- Continued.

(g) Concluded.

A	FRAME	TRIP	TYPE	A0	A1	Q	N	RE	K	B	FRAME
63320	N	US	2.5	10.0	.878	.303	3739575.		.0969	5.36	63321
63323	N	US	2.7	10.0	.880	.303	3746774.		.0969	5.36	63400
64019	Y	US	15.0	10.0	.844	.296	3865490.		.0247	1.31	64020
64021	Y	US	15.0	10.0	.840	.295	3813567.		.0493	2.62	64022
64023	Y	US	15.0	10.0	.821	.292	3752005.		.0997	5.24	64100
64107	Y	US	15.0	10.0	.840	.185	2448919.		.0496	1.65	64108
64109	Y	US	15.0	10.0	.840	.184	2439010.		.0991	3.30	64110
64111	Y	US	15.0	10.0	.841	.185	2439626.		.1481	4.95	64112
64119	Y	US	2.5	10.0	.876	.302	3823417.		.0099	5.4	64120
64121	Y	US	2.5	10.0	.875	.302	3785031.		.0244	1.34	64122
64202	Y	US	2.5	10.0	.879	.303	3794515.		.0487	2.68	64203
64204	Y	US	2.5	10.0	.878	.302	3774318.		.0974	5.36	64205
64212	Y	US	-2.0	10.0	.877	.302	3717936.		.0098	5.4	
64213	Y	US	-2.0	10.0	.878	.303	3695424.		.0241	1.34	
64214	Y	US	-2.0	10.0	.878	.302	3685179.		.0482	2.68	
64215	Y	US	-2.0	10.0	.880	.303	3683703.		.0963	5.36	
65121	N	US	-2.0	10.0	.869	.300	3717371.		.0098	5.4	
65122	N	US	-2.0	10.0	.873	.301	3700235.		.0243	1.34	
65123	N	US	-2.0	10.0	.874	.301	3694893.		.0485	2.68	
65200	N	US	-2.0	10.0	.877	.302	3694943.		.0958	5.36	
65207	N	US	15.0	10.0	.895	.199	264668.		.0997	3.57	
65209	N	US	15.0	10.0	.828	.292	3779170.		.1019	5.36	
65223	N	US	7.0	5.0	.121	.109	1475396.		.0249	4.9	
65300	N	US	7.0	5.0	.121	.109	1472656.		.1996	3.92	
65311	N	US	7.0	5.0	.879	.301	3862901.		.1969	10.72	
65309	N	US	7.0	5.0	.876	.301	3889117.		.0100	5.4	
63222	N	US	15.0	2.0	.818	.291	3675798.		.2028	10.72	63223

TABLE 11.- Continued.

(h) NLR-7301.

A										B									
FRAME	TRIP	TYPE	AO	A1	G	M	RE	K	FREQ	FRAME	TRIP	TYPE	AO	A1	G	M	RE	K	FREQ
66019	N	ST	5.0	0.0	872	300	4003817	0.0000	0.00	66020	N	ST	20.0	0.0	122	109	1517157	0.0000	0.00
66021	N	ST	2.0	0.0	876	300	3999020	0.0000	0.00	66023	N	ST	25.0	0.0	122	109	1520439	0.0000	0.00
66022	N	ST	0.0	0.0	883	301	3992026	0.0000	0.00	66023	N	ST	17.0	0.0	122	109	1519469	0.0000	0.00
66101	N	ST	2.0	0.0	881	301	3987844	0.0000	0.00	66103	N	ST	15.0	0.0	121	108	1513500	0.0000	0.00
66109	N	ST	5.0	0.0	877	300	3982368	0.0000	0.00	66103	N	ST	13.0	0.0	121	109	1513362	0.0000	0.00
66110	N	ST	8.0	0.0	876	300	3968075	0.0000	0.00	66111	N	ST	12.0	0.0	122	109	1519732	0.0000	0.00
66112	N	ST	10.0	0.0	867	299	3933468	0.0000	0.00	66111	N	ST	11.5	0.0	122	109	1517895	0.0000	0.00
66114	N	ST	12.0	0.0	872	287	3704350	0.0000	0.00	66115	N	ST	15.0	0.0	121	109	1516191	0.0000	0.00
66116	N	ST	14.0	0.0	717	270	3554317	0.0000	0.00	66115	N	ST	10.0	0.0	124	110	1528731	0.0000	0.00
66118	N	ST	16.0	0.0	701	267	3518002	0.0000	0.00	66117	N	ST	0.0	0.0	337	183	2468560	0.0000	0.00
66120	N	ST	17.6	0.0	733	274	3568933	0.0000	0.00	66119	Y	ST	0.0	0.0	338	183	2463486	0.0000	0.00
66122	N	ST	18.3	0.0	737	274	3591274	0.0000	0.00	66121	Y	ST	0.0	0.0	338	182	2456240	0.0000	0.00
66200	N	ST	20.0	0.0	702	274	3499749	0.0000	0.00	66123	Y	ST	12.0	0.0	338	182	2456043	0.0000	0.00
66201	N	ST	17.0	0.0	709	269	3499749	0.0000	0.00	66200	Y	ST	14.7	0.0	338	182	2454470	0.0000	0.00
66208	N	ST	15.0	0.0	709	269	3515184	0.0000	0.00	66209	Y	ST	15.5	0.0	343	184	2472156	0.0000	0.00
66209	N	ST	5.0	0.0	877	300	3932765	0.0000	0.00	66210	Y	ST	17.0	0.0	337	183	2452276	0.0000	0.00
66214	N	ST	0.0	0.0	875	300	3922572	0.0000	0.00	66211	Y	ST	18.0	0.0	338	183	2453445	0.0000	0.00
66216	N	ST	5.0	0.0	609	248	3274639	0.0000	0.00	66212	Y	ST	20.0	0.0	338	183	2453475	0.0000	0.00
66221	N	ST	8.0	0.0	608	248	3269675	0.0000	0.00	66213	Y	ST	25.0	0.0	343	184	2466074	0.0000	0.00
66222	N	ST	10.0	0.0	610	248	3271957	0.0000	0.00	66214	Y	ST	17.0	0.0	343	184	2464659	0.0000	0.00
66223	N	ST	12.0	0.0	606	247	3251575	0.0000	0.00	66215	Y	ST	14.7	0.0	339	183	2452952	0.0000	0.00
66300	N	ST	14.0	0.0	607	248	3245841	0.0000	0.00	66216	Y	ST	10.0	0.0	341	184	2459672	0.0000	0.00
66301	N	ST	16.0	0.0	608	248	3245841	0.0000	0.00	66217	Y	ST	5.0	0.0	873	300	3962919	0.0000	0.00
66302	N	ST	17.2	0.0	612	248	3235888	0.0000	0.00	66218	Y	ST	8.0	0.0	875	300	3952795	0.0000	0.00
66304	N	ST	20.0	0.0	612	249	3234835	0.0000	0.00	66219	Y	ST	10.0	0.0	875	300	3952795	0.0000	0.00
66305	N	ST	25.0	0.0	602	247	3196460	0.0000	0.00	66220	Y	ST	12.0	0.0	820	290	3965900	0.0000	0.00
66306	N	ST	17.0	0.0	608	248	3218130	0.0000	0.00	66221	Y	ST	13.0	0.0	874	300	3915017	0.0000	0.00
66307	N	ST	15.0	0.0	612	249	3223516	0.0000	0.00	66222	Y	ST	15.0	10.0	339	183	2438650	0.0000	0.00
66308	N	ST	14.0	0.0	612	249	3229433	0.0000	0.00	66223	Y	US	15.0	10.0	340	184	2433341	0.0000	0.00
66313	N	ST	5.0	0.0	606	248	3252538	0.0000	0.00	66224	Y	US	10.0	5.0	880	301	3908675	0.0000	0.00
66314	N	ST	5.0	0.0	606	248	3252538	0.0000	0.00	66225	Y	US	10.0	5.0	880	301	3908675	0.0000	0.00
66320	N	ST	5.0	0.0	340	184	2457291	0.0000	0.00	66226	Y	US	10.0	5.0	862	298	3742499	0.0000	0.00
66321	N	ST	5.0	0.0	339	183	2457291	0.0000	0.00	66227	Y	US	10.0	5.0	862	298	3742499	0.0000	0.00
66405	N	ST	8.0	0.0	339	183	2463521	0.0000	0.00	66228	Y	US	10.0	5.0	862	298	3742499	0.0000	0.00
66406	N	ST	10.0	0.0	339	183	2464683	0.0000	0.00	66229	Y	US	10.0	5.0	862	298	3742499	0.0000	0.00
66408	N	ST	12.0	0.0	340	184	2457696	0.0000	0.00	66230	Y	US	10.0	5.0	862	298	3742499	0.0000	0.00
66410	N	ST	14.0	0.0	340	184	2457291	0.0000	0.00	66231	Y	US	10.0	5.0	862	298	3742499	0.0000	0.00
66412	N	ST	16.0	0.0	339	183	2452670	0.0000	0.00	66232	Y	US	10.0	5.0	862	298	3742499	0.0000	0.00
66421	N	ST	17.4	0.0	341	184	2455643	0.0000	0.00	66233	Y	US	10.0	5.0	862	298	3742499	0.0000	0.00
66423	N	ST	20.0	0.0	338	183	2458201	0.0000	0.00	66234	Y	US	10.0	5.0	862	298	3742499	0.0000	0.00
66500	N	ST	25.0	0.0	339	183	2447905	0.0000	0.00	66235	Y	US	10.0	5.0	862	298	3742499	0.0000	0.00
66501	N	ST	17.0	0.0	339	183	2450544	0.0000	0.00	66236	Y	US	10.0	5.0	862	298	3742499	0.0000	0.00
66502	N	ST	15.0	0.0	339	183	2452240	0.0000	0.00	66237	Y	US	10.0	5.0	862	298	3742499	0.0000	0.00
66503	N	ST	14.0	0.0	337	183	2448905	0.0000	0.00	66238	Y	US	10.0	5.0	862	298	3742499	0.0000	0.00
66504	N	ST	13.0	0.0	338	183	2449911	0.0000	0.00	66239	Y	US	10.0	5.0	862	298	3742499	0.0000	0.00
66510	N	ST	5.0	0.0	339	183	2451875	0.0000	0.00	66240	Y	US	10.0	5.0	862	298	3742499	0.0000	0.00
66511	N	ST	5.0	0.0	338	183	2553873	0.0000	0.00	66241	Y	US	10.0	5.0	862	298	3742499	0.0000	0.00
66516	N	ST	5.0	0.0	339	183	2555680	0.0000	0.00	66242	Y	US	10.0	5.0	862	298	3742499	0.0000	0.00
66518	N	ST	5.0	0.0	121	108	1533072	0.0000	0.00	66243	Y	US	10.0	5.0	862	298	3742499	0.0000	0.00
66600	N	ST	5.0	0.0	122	109	1533757	0.0000	0.00	66244	Y	US	10.0	5.0	862	298	3742499	0.0000	0.00
66601	N	ST	5.0	0.0	121	109	1534255	0.0000	0.00	66245	Y	US	10.0	5.0	862	298	3742499	0.0000	0.00
66602	N	ST	10.0	0.0	122	109	1527646	0.0000	0.00	66246	Y	US	10.0	5.0	862	298	3742499	0.0000	0.00
66603	N	ST	12.0	0.0	120	109	1519094	0.0000	0.00	66247	Y	US	10.0	5.0	862	298	3742499	0.0000	0.00
66604	N	ST	14.0	0.0	120	109	1516730	0.0000	0.00	66248	Y	US	10.0	5.0	862	298	3742499	0.0000	0.00
66605	N	ST	16.0	0.0	121	108	1516123	0.0000	0.00	66249	Y	US	10.0	5.0	862	298	3742499	0.0000	0.00
66606	N	ST	16.5	0.0	121	109	1517915	0.0000	0.00	66250	Y	US	10.0	5.0	862	298	3742499	0.0000	0.00

TABLE 11.- Concluded.  
(h) Concluded.

A				B						
FRAME	TRIP	TYPE	AO	A1	Q	H	RE	K	FREQ	FRAME
69100	N	US	10.0	10.0	.873	.300	3918788.	.0249	1.34	69101
69102	N	US	10.0	10.0	.874	.300	3900063.	.0496	2.68	69103
69105	N	US	10.0	10.0	.877	.301	3904003.	.0991	5.36	69106
69107	N	US	10.0	10.0	.876	.300	3684160.	.1484	8.04	69108
69119	N	US	16.8	2.0	.727	.273	3492462.	.0270	1.34	69120
69121	N	US	16.8	2.0	.710	.270	3430737.	.0546	2.68	69122
69123	N	US	16.8	2.0	.700	.268	3396634.	.1100	5.36	69200
69201	N	US	16.8	2.0	.692	.267	3366793.	.2308	10.72	69202
69206	N	US	17.2	2.0	.734	.275	3160151.	.0268	1.34	69207
69208	N	US	17.2	2.0	.745	.277	3469110.	.0530	2.68	69209
69211	N	US	17.2	2.0	.709	.270	3370669.	.1086	5.36	69212
69213	N	US	17.2	2.0	.719	.272	3397722.	.1616	8.04	69214
69215	N	US	17.2	2.0	.755	.279	3459727.	.2098	10.72	69216
69221	N	US	17.5	2.0	.726	.273	3404711.	.0536	2.68	69222
69223	N	US	17.5	2.0	.654	.265	3296912.	.2205	10.72	69300
69304	N	US	18.5	2.0	.688	.266	3265767.	.0549	2.68	69305
69310	N	US	18.5	2.0	.671	.262	3218013.	.0554	2.68	69311
70019	N	US	9.4	10.0	.341	.185	2344307.	.0245	.83	70020
70021	N	US	9.4	10.0	.340	.185	2326519.	.0973	3.30	70022
70023	N	US	9.4	10.0	.340	.185	2336677.	.1948	6.60	70100
70107	N	US	5.7	10.0	.875	.301	3916444.	.0104	.56	70108
70109	N	US	5.7	10.0	.876	.301	3876178.	.0247	1.34	70110
70113	N	US	5.7	10.0	.872	.300	3851569.	.0495	2.68	70114
70115	N	US	5.7	10.0	.875	.301	3854554.	.0936	5.36	70116
70117	N	US	5.7	10.0	.874	.301	3843662.	.1479	8.04	70118

TABLE 12.- LIST OF STATIC DATA

Airfoil <sup>a</sup>	M <sub>∞</sub>	First frame	Last frame	No. of frames	α <sub>min</sub>	α <sub>max</sub>	Figure	Airfoil <sup>a</sup>	M <sub>∞</sub>	First frame	Last frame	No. of frames	α <sub>min</sub>	α <sub>max</sub>	Figure
N-0012	0.30	04019	04412	24	-5.0	20.0		FX-098T	0.30	17208	17314	8	0.0	20.0	
	.30	11018	11309	33	-5.0	30.0	9,12,16	FX-098T	.18	18019	18206	10	0.0	20.0	
	.30	12102	(quasi-steady)		-5.0	15.0	16	SC-1095	.30	35021	35214	17	-5.0	16.0	19
	.28	12109			-4.0	16.0		SC-1095	.25	35220	35401	20	-5.0	25.0	
	.28	13222			10.1	29.9		SC-1095	.18	36019	36120	10	-5.0	20.0	
	.27	12020			10.1	29.9		SC-1095	.11	36202	36218	11	-5.0	20.0	
	.26	12118			10.1	29.9		SC-1095T	.30	34022	34115	8	0.0	16.0	
	.25	12208			-3.0	17.0		SC-1095T	.18	34200	34214	7	0.0	16.0	
	.25	13303			-3.0	17.0		HH-02	.30	40222	41103	20	-5.0	20.0	20
	.23	12203			10.1	29.9		HH-02	.25	41110	41215	20	-5.0	20.0	
	.22	13308			-3.0	17.0		HH-02	.18	40114	40215	10	-5.0	20.0	
	.22	13310			-3.0	17.0		HH-02	.11	40018	40108	11	-5.0	20.0	
	.20	12300			10.1	29.9		HH-02T	.30	41221	41314	8	0.0	16.0	
	.18	12310			-3.0	17.0		HH-02T	.18	41401	41419	10	0.0	16.0	
	.17	12305			10.1	29.9		VR-7	.30	46418	46615	18	-5.0	25.0	11,21
	.11	13021			-3.0	17.0		VR-7	.25	46307	46412	19	-5.0	25.0	
	.11	13107			10.1	29.9		VR-7	.18	46116	46301	13	-5.0	25.0	
	.07	13120			-3.0	17.0		VR-7	.11	46018	46110	13	-5.0	25.0	
	.07	13115			10.1	29.9		VR-7T	.30	46802	46823	10	0.0	20.0	
	.04	13205			-5.0	15.0		VR-7T	.18	46621	46718	10	0.0	20.0	
	.04	13217			10.1	29.9		NLR-1	.30	61407	61606	19	-5.0	25.0	22
N-0012T	.29	13321			-3.0	17.0		NLR-1	.25	61221	61401	19	-5.0	25.0	
N-0012T	.18	13313			-3.0	17.0		NLR-1	.18	61114	61215	10	-5.0	20.0	
Ames-01	.30	26020	26307	23	-5.0	25.0	17	NLR-1	.11	61018	61108	11	-5.0	20.0	
Ames-01	.25	26313	27117	22	-5.0	25.0		NLR-1T	.30	65019	65115	13	-11.0	16.0	
Ames-01	.18	27123	27318	22	-5.0	25.0		NLR-1T	.18	64221	64311	8	0.0	16.0	
Ames-01	.11	27400	28120	21	-5.0	25.0		NLR-7301	.30	66019	66209	17	-5.0	20.0	23
Ames-01T	.30	28312	28410	9	0.0	16.0		NLR-7301	.25	66214	66314	17	-5.0	25.0	
Ames-01T	.19	28207	28304	10	0.0	20.0		NLR-7301	.18	66320	66511	18	-5.0	25.0	
FX-098	.30	20118	20322	21	-5.0	25.0	18	NLR-7301	.11	66516	66617	17	-5.0	25.0	
FX-098	.25	19314	20112	22	-5.0	25.0		NLR-7301T	.30	66810	66822	6	0.0	13.0	
FX-098	.18	19020	19308	23	-5.0	25.0		NLR-7301T	.18	66623	66802	13	0.0	25.0	
FX-098	.11	18215	18502	23	-5.0	25.0	10								

<sup>a</sup>T = trip.

TABLE 13.- MACH NUMBER SWEEP AT  $\alpha = 15^\circ + 10^\circ \sin \omega t$ ,  $k = 0.10$

$M_\infty^\alpha$	NACA 0012	A-01	FX-098	SC-1095	HH-02	VR-7	NLR-1	NLR-7301
0.035	8102		16019			58102		
.07	8114	24323	16105	33022	42121	47123	62020	
.11	8214	24314	16114	33106	42321	{47206 58111	62104	67120
.18	8220	{24217 31209	16200	33110	42302	{47213 58121	62112	67220
.18T	{14021 14106	29117	17103	34321	42110	47112	64109	67021
.20							{62114 65207	
.22	9202	24209	16300	33205	42309	47217	62208	
.25	9203	24201	16308	33207	42313	47301	62210	67305
.28	9208	24117	22208	33215	42218	47305	62218	
.29	{9217 14220	24105	22201	33300	42210	45023	{62307 65209	
.29T	{14208 14210	29106	17200	34308	42100	47100	64023	

$\alpha_T = \text{trip.}$

TABLE 14.- FREQUENCY SWEEP AT  $M_\infty = 0.29$ ,  $\alpha = 15^\circ + 10^\circ \sin \omega t$

$k^\alpha$	NACA 0012	A-01	FX-098	SC-1095	HH-02	VR-7	NLR-1	NLR-7301
0.01	9210	{30019 30020	21100	38300				
.025	{9213 14218	24022	22023	33217	42206	45019	62302	
.025T	{14117 14200	29023	17117		42019	47020	64019	
.05	{9214 14219	24100	22103	33222	42208	45021	62304	
.05T	{14119 14202	29101	17119	34306	42021	47022	64021	
.10	{9217 14220	24105	22201	33300	42210	45023	{62307 65209	
.10T	{14208 14210	29106	17200	34308	42100	47100	64023	
.15	9218	24109	22206	34409	{42212 42217	45101	62309	

$\alpha_T = \text{trip.}$

TABLE 15.- FREQUENCY SWEEP AT  $M_\infty = 0.30$ ,  $\alpha = 10^\circ + 10^\circ \sin \omega t$

k	NACA 0012	A-01	FX-098	SC-1095	HH-02	VR-7	NLR-1	NLR-7301
0.01	9221	30105	21107	38306	43019	45109	62317	69019
.025	9222	{25022 31102	22216	37023	43106	45111	62320	69100
.05	9223	{25102 31104	22217	37101	43108	45113	62322	69102
.10	9302	25104	22218	37107	43112	45117	62400	69105
.12							62403	
.15	9307	{25109 31110 31112	22219	37109	{43114 43117	45119	62405	69107

TABLE 16.- FREQUENCY SWEEP AT  $M_\infty = 0.30$ ,  $\alpha = 15^\circ + 5^\circ \sin \omega t$

k	NACA 0012	A-01	FX-098	SC-1095	HH-02	VR-7	NLR-1	NLR-7301
0.01	10113	30110	21112	39104		45203	63018	68019
.025	10114	25204	23021	38021	43303	45205	63019	68100
.05	10117	25205	23022	38022	43304	45207	63020	68102
.10	10118	25208	23023	38102	43305	45209	63021	68104
.12							63100	
.15	10120	25209	23100	38103	43308	45211	63101	68109
.20	10123	25210	23101	38104	43309	45213	63102	68111

TABLE 17.- FREQUENCY SWEEP AT  $M_\infty = 0.30$ ,  $\alpha = 10^\circ + 5^\circ \sin \omega t$

k	NACA 0012	A-01	FX-098	SC-1095	HH-02	VR-7	NLR-1	NLR-7301	NLR-7301T
0.01	10202	30119	21200	39107	44019			68119	
.025	{7112 10203	25117	22307	37207	{44021 44119	45221	63108	68121	67108
.05	{7222 10204	25118	22308	37208	44023	45223		68123	67110
.075	10207								
.10	{7113 10208	25119	22309	37210	{44104 44118	45300	63112	68201	67112
.15	{7300 10211	{25121 25122	22311	37213	44106	45302			
.20	{7114 10212	25123	22312	37215	{44112 44120	45303	63114	68203	



TABLE 18.- STALL ONSET AT  $M_\infty = 0.30$ ,  $\alpha = \alpha_0 + 10^\circ \sin \omega t$ ,  $k = 0.10$

NACA 0012, $\alpha_0 = 3.8^\circ$	A-01, $\alpha_0 = 5.5^\circ$	FX-098, $\alpha_0 = 3.8^\circ$	SC-1095, $\alpha_0 = 4.4^\circ$	HH-02, $\alpha_0 = 4.0^\circ$	VR-7, $\alpha_0 = 4.6^\circ$	NLR-1, $\alpha_0 = 2.7^\circ$	NLR-7301, $\alpha_0 = 5.7^\circ$
10305	25319	23201	34418	43219	63323	70115	

TABLE 19.- STALL SUPPRESSION AT  $M_\infty = 0.30$ ,  $\alpha = \alpha_0 + 10^\circ \sin \omega t$

k	NACA 0012 $\alpha_0 = 5.0^\circ$	A-01, $\alpha_0 = 5.0^\circ$	FX-098, $\alpha_0 = 3.3^\circ$	SC-1095, $\alpha_0 = 4.1^\circ$	HH-02, $\alpha_0 = 3.8^\circ$	VR-7, $\alpha_0 = 4.1^\circ$	NLR-1, $\alpha_0 = 2.5^\circ$	NLR-7301, $\alpha_0 = 5.7^\circ$
0.01	29205	21208	39021	43215	48019	63312	70107	
.025	31119			43202	48023	63314	70109	
.05	{29207 31121 25311	23206	37119	43204	48101	63318	70113	
.10	{29211 31123 29213	23208	37121	43206	48103	63320	70115	
.15	{29215 31201	23211	37123	43209			70117	

<sup>a</sup>See table 24.

TABLE 20.- STALL SUPPRESSION AT  $M_\infty = 0.18$ ,  $\alpha = \alpha_0 + 10^\circ \sin \omega t$

k	NACA 0012, $\alpha_0 = 8.0^\circ$	A-01, $\alpha_0 = 7.5^\circ$	FX-098, $\alpha_0 = 6.5^\circ$	SC-1095, $\alpha_0 = 6.2^\circ$	HH-02	VR-7, $\alpha_0 = 4.7^\circ$	NLR-1	NLR-7301, $\alpha_0 = 9.4^\circ$
0.01	9110	30215	21219			50116		70019
.025						49216		
.05	9112	{24302 31215	16213	33118				
.10						49300		70021
.20	9118	{24306 31217	16215	33121		49307		70023
.25						49310		

TABLE 21.- PITCH DAMPING STUDIES AT  $M_\infty = 0.30$ ,  $\alpha = \alpha_0 + 2^\circ \sin \omega t$

NACA 0012	A-01	FX-098	SC-1095	HH-02	VR-7	NLR-1	NLR-7301 $\alpha$
	$k = 0.01$						
	$\alpha_0 = 14.0^\circ$ 30206		$\alpha_0 = 14.0^\circ$ 39115	$\alpha_0 = 12.5^\circ$ 44221	$\alpha_0 = 12.5^\circ$ 48300		
				$\alpha_0 = 15.5^\circ$ 44212			
	$k = 0.025$						
				$\alpha_0 = 12.5^\circ$ 44222	$\alpha_0 = 12.5^\circ$ 48301		$\alpha_0 = 16.8^\circ$ 69119
				$\alpha_0 = 15.5^\circ$ 44214	$\alpha_0 = 13.0^\circ$ 48116		$\alpha_0 = 17.2^\circ$ 69206
	$k = 0.05$						
				$\alpha_0 = 12.5^\circ$ 44223	$\alpha_0 = 12.5^\circ$ 48302	$\alpha_0 = 11.1^\circ$ 63302	$\alpha_0 = 16.5^\circ$ 69310
				$\alpha_0 = 15.5^\circ$ 44215	$\alpha_0 = 13.0^\circ$ 48118	$\alpha_0 = 15.0^\circ$ 63220	$\alpha_0 = 16.8^\circ$ 69121
					$\alpha_0 = 14.0^\circ$ 48215	$\alpha_0 = 17.0^\circ$ 63213	$\alpha_0 = 17.2^\circ$ 69208
							$\alpha_0 = 17.5^\circ$ 69221
							$\alpha_0 = 18.5^\circ$ 69304
	$k = 0.10$						
				$\alpha_0 = 12.5^\circ$ 44300	$\alpha_0 = 12.5^\circ$ 48303		$\alpha_0 = 16.8^\circ$ 69123
				$\alpha_0 = 14.0^\circ$ 44202	$\alpha_0 = 13.0^\circ$ 48122		$\alpha_0 = 17.2^\circ$ 69211
				$\alpha_0 = 15.5^\circ$ 44216	$\alpha_0 = 14.0^\circ$ 48216		

Table 21.- Concluded.

NACA 0012	A-01	FX-098	SC-1095	HH-02	VR-7	NLR-1	NLR-7301 <sup>a</sup>
k = 0.15							
$\alpha_o = 14.5^\circ$ 31310				$\alpha_o = 12.5^\circ$ 44303	$\alpha_o = 12.5^\circ$ 48304		$\alpha_o = 17.2^\circ$ 69213
				$\alpha_o = 15.5^\circ$ 44217			
k = 0.20							
$\alpha_o = 13.5^\circ$ 29223	$\alpha_o = 12.0^\circ$ 23219	$\alpha_o = 12.3^\circ$ 38201	$\alpha_o = 12.5^\circ$ 44304	$\alpha_o = 12.5^\circ$ 48308	$\alpha_o = 12.5^\circ$ 48308	$\alpha_o = 11.1^\circ$ 63304	$\alpha_o = 16.8^\circ$ 69201
$\alpha_o = 14.5^\circ$ 29304	$\alpha_o = 14.0^\circ$ 23305	$\alpha_o = 14.0^\circ$ 38119	$\alpha_o = 14.0^\circ$ 44204	$\alpha_o = 13.0^\circ$ 48200	$\alpha_o = 13.0^\circ$ 48200	$\alpha_o = 15.0^\circ$ 63222	$\alpha_o = 17.2^\circ$ 69215
31302	$\alpha_o = 16.0^\circ$ 23310	$\alpha_o = 16.0^\circ$ 38110	$\alpha_o = 15.5^\circ$ 42218	$\alpha_o = 14.0^\circ$ 48217	$\alpha_o = 14.0^\circ$ 48217	$\alpha_o = 16.4^\circ$ 63208	$\alpha_o = 17.5^\circ$ 69223
$\alpha_o = 16.5^\circ$ 29309			$\alpha_o = 17.5^\circ$ 44209	$\alpha_o = 16.0^\circ$ 48209	$\alpha_o = 16.0^\circ$ 48209	$\alpha_o = 17.0^\circ$ 63215	

<sup>a</sup>See table 24.

TABLE 22.- NO SEPARATION:  $M_\infty = 0.30$ ,  $\alpha = 5^\circ + 5^\circ \sin \omega t$

k	NACA 0012	A-01	FX-098	SC-1095	HH-02	VR-7	NLR-1 <sup>a</sup>	NLR-7301 <sup>a</sup>
0.01	10218							
.10	10221	25301	23107					
.20	10222	25303	23109					68211

<sup>a</sup>See table 24.

TABLE 23.- DYNAMIC BOUNDARY-LAYER TRIP DATA

$M_\infty$	k	NACA 0012	A-01	FX-098	SC-1095	HH-02	VR-7	NLR-1	NLR-7301
0.18	0.05	14019	29115	17100	34318	42108	47110	64107	67019
		14104							
.18	.10	14021	29117	17103	34321	42110	47112	64109	67021
		14106							
.18	.15	14023	29119	17109	34323	42113	47114	64111	
		14108							
.18	.20								67023
.30	.025	14117	29023	17117		42019	47020	64019 <sup>a</sup>	(a)
		14200							
.30	.05	14119	29101	17119	34306	42021	47022	64021 <sup>a</sup>	(a)
		14202							
.30	.10	14208	29106	17200	34308	42100	47100	64023 <sup>a</sup>	(a)
		14210							

<sup>a</sup>See table 24.

TABLE 24.- MISCELLANEOUS DYNAMIC DATA

Airfoil	Frame	$M_\infty$	$\alpha_0$	$\alpha_1$	k	Remarks
N-0012	8019	0.035	10.0	10.0	0.10	Low Reynolds number, $0.5 \times 10^6$
	8021	.035	10.0	10.0	.15	
	8023	.035	10.0	10.0	.25	
	8104	.035	15.0	10.0	.15	
	8106	.035	15.0	14.0	.10	
	8116	.07	15.0	10.0	.15	Match reference 3
	8118	.07	15.0	10.0	.25	
	8123	.07	15.0	14.0	.10	Match reference 3
	8203	.07	10.0	10.0	.25	
	8210	.11	10.0	10.0	.25	
	8222	.18	15.0	10.0	.15	Match reference 3
	8306	.18	15.0	14.0	.10	Match reference 3
	9022	.18	15.0	6.0	.24	Match reference 3
	9101	.18	15.0	5.0	.29	
	9106	.18	10.0	10.0	.25	
	7108	.30	8.0	5.0	.025	Variable $\alpha_0$
	7110		8.0		.10	
	7111		8.0		.20	
	7216		8.8		.05	
	7214		8.8		.10	
	7212		8.8		.15	
	7104		9.0		.025	
	7019		9.0		.05	
	7021		9.0		.10	
	7101		9.0		.15	
	7023		9.0		.20	
			10.0			See table 17
	7117		11.0		.025	
	7118		11.0		.05	
	7119		11.0		.10	
	7120		11.0		.15	
	7121		11.0		.20	
	7200		12.0		.025	
	7202		12.0		.05	
	7205		12.0		.10	
	7305		12.0		.15	
	7207		12.0		.20	
			15.0			See table 16
	10309		2.8	10.0	.10	
	10305		3.8			
	10303		5.0			
	9302		10.0			
	10022		12.0			
	9217	.29	15.0			
	14220	.29	15.0			
	10101	.27	20.0			
	10104	.30	12.0	8.0	.05	Match reference 17
	10105	.30	12.0	8.0	.10	Match reference 17
	10108	.30	12.0	8.0	.13	Match reference 17
	15218	.29	15.0	10.0	.10	Pressure orifices closed

TABLE 24.- Continued.

Airfoil	Frame	$M_\infty$	$\alpha_0$	$\alpha_1$	$k$	Remarks	
N-0012	Many	Variable	Variable	10.0	0.001	Quasi-static; see table 12	
W-098	23117	0.30	5.0	10.0	.10		
Ames-01	30201	↓	11.0	5.0	.01		
Ames-01	25214		↓	↓	.05		
Ames-01	25216		↓	↓	.10		
SC-1095	39110		↓	↓	.01		
	37219		↓	↓	.05		
	37221		↓	↓	.10		
	37304		↓	12.0	8.0	.05	Match reference 18
	37305		↓	12.0	8.0	.10	Match reference 18
	37306		↓	12.0	8.0	.13	Match reference 18
HH-02	43314		↓	11.0	5.0	.025	
HH-02	43315	↓	11.0	5.0	.05		
HH-02	43316	↓	11.0	5.0	.10		
VR-7	54019	.18	10.0	10.0	.025		
	54022	↓	10.0	↓	.05		
	54101	↓	10.0	↓	.10		
	54110	↓	10.0	↓	.15		
	54113	↓	10.0	↓	.20		
	54116	↓	10.0	↓	.25		
	49023	↓	15.0	↓	.01		
	49110	↓	↓	↓	.025		
	49117	↓	↓	↓	.05		
	49120	↓	↓	↓	.10		
	58121	↓	↓	↓	.10		
	49203	↓	↓	↓	.15		
	54216	↓	↓	↓	.15		
	57018	↓	↓	↓	.15		
	58018	↓	↓	↓	.15		
	58120	↓	↓	↓	.15		
	49206	↓	↓	↓	.20		
NLR-1	65223	.11	7.0	5.0	.025	No separation	
	65300	.11	7.0	5.0	.20	No separation	
	62114	.20	15.0	10.0	.10		
	65207	.20	15.0	10.0	.10		
	62121	.20	10.0	10.0	.17	Match reference 19	
	62202	.20	15.0	5.0	.17		
	62201	.20	15.0	5.0	.28		
	62403	.30	10.0	10.0	.12		
	63100	↓	15.0	5.0	.12		
	63122	↓	12.0	8.0	.12		
	65309	↓	7.0	5.0	.01	No separation	
	65311	↓	7.0	5.0	.20	No separation	
	65121	↓	-2.0	10.0	.01	Stall at negative $\alpha$	
	65122	↓	↓	↓	.025	Stall at negative $\alpha$	
	65123	↓	↓	↓	.05	Stall at negative $\alpha$	
	65200	↓	↓	↓	.10	Stall at negative $\alpha$	
NLR-1T	64212	↓	↓	↓	.01	Trip; stall at negative $\alpha$	
NLR-1T	64213	↓	↓	↓	.025	Trip; stall at negative $\alpha$	
NLR-1T	64214	↓	↓	↓	.05	Trip; stall at negative $\alpha$	

TABLE 24.- Concluded.

Airfoil	Frame	$M_\infty$	$\alpha_0$	$\alpha_1$	k	Remarks
NLR-1T	64215	0.30	-2.0	10.0	0.10	Trip; stall at negative $\alpha$
NLR-1T	64119	.30	2.5		.01	Trip; stall suppression
NLR-1T	64121	.30	2.5		.025	Trip; stall suppression
NLR-1T	64202	.30	2.5		.05	Trip; stall suppression
NLR-1T	64204	.30	2.5		.10	Trip; stall suppression
NLR-7	67201	.11	10.0		.10	
	67208	.18	10.0		.025	
	67210	.18	10.0		.10	
	67212	.18	10.0		.20	
	67218	.18	15.0		.025	
	67220	.18	15.0		.10	
	67222	.18	15.0		.20	
	67310	.25	10.0		.10	
	68219	.30	12.0	2.0	.05	No separation
	68221	.30	12.0	2.0	.10	No separation
	68304	.30	12.0	2.0	.20	No separation
NLR-7T	67108	.30	10.0	5.0	.025	Trip
NLR-7T	67110	.30	10.0	5.0	.05	Trip
NLR-7T	67112	.30	10.0	5.0	.10	Trip

TABLE 25.- TEST CASES FOR NUMERICAL ANALYSIS (ref. 1)

Case	Frame	Airfoil	$\alpha_0$	$\alpha_1$	k	Case	Frame	Airfoil	$\alpha_0$	$\alpha_1$	k
1	10222	NACA 0012	5	5	0.20	7	10212	NACA 0012	10	5	0.20
2	68211	NLR-7301	5	↓	↓	8	9302	↓	10	10	.10
3	7111	NACA 0012	8	↓	↓	9	10113	↓	15	5	.01
4	68203	NLR-7301	10	↓	↓	↓	10114	↓	↓	↓	.025
5	7023	NACA 0012	9	↓	↓	↓	10117	↓	↓	↓	.05
6	45221	VR-7	10	↓	.025	↓	10118	↓	↓	↓	.10
↓	45223	↓	↓	↓	.05	↓	10120	↓	↓	↓	.15
↓	45300	↓	↓	↓	.10	↓	10123	↓	↓	↓	.20
↓	45302	↓	↓	↓	.15	10	45203	VR-7	↓	↓	.01
↓	45303	↓	↓	↓	.20	↓	45205	↓	↓	↓	.025
7	10202	NACA 0012	↓	↓	.01	↓	45207	↓	↓	↓	.05
↓	10203	↓	↓	↓	.025	↓	45209	↓	↓	↓	.10
↓	10204	↓	↓	↓	.05	↓	45211	↓	↓	↓	.15
↓	10208	↓	↓	↓	.10	↓	45213	↓	↓	↓	.20
↓	10211	↓	↓	↓	.15	↓	↓	↓	↓	↓	↓



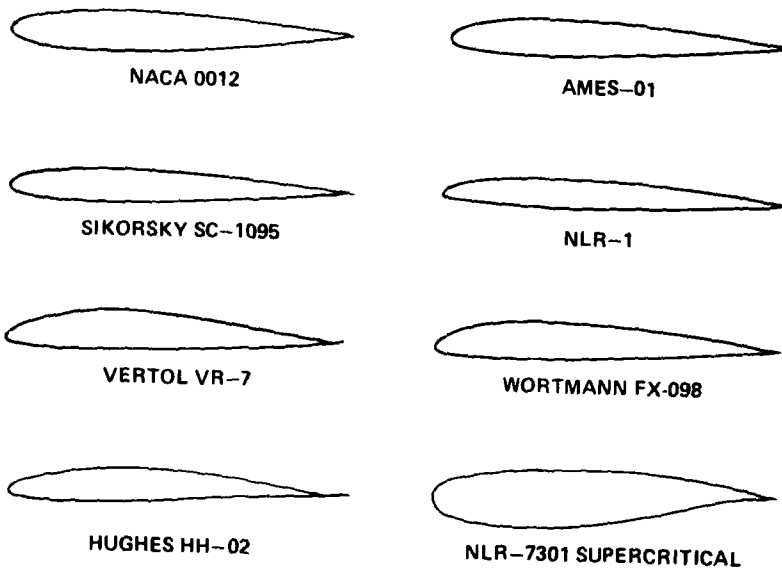


Figure 1.- Airfoils tested in the experiment.

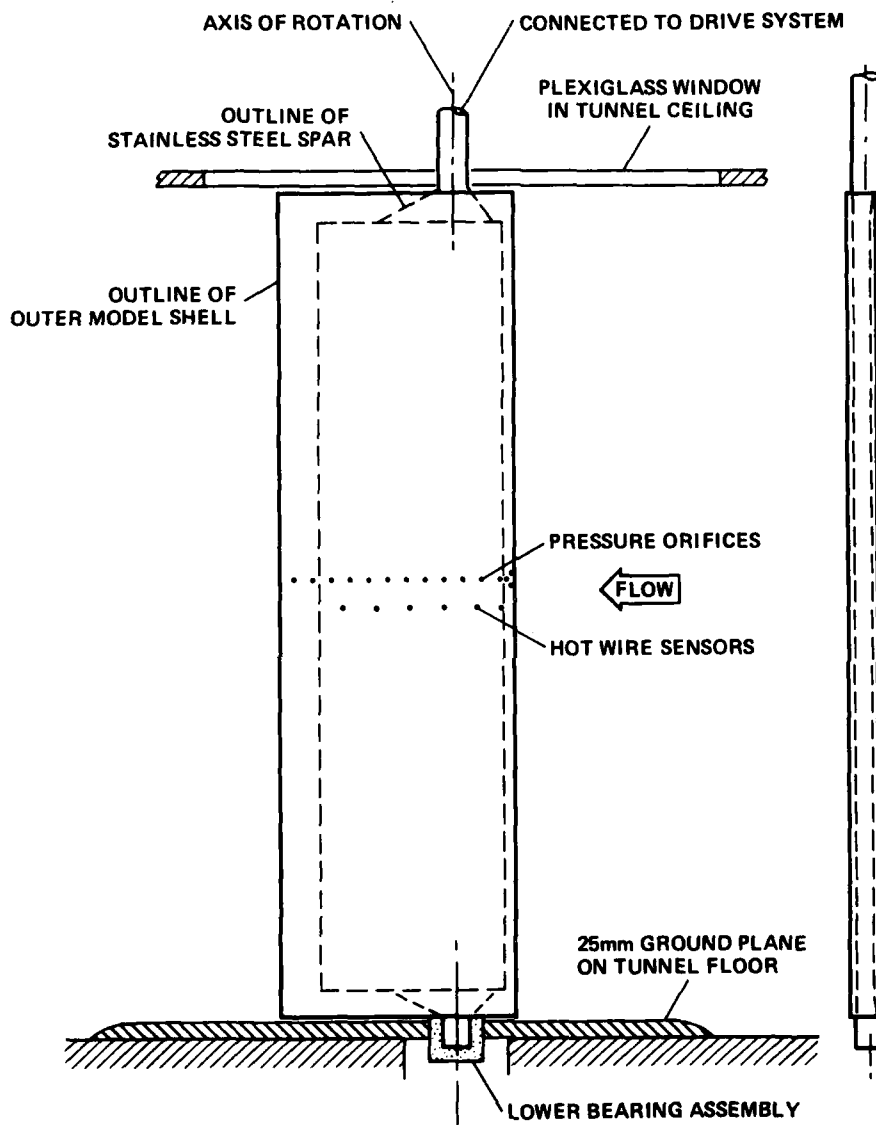


Figure 2.- Model installation in the test section.

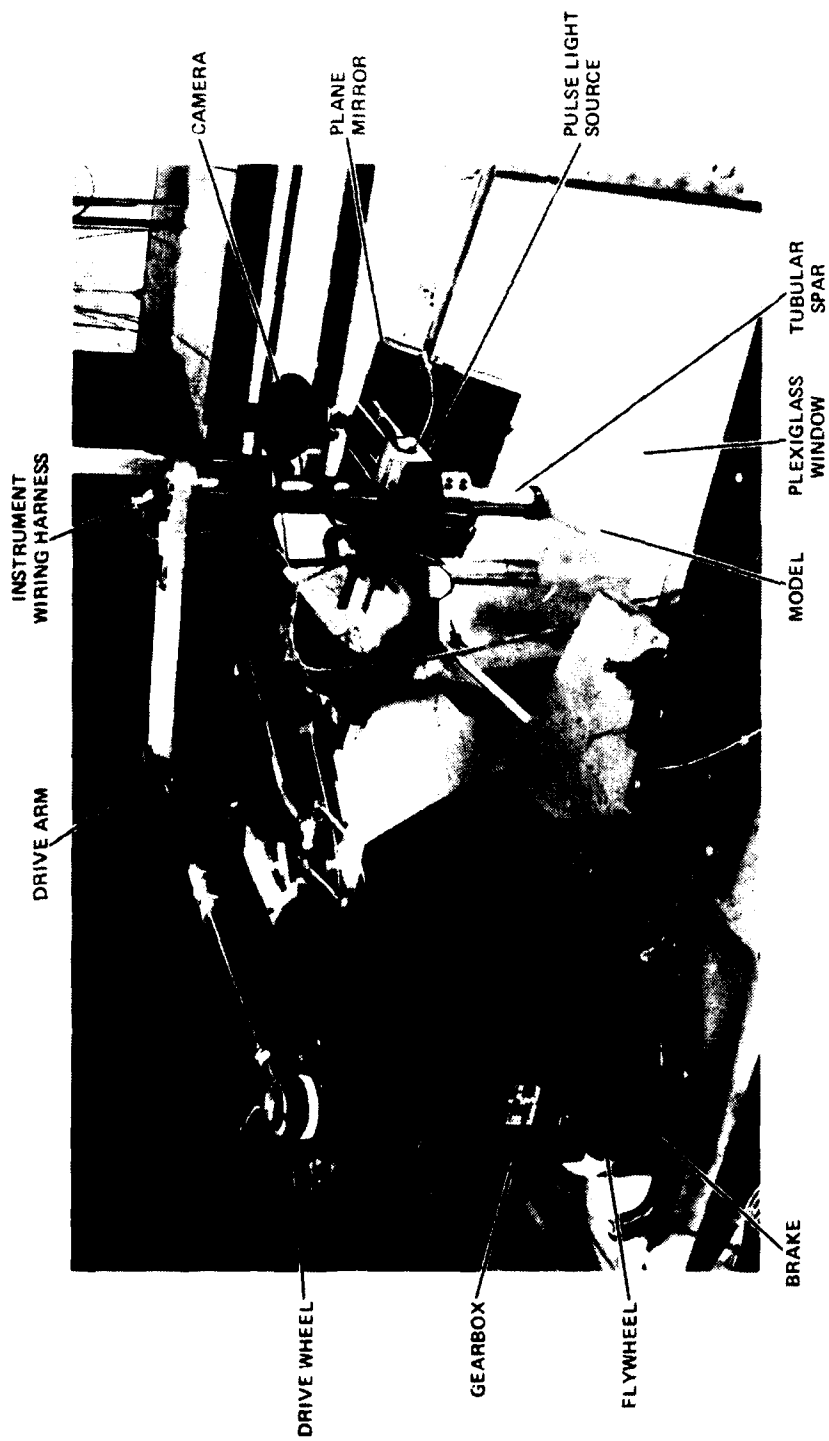
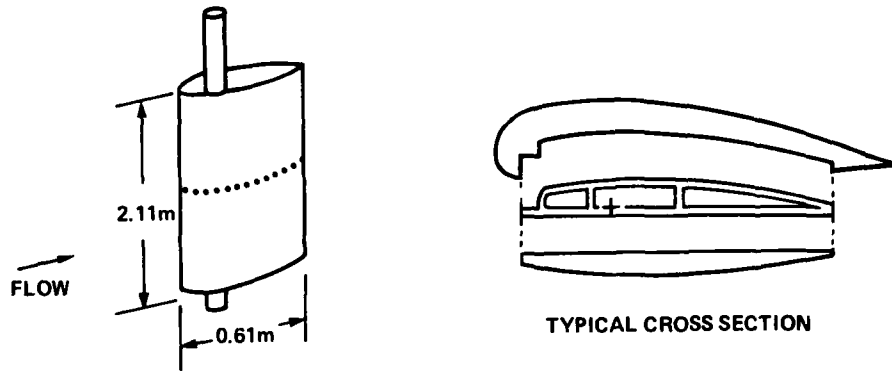


Figure 3.- Photograph of the oscillation mechanism.



WOODEN UPPER SHELL  
WITH FIBERGLASS SKIN

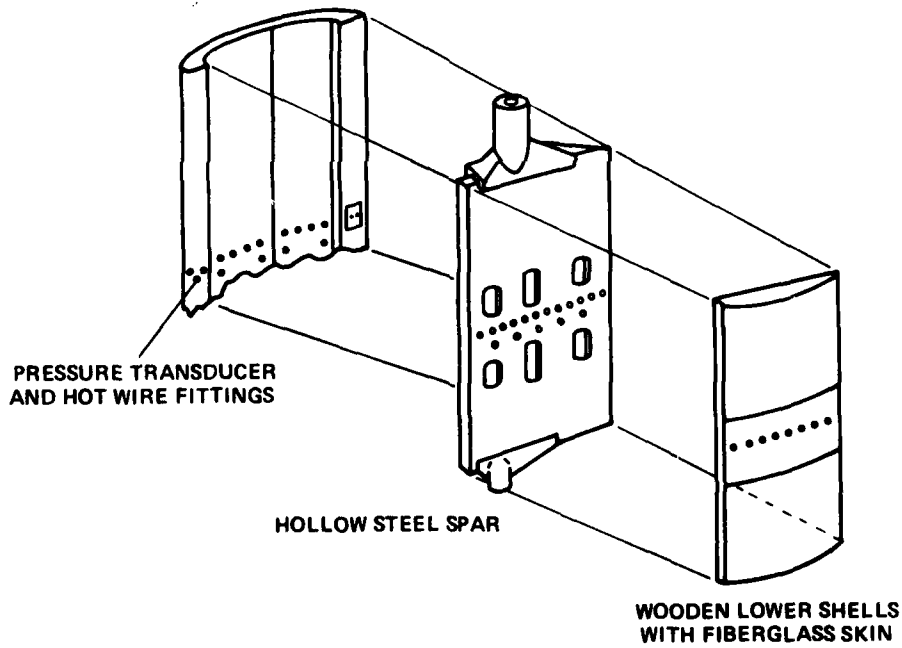


Figure 4.- Sketch of the wooden model shells surrounding the steel spar.

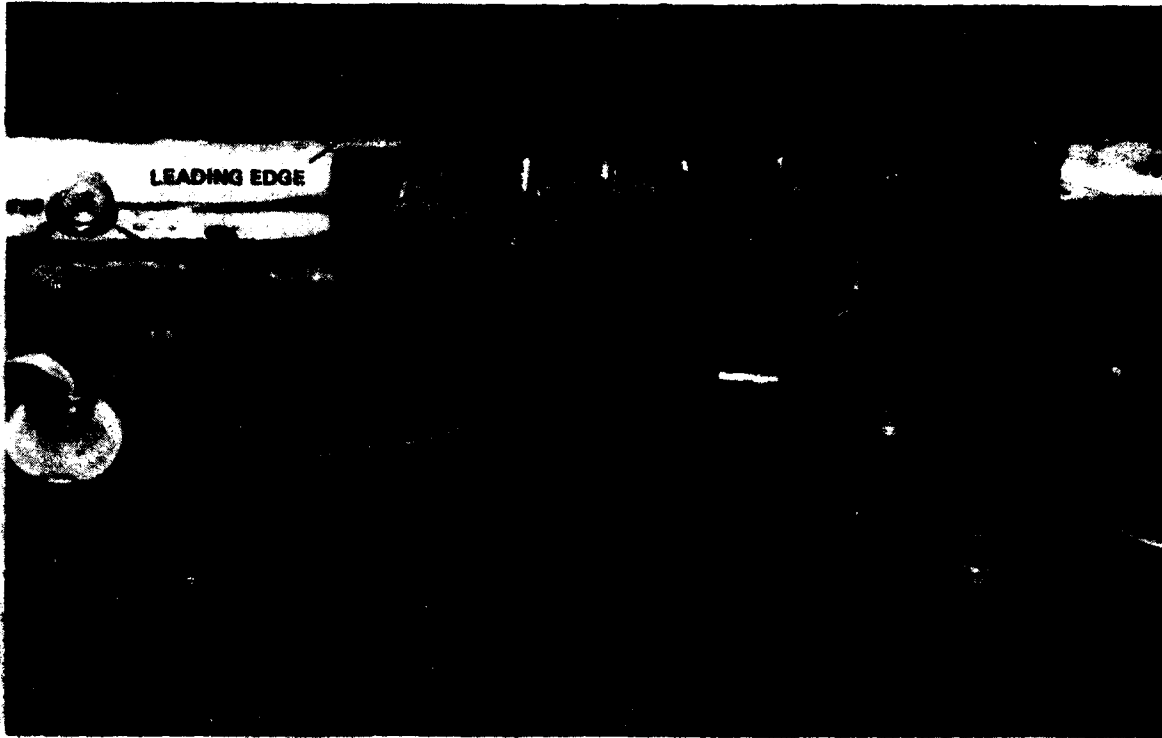


Figure 5.- Pressure transducer and hot-wire installation: view from inside the upper-surface shell.

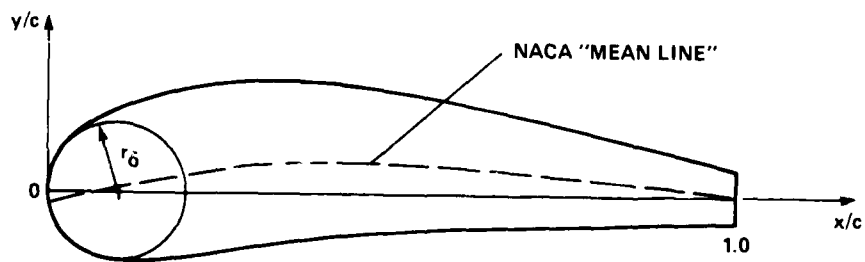


Figure 6.- Coordinate axes for the airfoils.

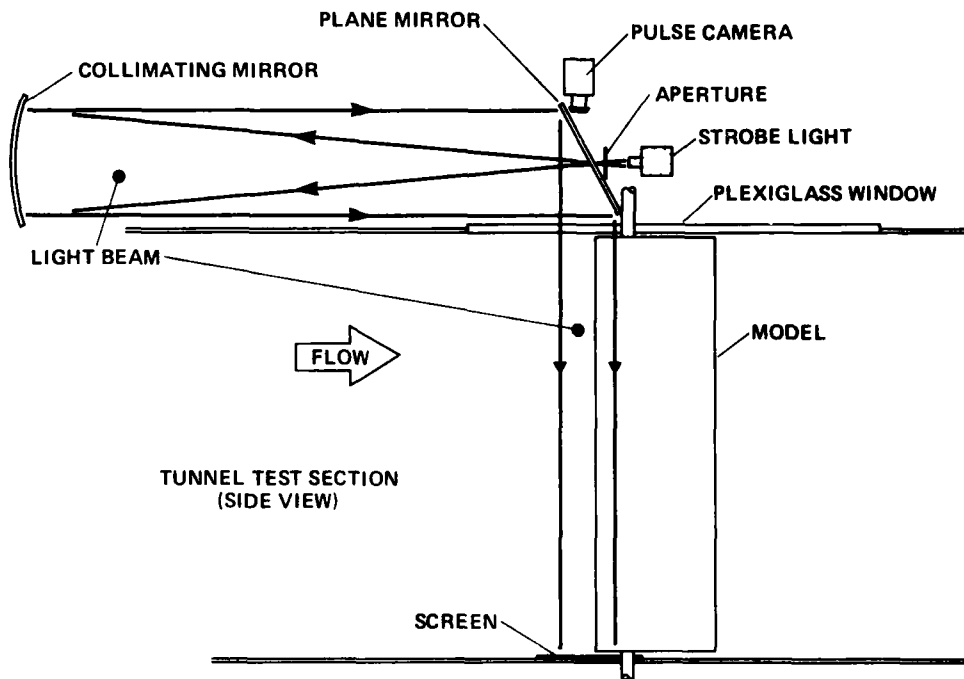


Figure 7.- Sketch of the shadowgraph system for visualizing the leading-edge region.

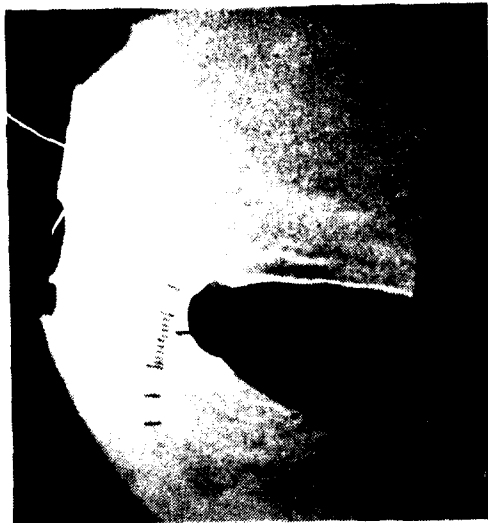


Figure 8.- Representative shadowgraphs before (upper) and during (lower) dynamic stall: Sikorsky SC-1095 airfoil,  $M_\infty = 0.30$ ,  $\alpha = 10^\circ + 10^\circ \sin \omega t$ ,  $k = 0.10$ .

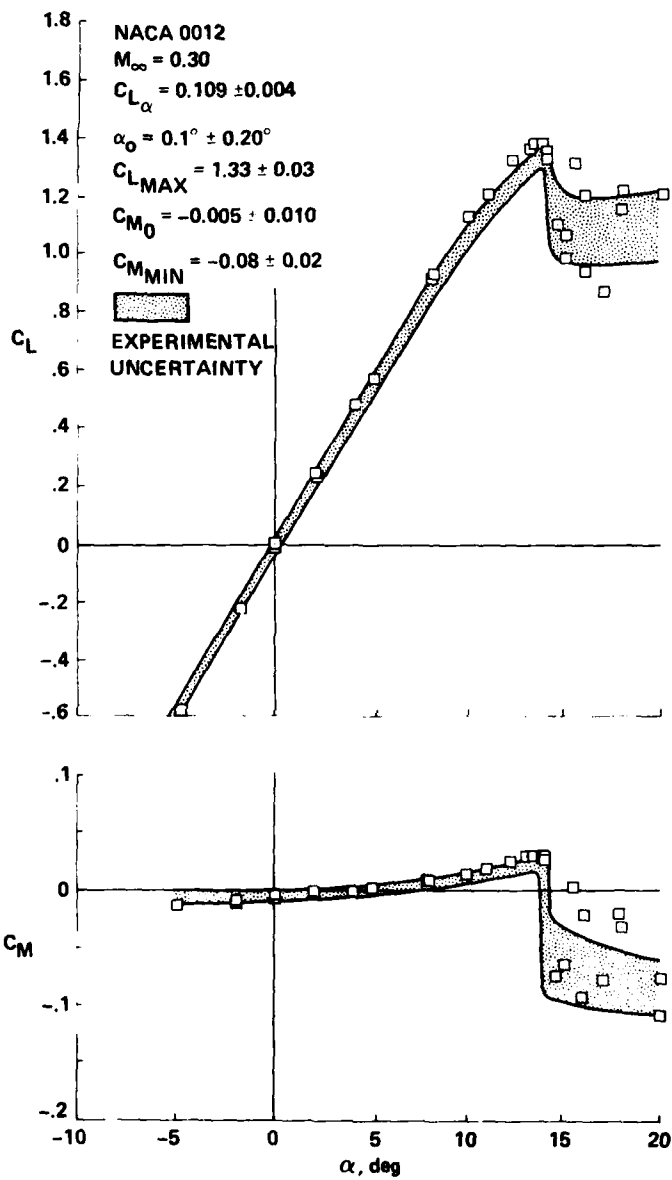


Figure 9.- Static lift and moment data on the NACA 0012 airfoil at  $M_\infty = 0.3$ ; shaded bands represent uncertainty limits of data corrected for wind-tunnel-wall effects.



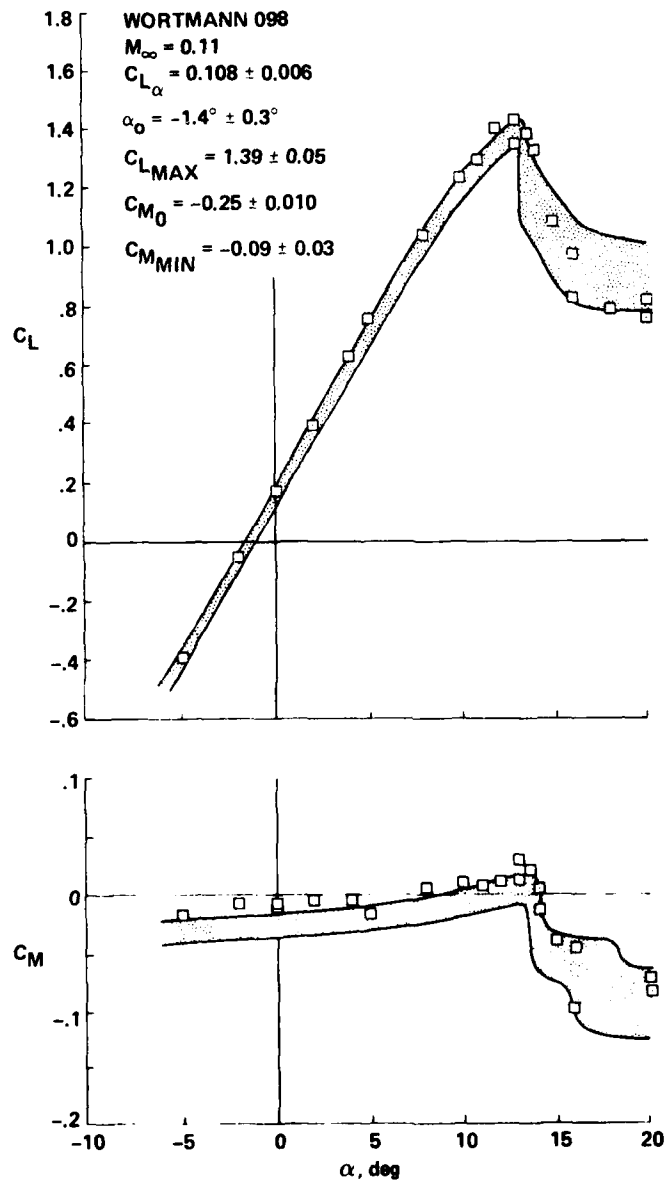


Figure 10.- Static lift and moment data on the Wortmann FX-098 airfoil at  $M_\infty = 0.11$ .

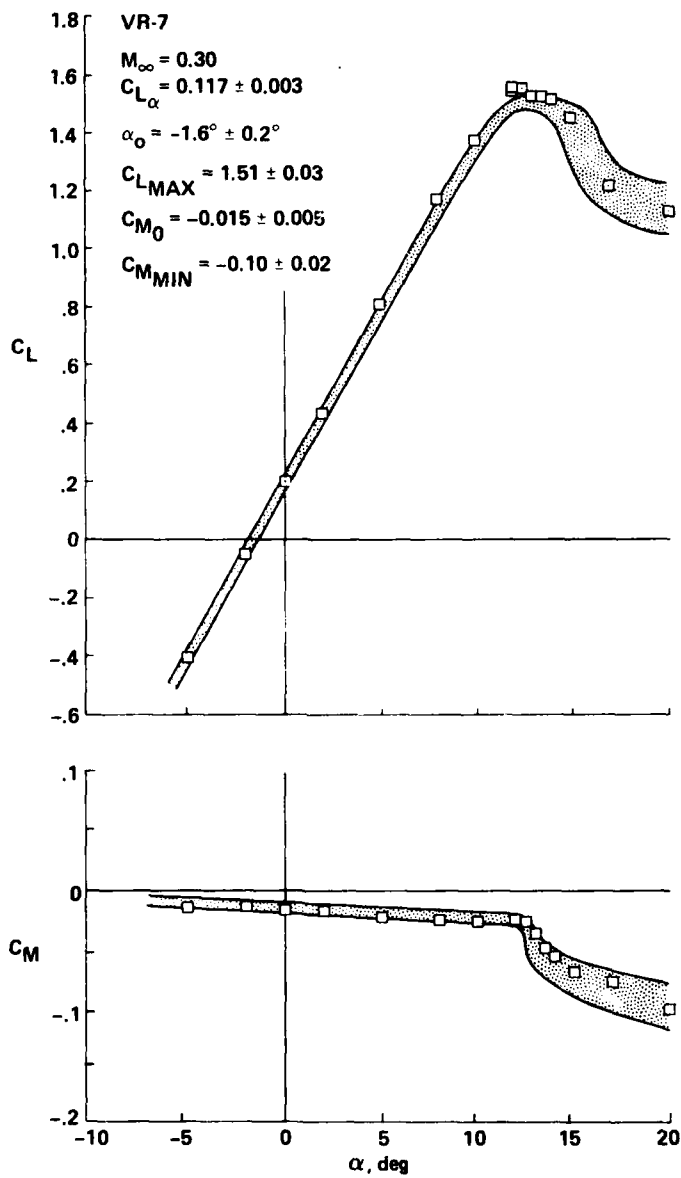


Figure 11.- Static lift and moment data on the Vertol VR-7 airfoil at  $M_\infty = 0.30$ .

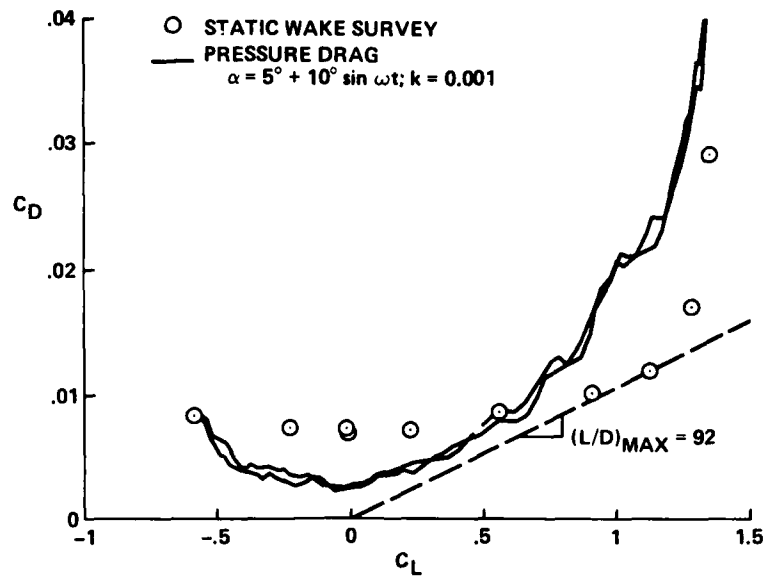


Figure 12.- Comparison of measured lift-drag polars for the NACA 0012 airfoil at  $M_\infty = 0.30$ , including wind-tunnel-wall corrections.

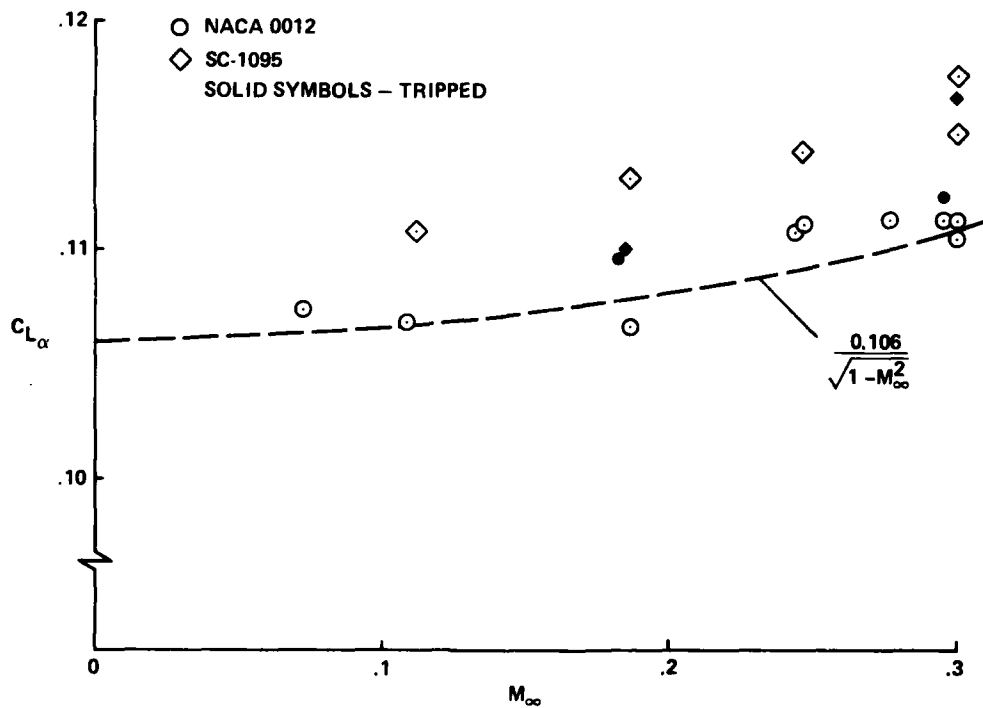


Figure 13.- Comparison of lift-curve slopes on the NACA 0012 and SC-1095 airfoils, including wind-tunnel-wall corrections.

NACA 0012 AIRFOIL  
 FRAME : 9302     $A_0 = 9.82^\circ$      $k = 0.096$   
 $Re = 3.66 E6$      $A_1 = 9.88^\circ$      $M = 0.302$   
 $C_{Lmax} = 1.84$      $C_{Mmin} = -0.25$      $C_{Dmax} = 0.53$   
 $\alpha_{Lmax} = 18.2^\circ$      $\xi = 0.272$      $M_{max} = 1.227$   
 $\alpha_{Cmin} = 9.4^\circ$      $-C_{Pmax} = 9.1$      $\alpha_{Mmax} = 14.8^\circ$

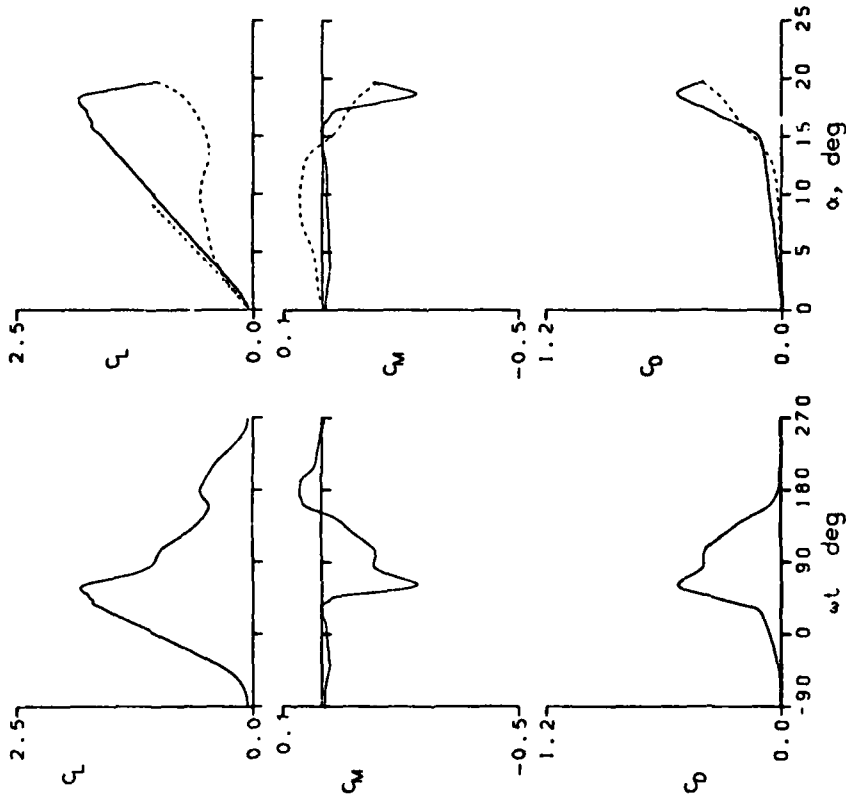
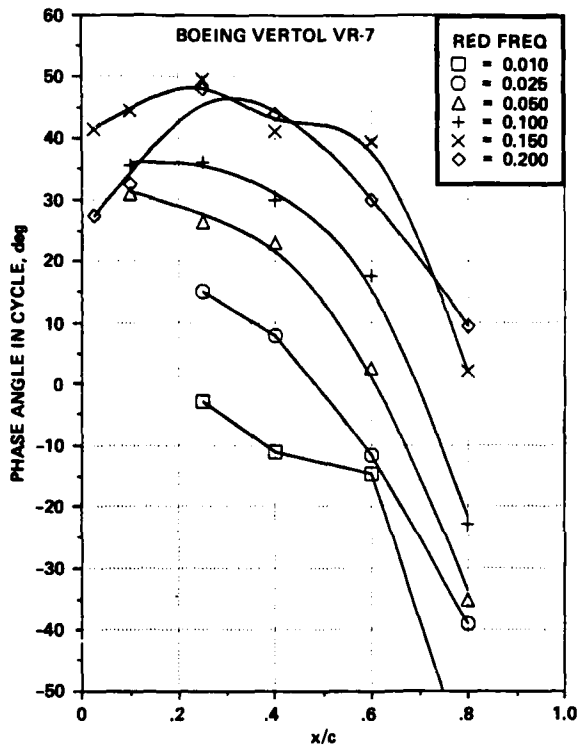
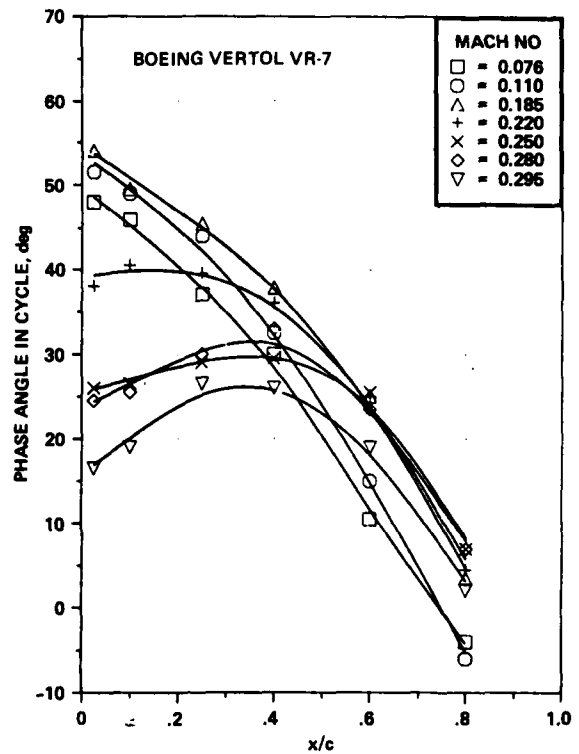


Figure 14.- Typical data presentation from volume 2; no wall corrections.



(a) Reduced frequency sweep:  
light stall.



(b) Mach number sweep:  
deep stall.

Figure 15.- Typical data presentation from volume 3.

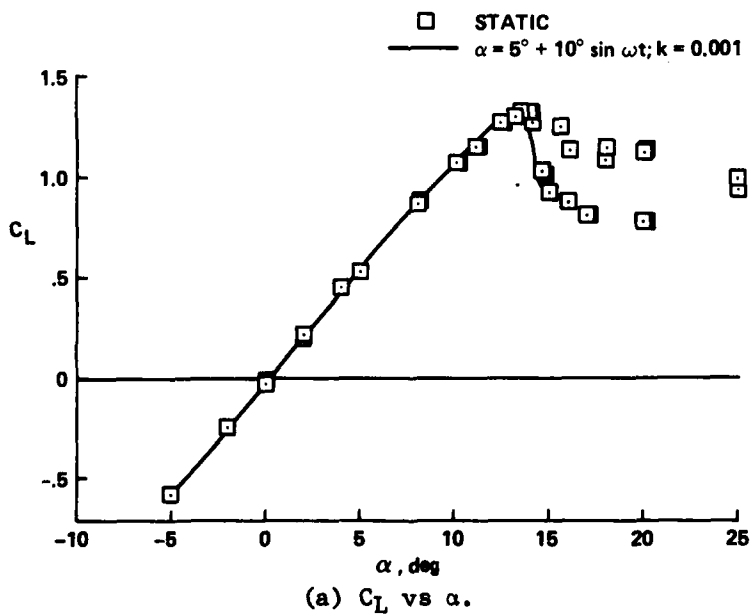
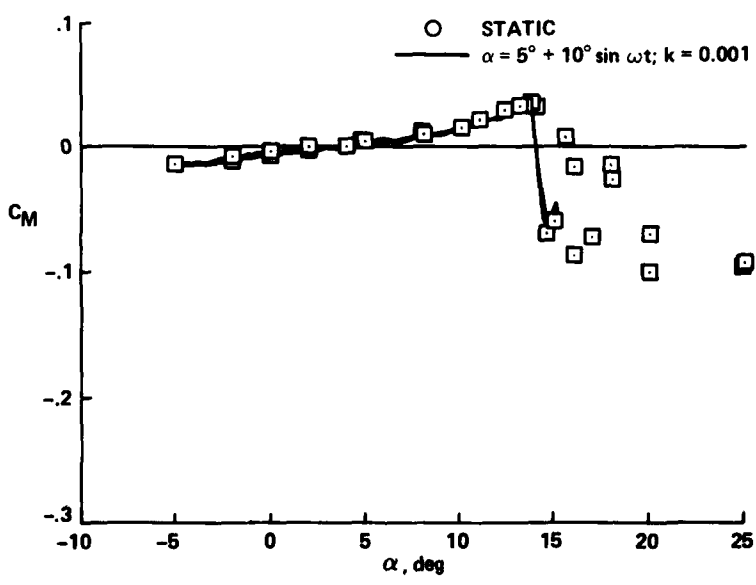
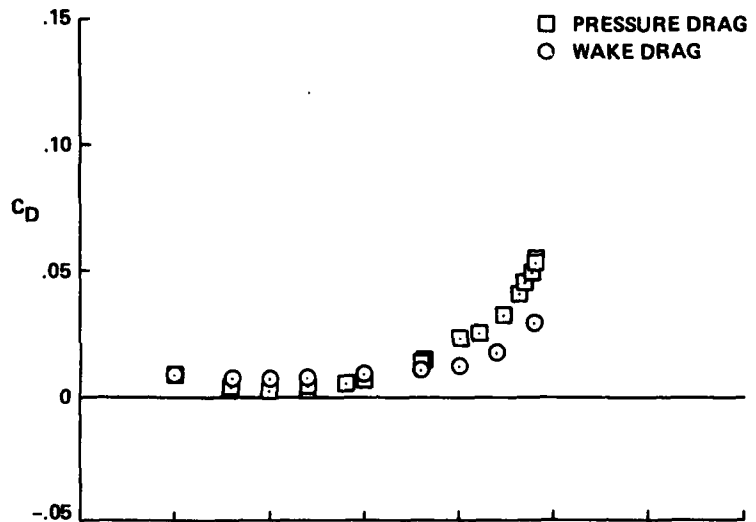
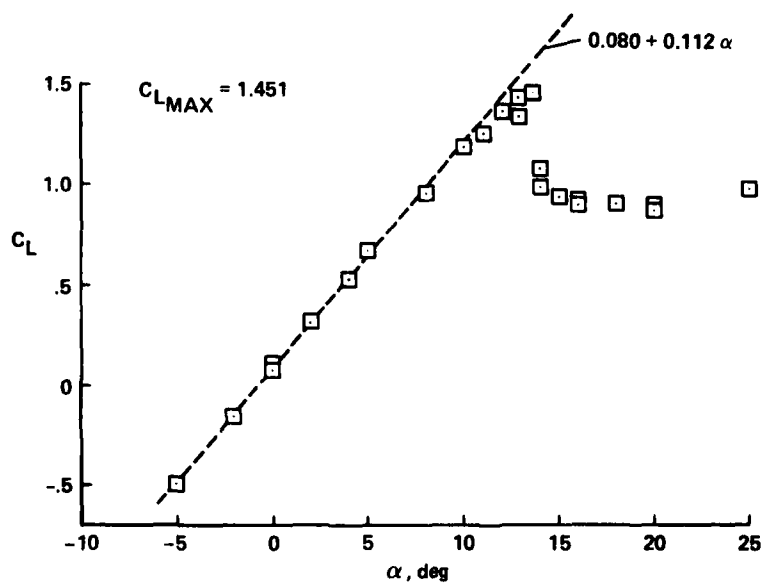


Figure 16.- Static characteristics of the NACA 0012 airfoil at  $M_\infty = 0.30$ , including wind-tunnel-wall corrections.



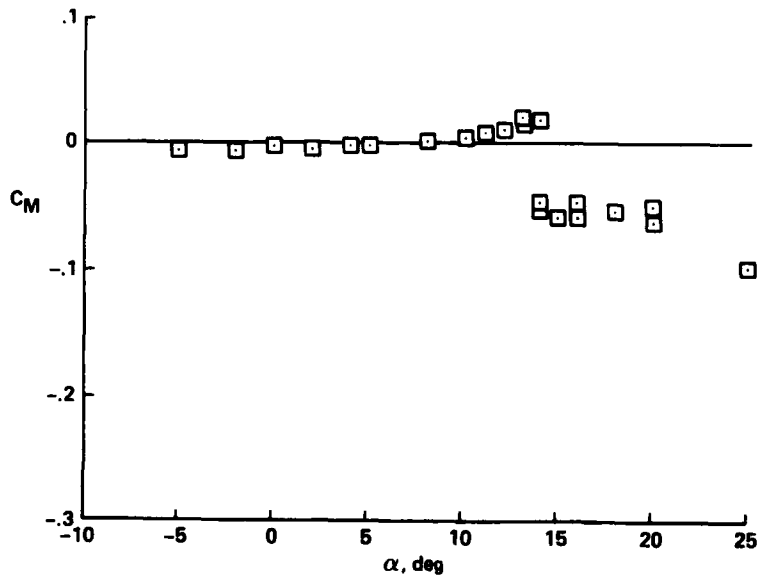
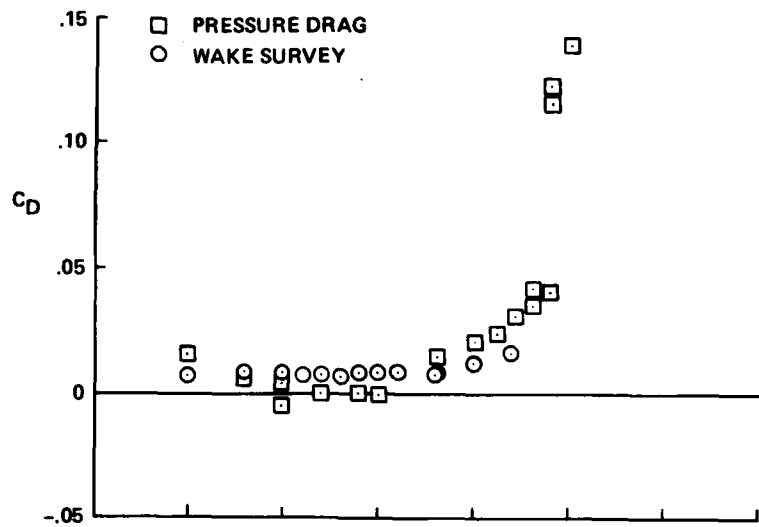
(b)  $C_D$  and  $C_M$  vs  $\alpha$ .

Figure 16.- Concluded.



(a)  $C_L$  vs  $\alpha$ .

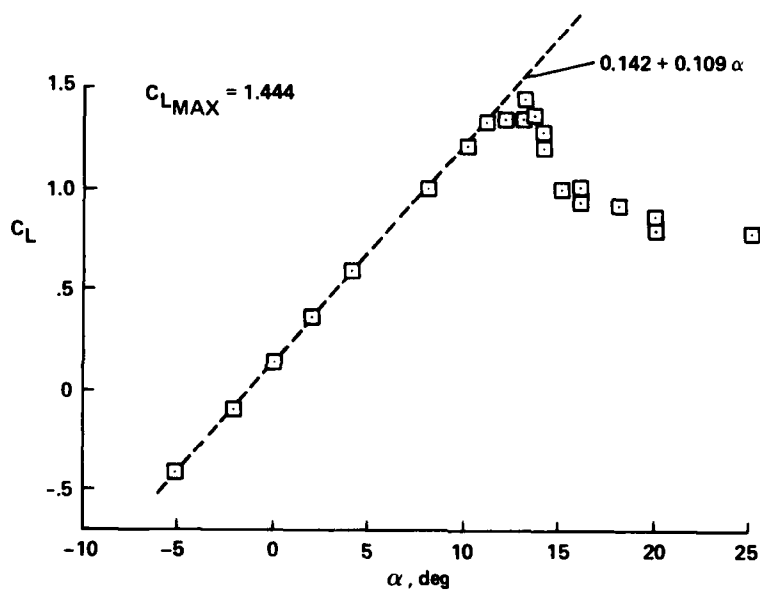
Figure 17.- Static characteristics of the Ames A-01 airfoil at  $M_\infty = 0.30$ , including wind-tunnel-wall corrections.



(b) C<sub>D</sub> and C<sub>M</sub> vs α.

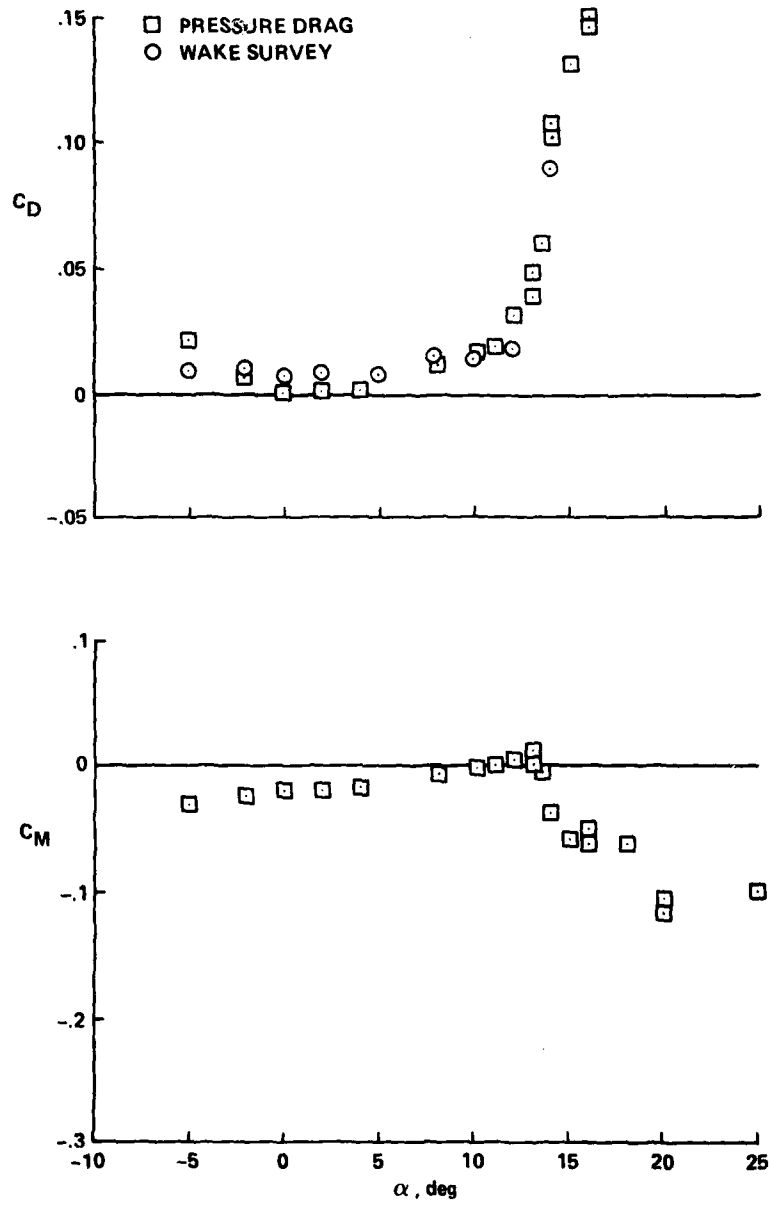
Figure 17.- Concluded.





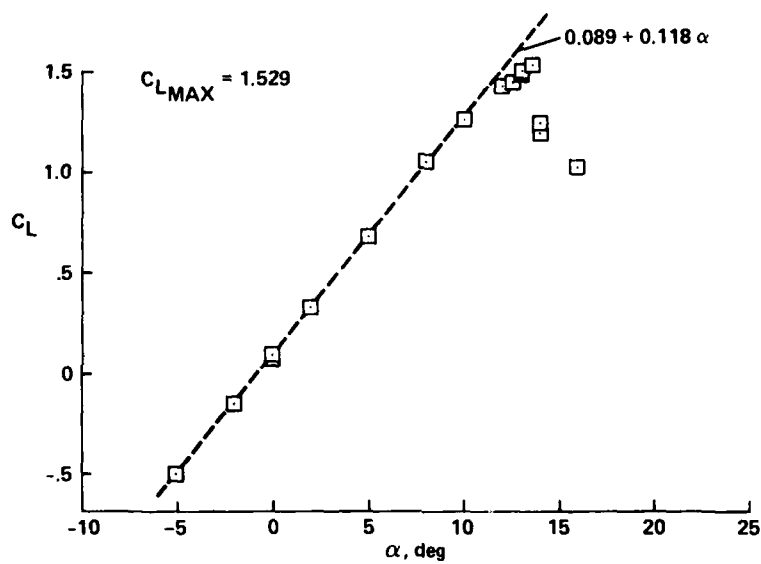
(a)  $C_L$  vs  $\alpha$ .

Figure 18.- Static characteristics of the Wortmann FX-098 airfoil at  $M_\infty = 0.30$ , including wind-tunnel-wall corrections.



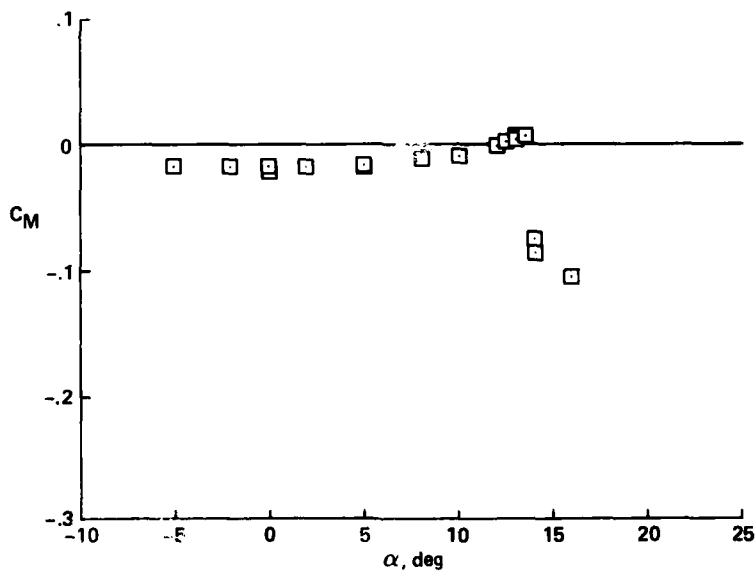
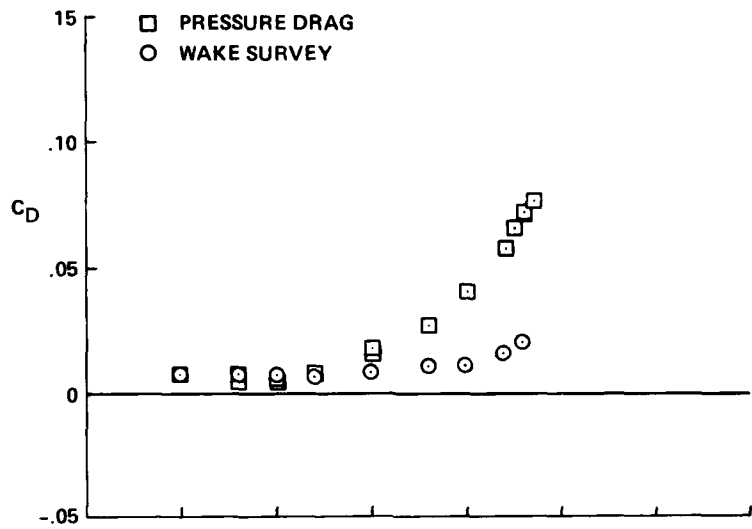
(b)  $C_D$  and  $C_M$  vs  $\alpha$ .

Figure 18.- Concluded.



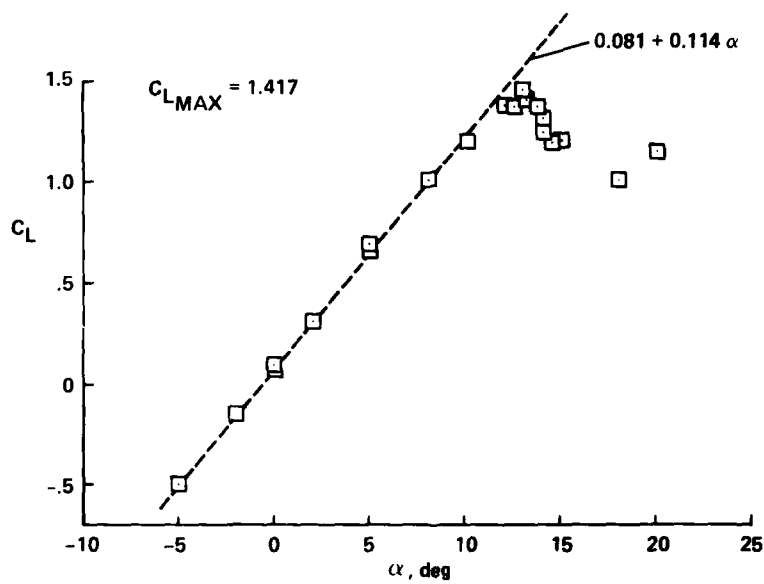
(a)  $C_L$  vs  $\alpha$ .

Figure 19.- Static characteristics of the Sikorsky SC-1095 airfoil at  $M_\infty = 0.30$ , including wind-tunnel-wall corrections.



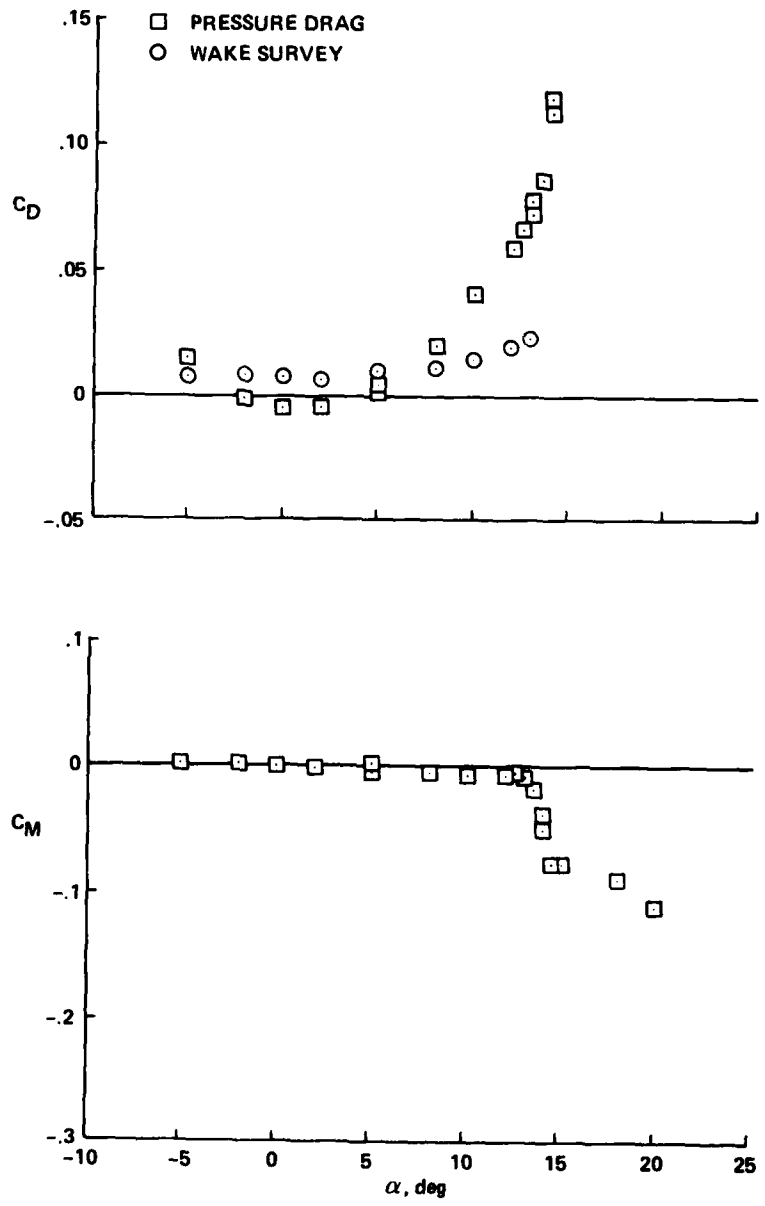
(b)  $C_D$  and  $C_M$  vs  $\alpha$ .

Figure 19.- Concluded.

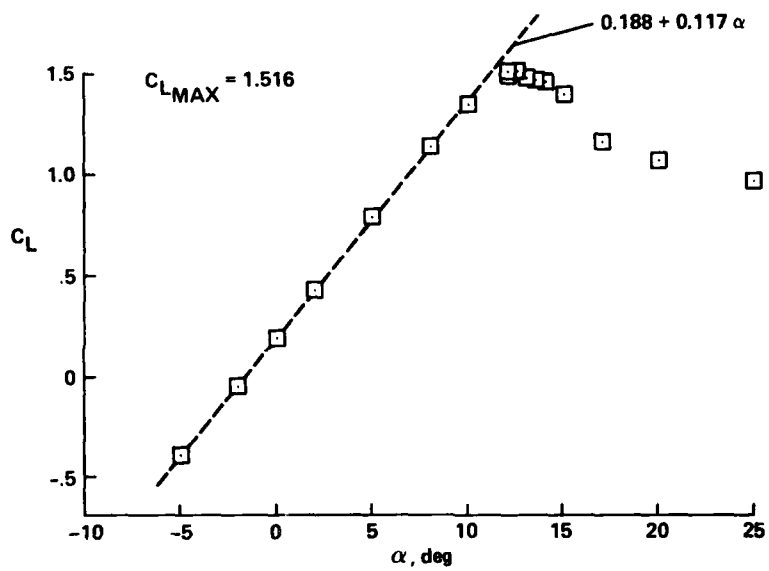


(a)  $C_L$  vs  $\alpha$ .

Figure 20.- Static characteristics of the Hughes HH-02 airfoil at  $M_\infty = 0.30$ , including wind-tunnel-wall corrections.

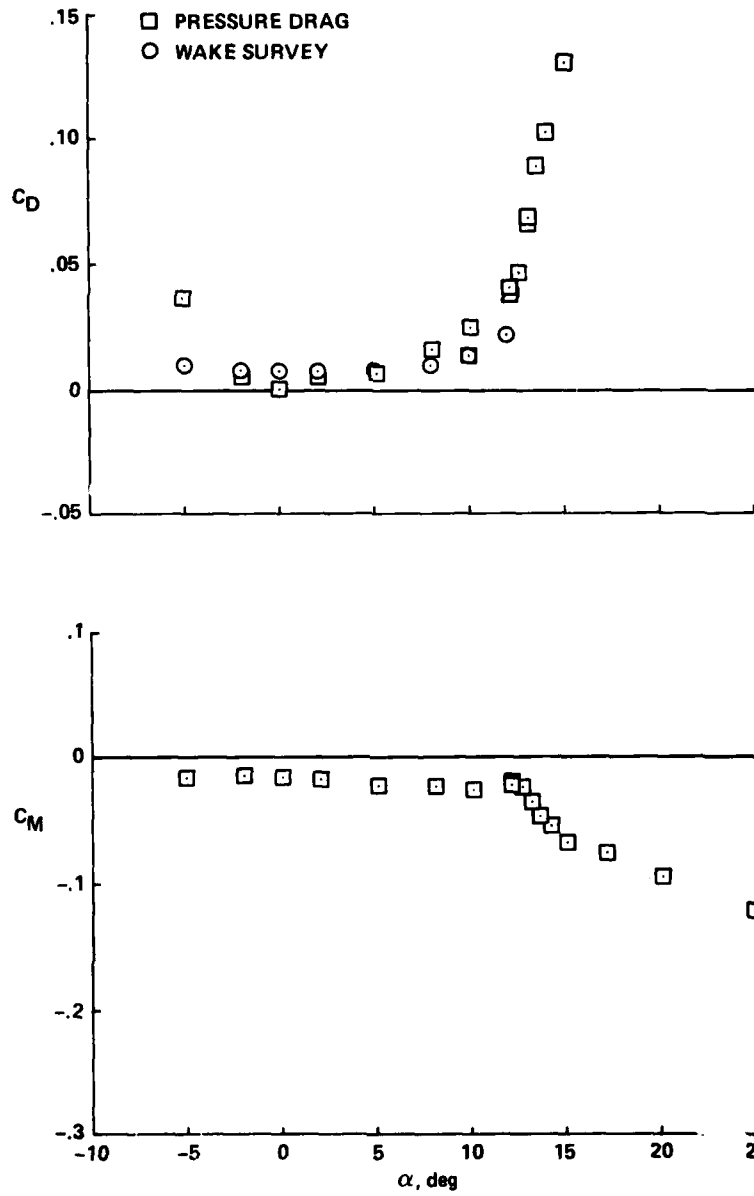


(b)  $C_D$  and  $C_M$  vs  $\alpha$ .  
 Figure 20.- Concluded.



(a)  $C_L$  vs  $\alpha$ .

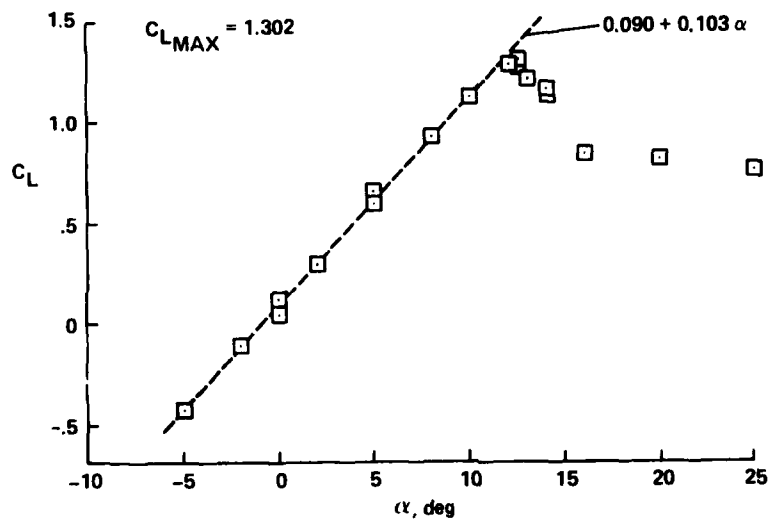
Figure 21.- Static characteristics of the Vertol VR-7 airfoil at  $M_\infty = 0.30$ , including wind-tunnel-wall corrections.



(b)  $C_D$  and  $C_M$  vs  $\alpha$ .

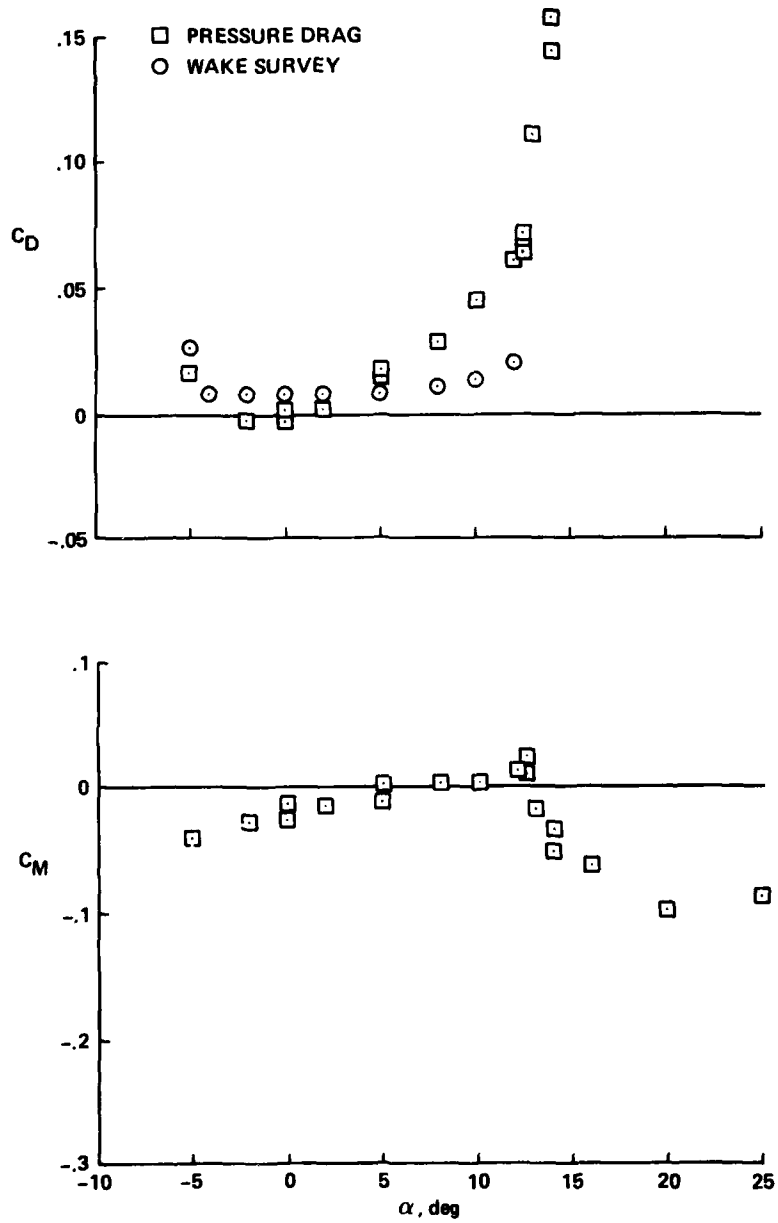
Figure 21.- Concluded.





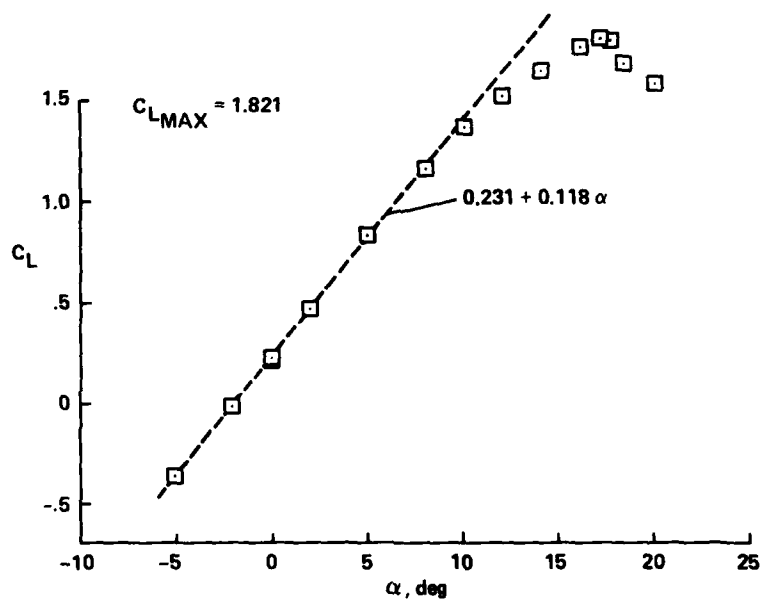
(a)  $C_L$  vs  $\alpha$ .

Figure 22.- Static characteristics of the NLR-1 airfoil at  $M_\infty = 0.30$ , including wind-tunnel-wall corrections.



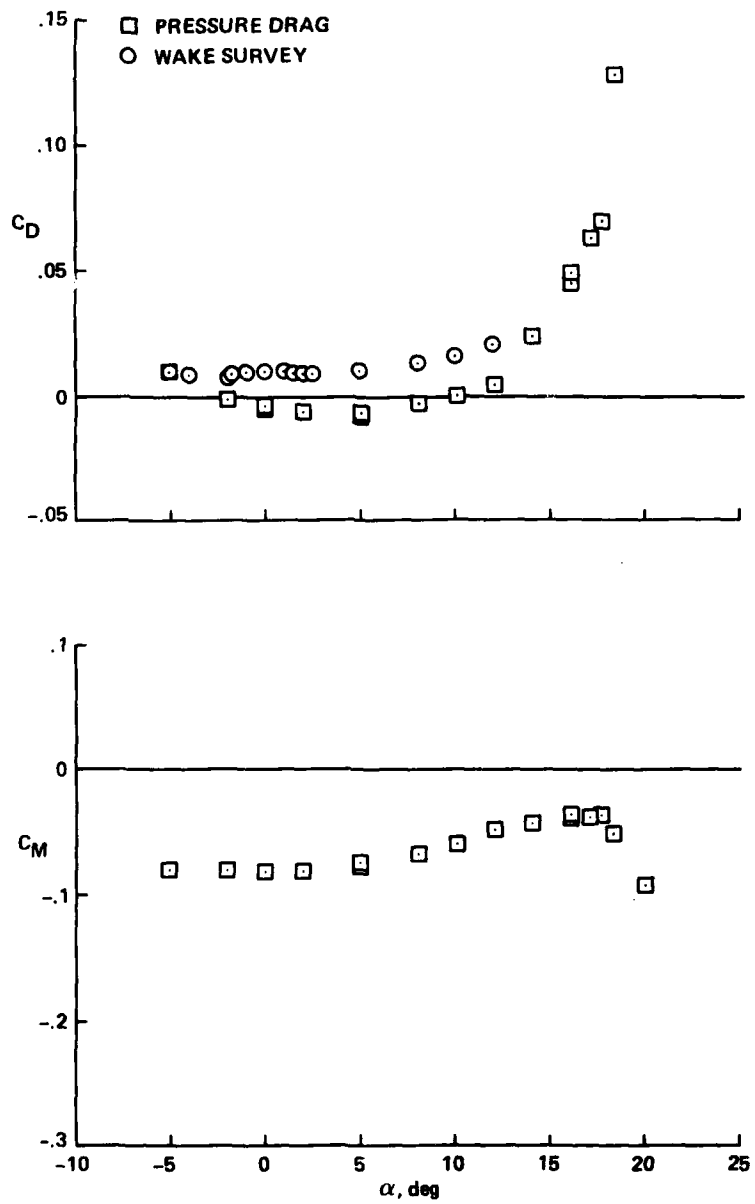
(b)  $C_D$  and  $C_M$  vs  $\alpha$ .

Figure 22.- Concluded.



(a)  $C_L$  vs  $\alpha$ .

Figure 23.- Static characteristics of the NLR-7301 airfoil at  $M_\infty = 0.30$ , including wind-tunnel-wall corrections.



(b)  $C_D$  and  $C_M$  vs  $\alpha$ .

Figure 23.- Concluded.

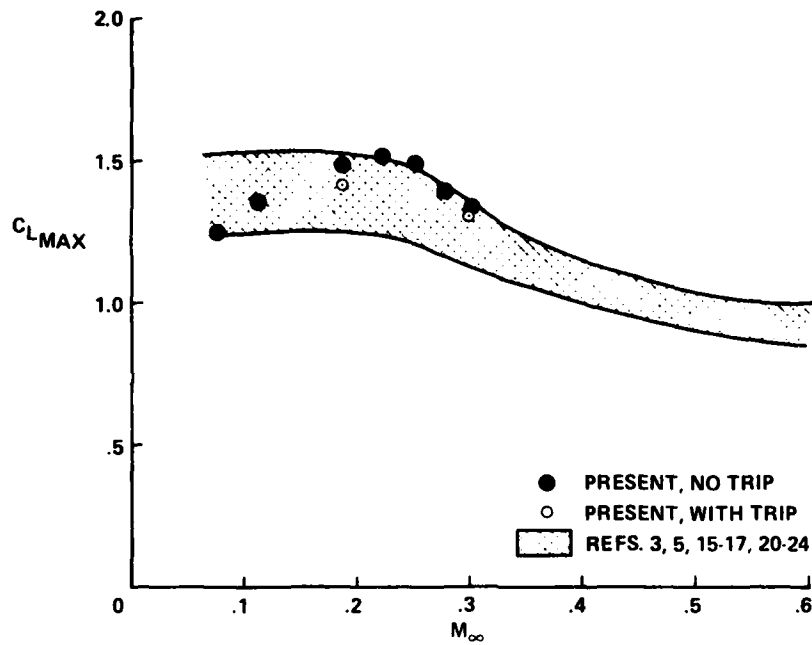


Figure 24.- Comparison of maximum static lift on the NACA 0012 airfoil.

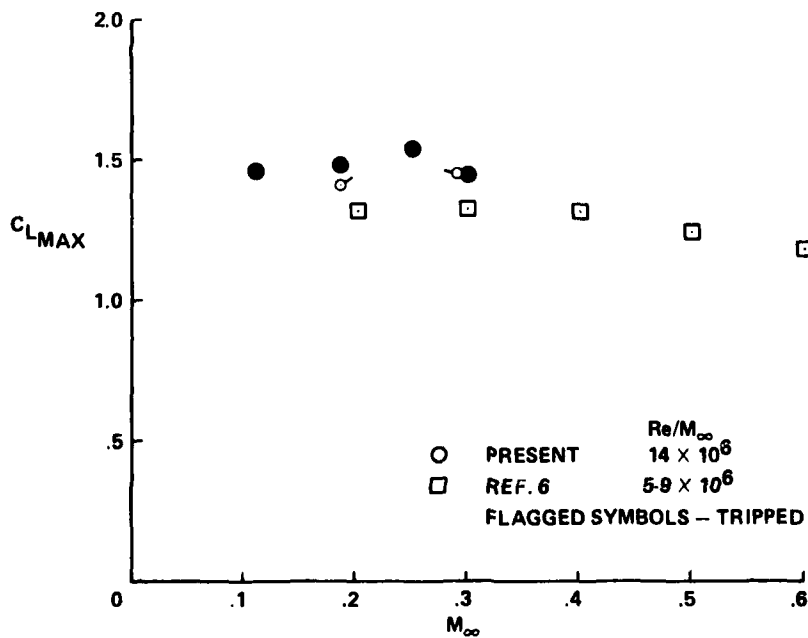


Figure 25.- Comparison of maximum static lift on the Ames A-01 airfoil.

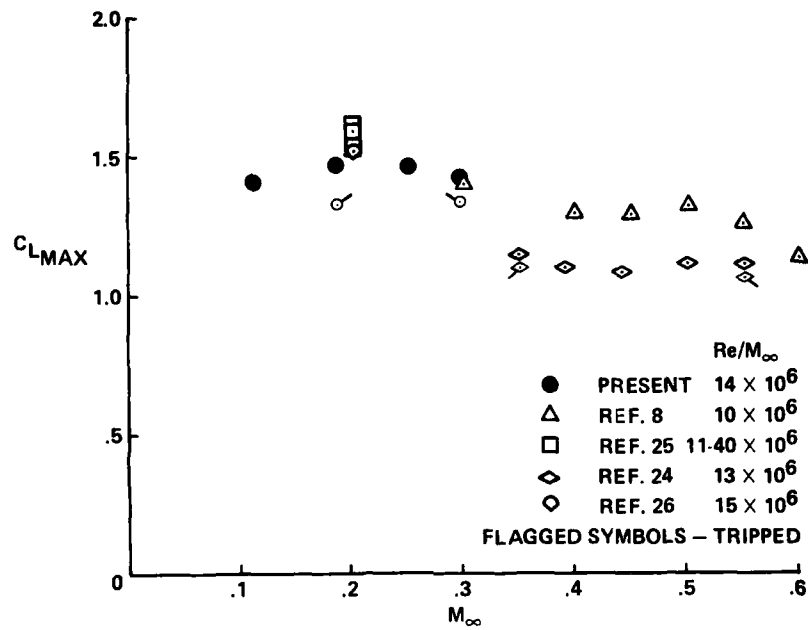


Figure 26.- Comparison of maximum static lift on the Wortmann FX-098 airfoil.

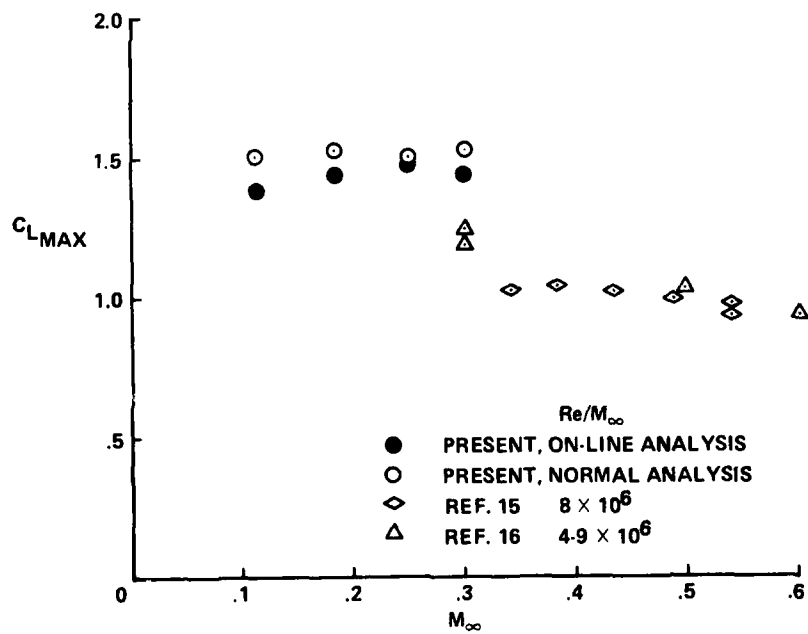


Figure 27.- Comparison of maximum static lift on the Sikorsky SC-1095 airfoil.

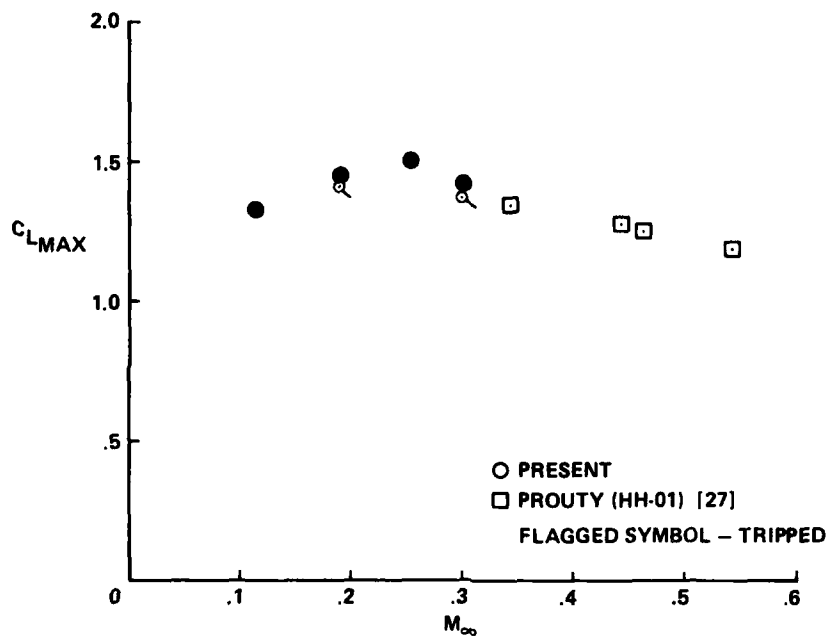


Figure 28.- Comparison of maximum static lift on the Hughes HH-02 airfoil.

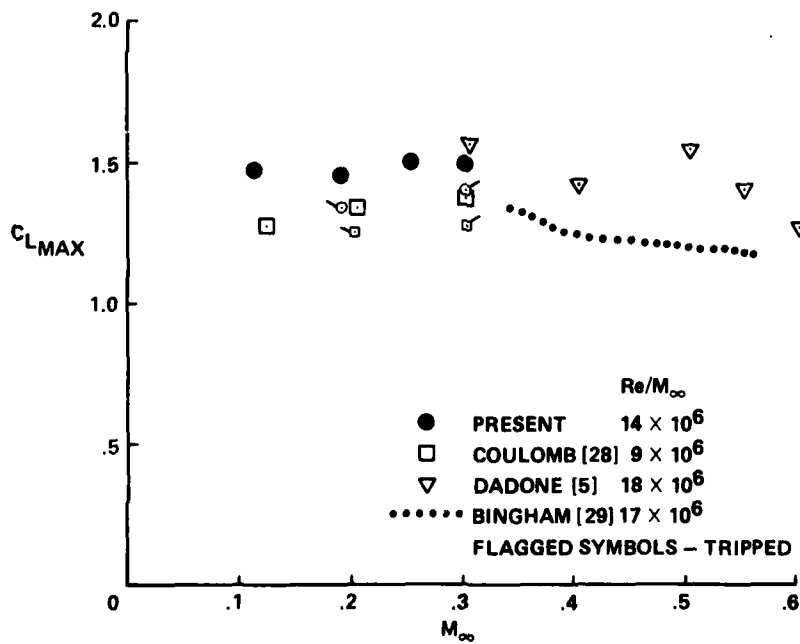


Figure 29.- Comparison of maximum static lift on the Vertol VR-7 airfoil.

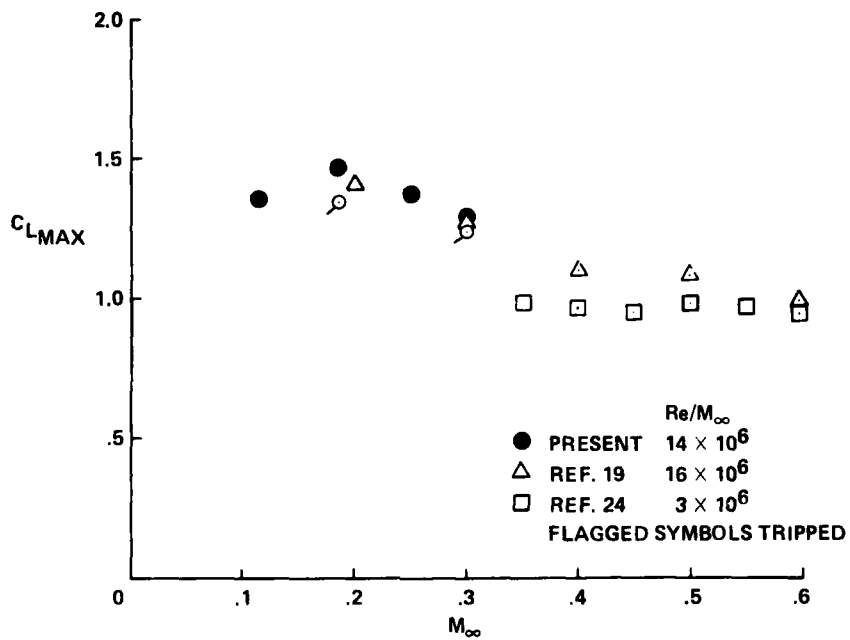


Figure 30.- Comparison of maximum static lift on the NLR-1 airfoil.

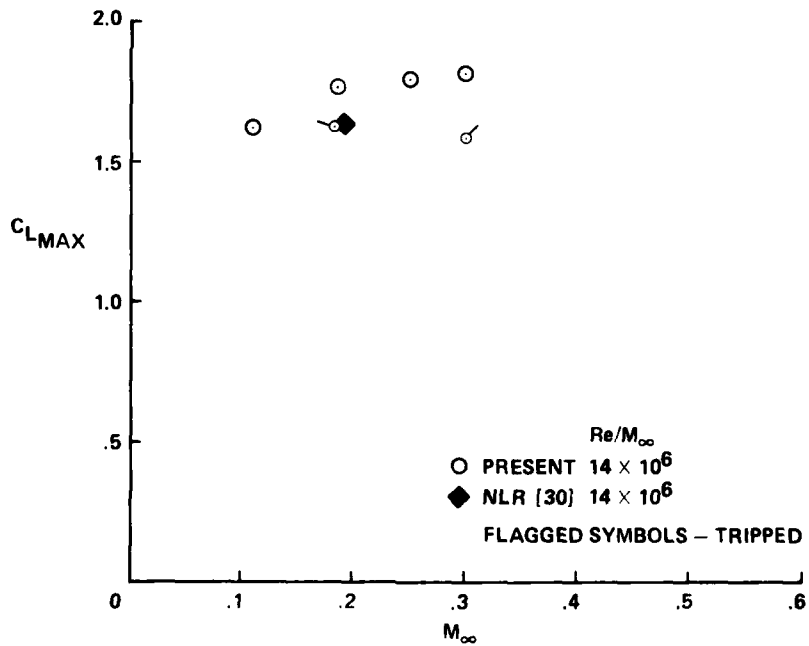


Figure 31.- Comparison of maximum static lift on the NLR-7301 airfoil.





AD-A119 827

NATIONAL AERONAUTICS AND SPACE ADMINISTRATION MOFFET--ETC F/G 20/4  
AN EXPERIMENTAL STUDY OF DYNAMIC STALL ON ADVANCED AIRFOIL SECT--ETC (U)  
JUL 82 W J MCCROSKEY, K W MCALISTER, L W CARR

UNCLASSIFIED

NASA-A-8924-VOL-1

NASA-TN-89245-VOL-1

NL

2 of 2

3000



END

DATE

FORMED

11 82

DTIC

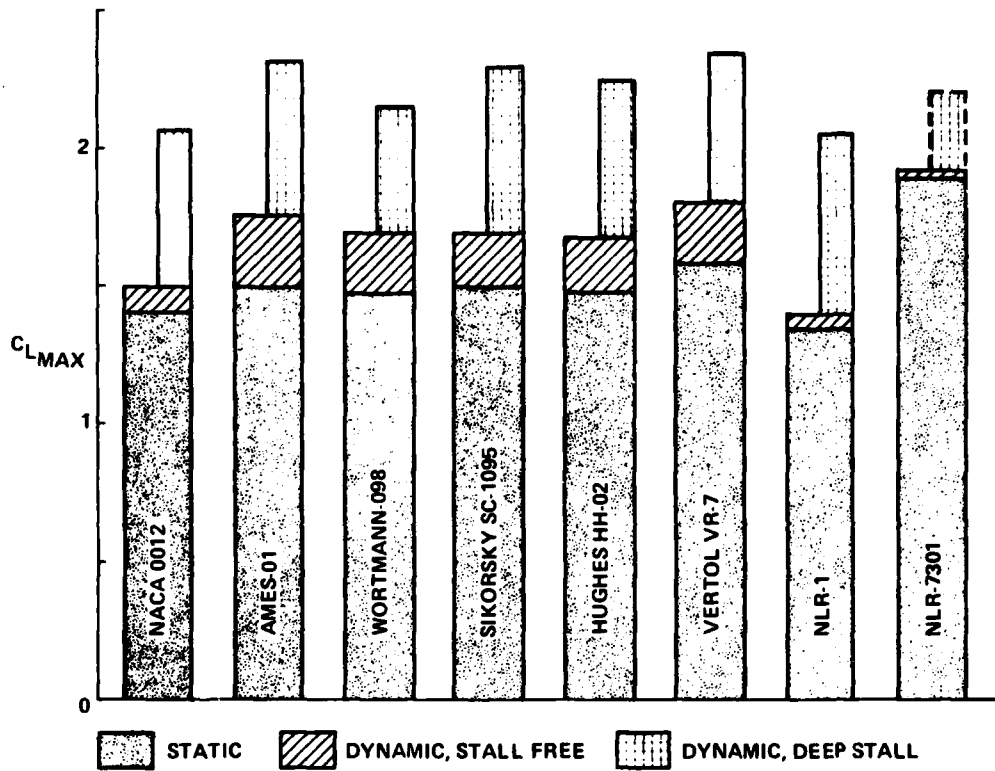


Figure 33.- Comparison of maximum lift on the eight airfoils at  $M_{\infty} = 0.30$ .

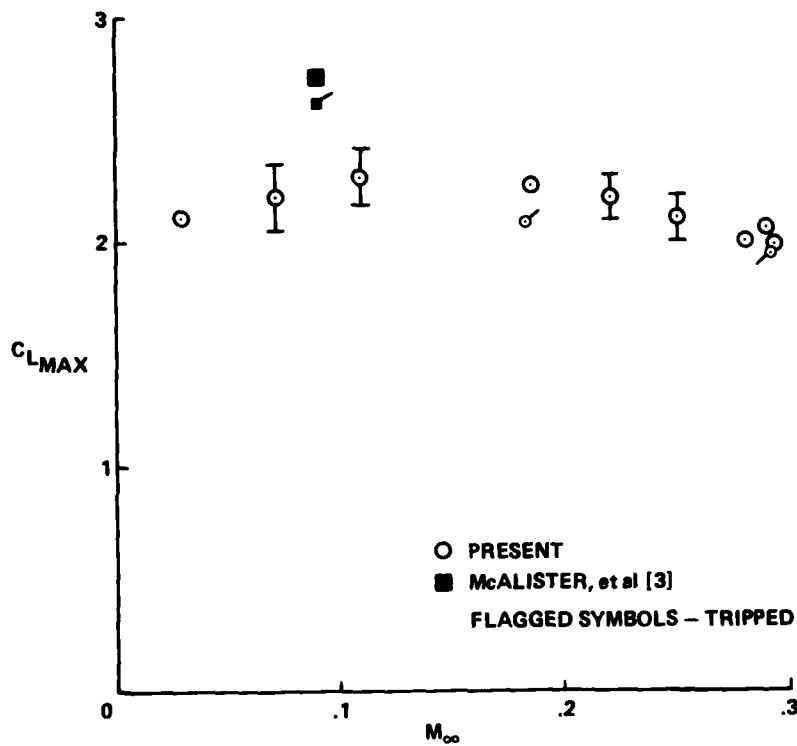


Figure 34.- Comparison of maximum lift on the NACA 0012 airfoil under deep-dynamic-stall conditions:  $\alpha = 15^\circ + 10^\circ \sin \omega t$ ,  $k = 0.10$ .

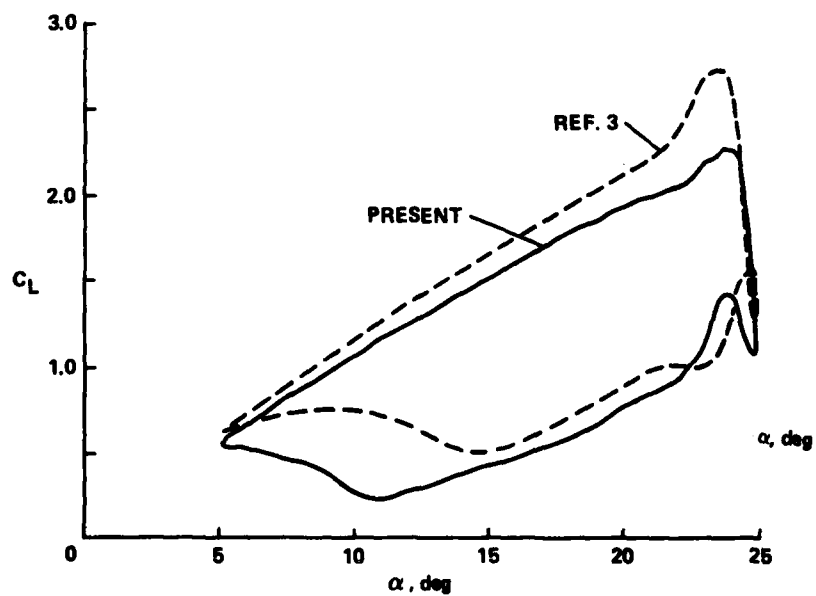


Figure 35.- Comparison of the lift hysteresis on the NACA 0012 airfoil:  $M_\infty \approx 0.1$ ,  $\alpha = 15^\circ + 10^\circ \sin \omega t$ ,  $k = 0.10$ .

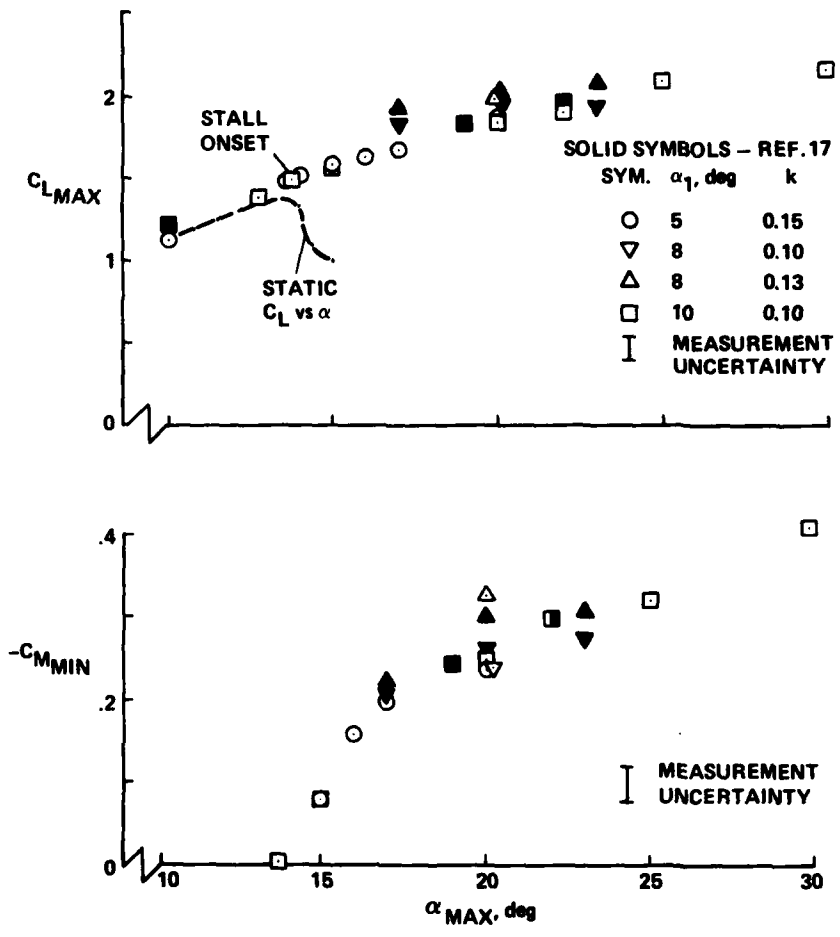


Figure 36.- Comparison of maximum airloads on the NACA 0012 airfoil at  $M_\infty = 0.30$  and  $\alpha_1 k^2 \cong \text{constant}$ .

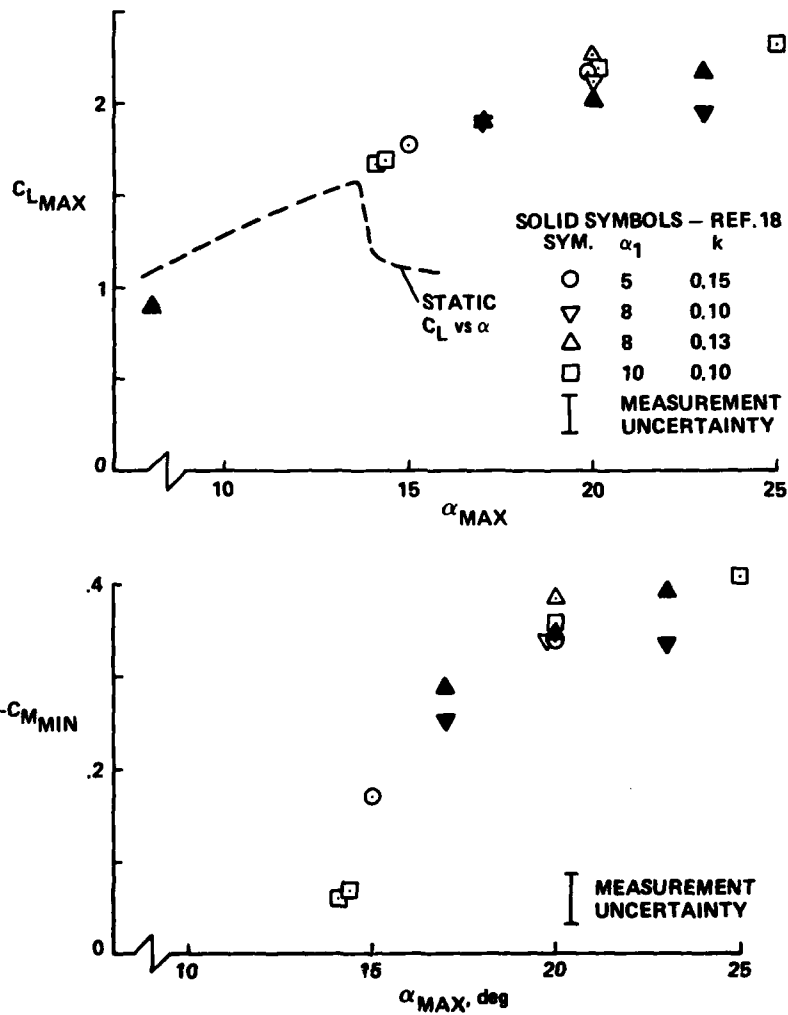


Figure 37.- Comparison of maximum airloads on the Sikorsky SC-1095 airfoil at  $M_\infty = 0.30$  and  $\alpha_1 k^2 = \text{constant}$ .

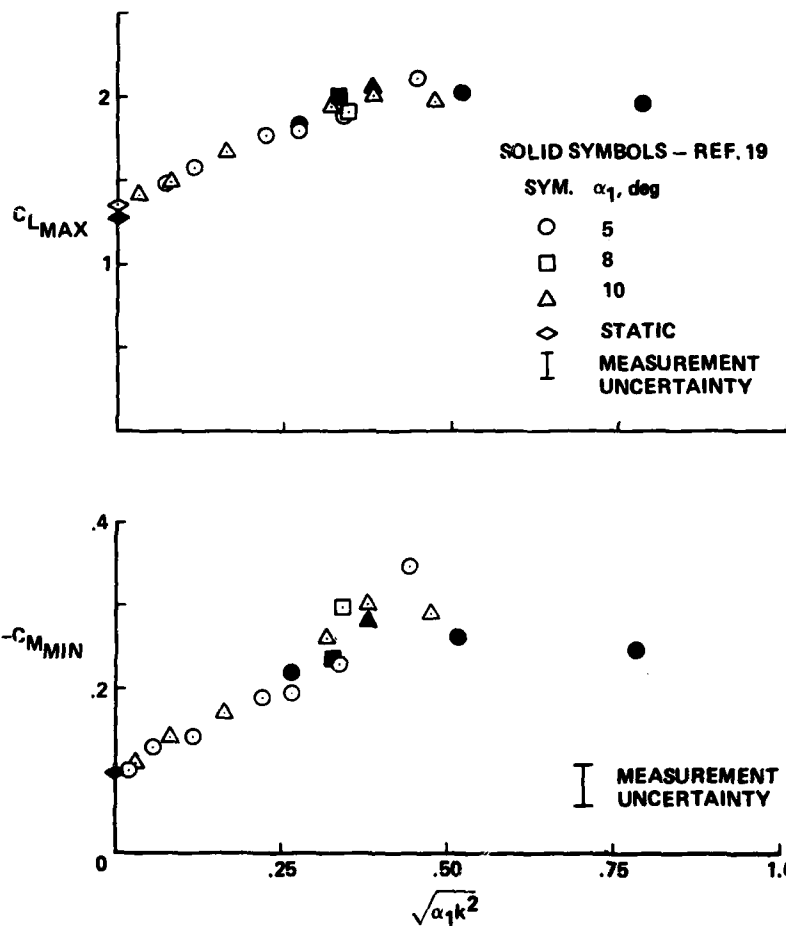


Figure 38.- Comparison of maximum airloads on the NLR-1 airfoil at  $M_\infty = 0.3$  and  $\alpha_{max} = 20^\circ$ .

1. Report No. NASA TM 84245 USAAVRADCOM TR-82-A-8	2. Government Accession No. <b>AD-A119 827</b>	3. Recipient's Catalog No.	
4. Title and Subtitle AN EXPERIMENTAL STUDY OF DYNAMIC STALL ON ADVANCED AIRFOIL SECTIONS VOLUME 1. SUMMARY OF THE EXPERIMENT		5. Report Date July 1982	
		6. Performing Organization Code	
7. Author(s) W. J. McCroskey, K. W. McAlister, L. W. Carr, and S. L. Pucci		8. Performing Organization Report No. A-8924	
		10. Work Unit No. K-1585	
9. Performing Organization Name and Address NASA Ames Research Center, Moffett Field, Calif. 94035, and U.S. Army Aero- mechanics Laboratory (AVRADCOM), Ames Research Center, Moffett Field, Calif. 94035		11. Contract or Grant No.	
		13. Type of Report and Period Covered Technical Memorandum	
12. Sponsoring Agency Name and Address National Aeronautics and Space Administration, Washington, D.C. 20546, and U.S. Army Aviation R&D Command, St. Louis, MO 93166		14. Sponsoring Agency Code	
		15. Supplementary Notes Point of Contact: W. J. McCroskey, Ames Research Center, MS 202A-1 Moffett Field, Calif. 94035 (415) 965-6428 or FTS 448-6428	
16. Abstract <p>The static and dynamic characteristics of seven helicopter sections and a fixed-wing supercritical airfoil were investigated over a wide range of nominally two-dimensional flow conditions, at Mach numbers up to 0.30 and Reynolds numbers up to <math>4 \times 10^6</math>. Details of the experiment, estimates of measurement accuracy, and test conditions are described in this volume (the first of three volumes). Representative results are also presented and comparisons are made with data from other sources. The complete results for pressure distributions, forces, pitching moments, and boundary-layer separation and reattachment characteristics are available in graphical form in volumes 2 and 3.</p> <p>The results of the experiment show important differences between airfoils, which would otherwise tend to be masked by differences in wind tunnels, particularly in steady cases. All of the airfoils tested provide significant advantages over the conventional NACA 0012 profile. In general, however, the parameters of the unsteady motion appear to be more important than airfoil shape in determining the dynamic-stall airloads.</p>			
17. Key Words (Suggested by Author(s)) Dynamic stall      Maximum lift Oscillating airfoils      Airfoil data Boundary layer measurements Unsteady pressure distributions		18. Distribution Statement Unlimited  Subject Category - 02	
19. Security Classif. (of this report) Unclassified	20. Security Classif. (of this page) Unclassified	21. No. of Pages 103	22. Price* A06